Thermophysical properties of hydrogen mixtures relevant for the development of the hydrogen economy: Review of available experimental data and thermodynamic models

Daniel Lozano-Martín, Alejandro Moreau, César R. Chamorro[*]

Grupo de Termodinámica y Calibración (TERMOCAL), Research Institute on Bioeconomy (BioEcoUVa), Escuela de Ingenierías Industriales, Universidad de Valladolid, Paseo Del Cauce, 59, E-47011, Valladolid, Spain

ABSTRACT

The accurate knowledge of the thermophysical and thermodynamic properties of pure hydrogen and hydrogen mixtures plays an important role in the design and operation of many processes involved in hydrogen production, transport, storage, and use. These data are needed for the development of theoretical models necessary for the introduction of hydrogen as a promising energy carrier in the near future. A literature survey on both the available experimental data and the theoretical models associated with the thermodynamic properties of hydrogen mixtures, within the operational ranges of industrial interest for composition, temperature, and pressure, is presented in this work. Considering the available experimental data and the requirements for the design and operation of hydrogen systems, the most relevant gaps in temperature, pressure and composition are identified.

1. Introduction

In recent years, hydrogen is being pursued as a sustainable energy carrier. Hydrogen allows renewable energy sources to contribute more efficiently to the future energy mix, helping to match the variable output from the main renewable sources (wind and solar) with the demand. Hydrogen provides a way to decarbonize the economy in a broad range of sectors, not only energy and transport, but also in such fields as chemicals or iron and steel production, where it is difficult to find alternatives that can reduce emissions.

Hydrogen is already in use in a number of important industrial sectors. Pure hydrogen, with only small amounts of contaminants allowed, is demanded for oil refining and fertilizer manufacturing. Hydrogen without prior separation from other gases, mainly in the form of synthesis gas (H_2, CO, CO_2), is also broadly used in industry.

Industry has already proved that hydrogen can be produced, stored and distributed on a large scale [1], but unfortunately, almost all the hydrogen for industrial use is nowadays produced from fossil fuels. Hydrogen obtained using renewable energy and sustainable processes, usually called 'green' hydrogen, is currently more expensive. For hydrogen to have a role in future low-carbon energy systems, it is necessary to demonstrate that it can be obtained economically from

low-carbon-emission processes, and it also needs to be adopted in sectors where it is almost completely absent at the moment, such as transport, heat supply for buildings and power generation [2].

Hydrogen, like electricity, is an energy carrier rather than an energy source. But unlike electricity, it is a chemical energy carrier, which gives it important advantages. Hydrogen has a higher energy content per unit of mass than most of the conventional fossil fuels and the possibility of higher energy conversion efficiencies when used in fuel cells. On the other hand, most of the 'green' hydrogen production methods are not mature enough, resulting in high production costs.

Hydrogen can be used in its pure form or it can also be combined with other inputs to produce hydrogen-based fuels and feedstock. Hydrogen-based fuels include such products as synthetic methane, synthetic liquid fuels and methanol, all of which require carbon as an input, alongside hydrogen. Hydrogen-based feedstock include such products as ammonia, which can be used as a chemical feedstock or potentially as a fuel.

One of the key elements to permit the hydrogen economy to progress is the development of appropriate thermodynamic models describing the behavior of hydrogen mixtures. The accurate knowledge of thermophysical and thermodynamic properties, such as PVTx, speed of sound, and vapor-liquid equilibrium (VLE), plays an important role in

---

the design and operation of any chemical plant in general [3,4], and of many processes involved in hydrogen production, transport and use in particular [5]. Generally speaking, precise knowledge of the thermodynamic and transport properties allows the feasibility of a given process, the design of the plant, and the sizing of the equipment to be determined; and it is particularly relevant for the optimization of processes. The requirement for accuracy and reliability varies depending on the application [3].

This work presents a review of both the experimental data and models for the thermodynamic properties of hydrogen mixtures needed in industry and by the energy sector for the development of the hydrogen economy and supersedes our preliminary research advanced in a previous report [6]. The components of the studied mixtures have been selected from among the main components involved in the processes to obtain, transport and use hydrogen with current and foreseeable technologies. The paper is focused on VLE, density, speed of sound and other caloric properties of binary hydrogen mixtures, as these are the main experimental data needed for the improvement of existing reference equations of state and the development of new ones. Phase equilibrium data are limited to VLE. Liquid-liquid, solid-liquid, or solid-vapor equilibrium data are not considered in this review. The purpose of the work is to summarize the available experimental data and theoretical models, evaluate their quality, and identify knowledge gaps, providing suggestions for future research into H_2 mixtures.

2. Obtaining, storing, transporting, and using hydrogen

Hydrogen is an abundant element but, unfortunately, it is not found as a pure substance in nature. Hydrogen must be extracted from fossil fuels, biomass or water, for which energy is needed and (if fossil fuels are used) CO_2 is emitted. Attending to the primary energy source used to produce hydrogen, we can consider thermal, electrical, photonic and biochemical processes. Hydrogen that meets certain sustainability criteria has been termed "green" hydrogen, but there is no universally agreed definition yet, as there is no international green hydrogen standard [2].

2.1. Production processes, components, and compositions

The main technologies for obtaining hydrogen from fossil fuels are hydrocarbon reforming and pyrolysis. These methods are the most commonly used today. Currently, up to 48% of hydrogen comes from natural gas steam reforming and another 48% from oil reforming and coal gasification. In hydrocarbon reforming, the other component involved, besides the hydrocarbon, can be steam (steam reforming) or oxygen (partial oxidation). Both processes can be combined (autothermal reaction). Carbon monoxide appears as a byproduct of these processes. The main components that may be involved in all of these processes, besides H_2, are CH_4 (or higher hydrocarbons), CO, CO_2 and H_2O. Hydrocarbon pyrolysis consists of the thermal decomposition (temperatures around 1000 °C) of the hydrocarbon in an oxygen free environment, producing hydrogen and pure carbon. No CO_2 or CO is produced [7].

Biomass can also be used as the raw material for hydrogen production. Two kinds of processes, thermochemical and biological, can be used. Thermochemical processes, which are much faster and effective than the biological ones, mainly involve pyrolysis and gasification. The main gaseous products are H_2, CH_4, CO, and CO_2. Nitrogen also appears in biomass gasification in the presence of air (syngas).

Biological processes are more environmentally friendly and less energy intensive, as they usually operate at ambient temperature, but they are less efficient. The main biological technologies used for the production of hydrogen are bio-photolysis (direct or indirect) and fermentation (dark or photo-fermentation, simple or multi-stage). The raw material for obtaining hydrogen is water for the bio-photolysis processes and biomass for the fermentation processes. Hydrogen appears

accompanied by oxygen in the photolysis processes and by CO_2 in the fermentative processes [8].

Water can be used as an abundant and inexpensive raw material for hydrogen production, but today less than 4% of hydrogen comes from water splitting, although its relevance is expected to increase in the future. Three main processes can be used: electrolysis, thermolysis or photo-electrolysis. Water electrolysis uses electricity as the required energy input. When the electricity comes from renewable or nuclear sources, the hydrogen produced does not involve the emission of greenhouse gases (GHG) into the atmosphere. Water thermolysis is the decomposition of water into hydrogen and oxygen at very high temperatures (over 2500 °C). In photo-electrolysis, water is decomposed into hydrogen and oxygen when visible light is absorbed with the help of some photo-catalyst [9,10]. Hydrogen can also be produced by mimicking photosynthesis reactions.

Various comprehensive reviews of the techniques for hydrogen production can be found in Refs. [11–13], and [14].

2.2. Transport and storage

Hydrogen, like electricity, is an energy carrier rather than an energy source, but unlike electricity, it is a chemical energy carrier, which gives it important advantages. Hydrogen has a higher energy content per unit of mass than conventional fossil fuels and, when used in fuel cells, higher energy conversion efficiencies. Hydrogen contains 33.33 kWh energy per kg, compared to 12 kWh for petrol and diesel [15]. However, due to its very low density, storing the same amount of energy requires larger volumes. The development of hydrogen storage technologies is fundamental for the generalization of the use of hydrogen as a fuel. For small-scale applications hydrogen can be stored as a compressed gas, at pressures up to 70 MPa, or as a cryogenic liquid, at temperatures below 20 K [16,17]. For large-scale applications, underground storage is a viable solution. A knowledge of the solubility of hydrogen in water is necessary for the optimization of underground storage, as in some cases the stored gas will be in direct contact with water or brine [18]. Solid-state hydrogen storage has obtained increasing attention in recent years, as it is considered a safer hydrogen storage mode. A classification and description of different technologies of hydrogen storage can be found in Refs. [19,20].

Hydrogen can be transported in its pure form, but blending hydrogen into the natural gas pipelines has important benefits for its transport, making use of the widespread natural gas network. Hydrogen-enriched natural gas can be used directly by the consumer, or alternatively, hydrogen can be separated again from the natural gas at the end of the transport line. The use of hydrogen-enriched natural gas will result in lower carbon dioxide emissions, assuming the hydrogen is produced in a low carbon manner [21]. Used as an alternative fuel, natural gas–hydrogen mixtures represent an intermediate step on the path to an ultimate hydrogen economy.

2.3. Use of hydrogen

Hydrogen can be used in its pure form, or it can also be combined with other inputs to produce hydrogen-based fuels for the energy sector, and feedstock for industry. Hydrogen-based fuels include such products as synthetic methane, synthetic liquid fuels and methanol, all of which require carbon as an input, alongside hydrogen. Hydrogen-based feedstock include such products as ammonia, which can be used as a chemical feedstock or potentially as a fuel.

The use of hydrogen in the energy sector may play a key role in achieving ambitious climate targets, but it is also central to industrial development. Hydrogen is one of the limited options for the decarbonization of many industrial sectors, particularly those that require chemical transformations that may not be amenable to other clean energy sources [22].

There are numerous possibilities for integrating the use of hydrogen

into the current power systems: power-to-gas systems as a way to store surplus renewable electricity, stationary fuel cells, vehicular applications, co-generation systems, or even as an alternative fuel for the aviation sector [23]. A review of some examples of the use of hydrogen in different applications can be found in Ref. [19].

3. Existing models for pure hydrogen and hydrogen mixtures

3.1. Equations of state for pure hydrogen

The current reference equation of state (EoS) for hydrogen is the one proposed in 2009 by Leachman et al. [24], which developed three different forms, one for orthohydrogen, one for parahydrogen, and one for normal-hydrogen. This EoS is included in commercial software of industrial and scientific use such as REFPROP [25]. The equation of state is explicit in the Helmholtz free energy, with 14 terms, and is valid for temperatures from the triple point (13.957 K) to 1000 K and for pressures up to 2000 MPa.

Actually, hydrogen is a mixture of two different kinds of molecules, namely ortho- and parahydrogen. The differentiating feature of the two forms is the relative orientation of the nuclear spin of the individual atoms, with orthohydrogen existing at higher energy states with parallel nuclear spins and parahydrogen at lower energy states with anti-parallel nuclear spins. Its equilibrium composition for temperatures higher than 200 K is approximately about 75% ortho- and 25% parahydrogen, which is the so-called normal-hydrogen. At lower temperatures, the concentration of parahydrogen continuously increases, although the conversion of nonequilibrium orthohydrogen into parahydrogen composition to an equilibrium hydrogen mixture is quite slow in the absence of a proper catalyst. In any case, the reference EoS of Leachman et al. [24] consider normal-hydrogen as a pure fluid, since the non-idealities associated with the mixing of orthohydrogen and parahydrogen are negligibly small.

The uncertainty in density for this reference equation of state is 0.1% at temperatures from the triple point to 250 K and at pressures of up to 40 MPa, except in the critical region, where the uncertainty rises to 0.2%. In the region between 250 and 450 K, and at pressures up to 300 MPa, the uncertainty in density is 0.04%. At temperatures between 450 and 1000 K, the uncertainty in density increases up to 1%. At pressures between 300 and 2000 MPa, the uncertainty in density is 8%. The speed of sound data are represented within 0.5% below 100 MPa. The claimed uncertainty for heat capacities is 1.0%. The estimated uncertainties of vapor pressures and saturated liquid densities are 0.2% for each property [24].

These uncertainties are estimated based on the comparison with the available experimental data sets in the literature, which include PVT, vapor pressure and speed of sound data for each kind of hydrogen, despite several experimental gaps: the most noteworthy are density data at temperatures lower than 50 K for normal-hydrogen, and density and speed of sound data at temperatures higher than 100 K for parahydrogen [26]. The data for orthohydrogen are based on a transformation of the para- and normal-hydrogen data using the quantum law of corresponding states. It should be noted, for the case of the claimed uncertainty of 1.0% for heat capacities, that only isochoric and isobaric data for parahydrogen are available, showing deviations between (1–2) %. However, for normal-hydrogen it may be assumed that the uncertainty for the heat capacity will be twice the uncertainty of the speed of sound data at the low pressure limit, which is also around the value of 1% mentioned above.

More questionable is the stated uncertainty of 0.2% of vapor pressures for normal-hydrogen, because the deviations from the literature data are mostly around 1% and even higher, both far from and near the critical point of 33.145 K.

The previous reference equation of state for hydrogen, used as a reference in former versions of NIST's standard properties package REFPROP, was the one proposed in 1982 by Younglove [27]. This equation was based on experimental data for the thermodynamic properties of pure parahydrogen and was modified to predict the thermodynamic properties of normal hydrogen by replacing the ideal-gas heat capacity equation and fixed-point properties of the parahydrogen model with values for normal hydrogen. The range of applicability of the equation of Younglove included pressures up to 121 MPa and temperatures up to 400 K. The model used the International Practical Temperature Scale of 1968. This pressure explicit equation of state for hydrogen was based on the well-known modified Benedict-Webb-Rubin (mBWR) equation of state which uses 32 terms.

Another equation of state for hydrogen, with reference quality, was developed in 2000 by Klimeck [28] for normal hydrogen, specifically designed for the development of the multicomponent GERG equation of state (GERG-2004 [29] and GERG-2008 [30], which is described later). The requirements for this equation were a similar structure to that of the other components and of the mixture, good accuracy, and a reasonable simplicity to achieve low computation times. This equation of state was developed by using multi-property fitting and optimization methods. It has an individually optimized structure with 14 terms. This equation is valid for temperatures of (14–700) K and pressures up to 300 MPa. The uncertainty in density at pressures up to 30 MPa is less than 0.2% over the temperature range (65–270) K and less than 0.1% at temperatures above 270 K. At pressures over 30 MPa, the uncertainty in density is less than (0.2–0.3) %.

All the EoS existing to date for hydrogen have been studied in terms of their uncertainty in the work of Sakoda et al. [31]. Briefly, with respect to density, the EoS of Leachman et al. [24] for parahydrogen agrees within 0.2% with that of Younglove [27] at temperatures below 100 K and pressures up to 45 MPa. Above that, the differences between the two EoS grow quickly by up to 0.9%, with a better agreement with the experimental data of the EoS of Leachman et al. For temperatures above 473 K, the EoS of Younglove [27], Klimeck [28], and Leachman et al. [24] are also in agreement within 0.2% at pressures up to 120 MPa. However, the limited data available do not allow us to know more. Regarding the vapor pressures, the mutual agreement between the EoS of Leachman et al. and Younglove is good and below 0.4% for parahydrogen; on the contrary, the EoS of Klimeck deviates significantly from the EoS of Leachman et al. and from the experimental data for normal hydrogen. The saturated liquid densities calculated from the EoS of Leachman et al., and from that of Younglove, match within 0.3% below the critical point; although the EoS of Leachman et al. yields better estimations of both saturated vapor and liquid densities. According to the speed of sound and heat capacity, the representation of experimental data by the EoS of Leachman et al. is much better than that of Younglove for parahydrogen, especially at temperatures below 100 K and pressures above 100 MPa. This is also true for the EoS of Leachman et al. with respect to the EoS of Klimeck for normal-hydrogen. The maximum deviations for both properties between the three EoS occur at temperatures near 50 K, with differences of up to 5%.

3.2. EoS for hydrogen mixtures

3.2.1. EoS for binary hydrogen mixtures

A model for hydrogen with ammonia binary mixtures was proposed by Neumann et al. [32] in 2020. The model is explicit in the reduced Helmholtz free energy as a function of temperature, density, and composition. The equation of state can be used to calculate all thermodynamic properties over the entire fluid region covering vapor, liquid, phase equilibrium, and supercritical states. Most of the experimental data used for the development of the EoS are reproduced within their experimental uncertainty. The range of validity is linked to the available data for each system; however, reasonable extrapolation behavior was ensured with the use of constraints during the fitting process.

A model for the hydrogen with carbon dioxide binary mixture was proposed by Demetriades and Graham in 2016 [33], developed from

Table 1
Experimental data used for the adjustment of the reducing functions developed for the hydrogen binary systems included in the GERG-2008 model [29,30].

hydrogen + …	Number of experimental $p\rho T$ data points used				Number of experimental VLE data points used			
	Number of points	Temperature range T / K	Pressure range p / MPa	Composition range x_{H2} / mole fraction	Number of points	Temperature range T / K	Pressure range p / MPa	Composition range x_{H2} / mole fraction
… + methane[a]	1427	130 to 600	0.2 to 107	0.05 to 0.91	90	90.3 to 174	1.0 to 27.6	0.00 to 0.35
… + nitrogen	1479	270 to 573	0.1 to 307	0.15 to 0.87	19	77.4 to 113	0.5 to 15.2	0.01 to 0.39
… + carbon dioxide	316	273 to 473	0.2 to 50.7	0.01 to 0.75	68	220 to 298	1.1 to 20.3	0.00 to 0.16
… + ethane	382	275 to 422	0.2 to 26.2	0.10 to 0.80	61	139 to 283	0.7 to 53.3	0.00 to 0.40
… + propane					140	172 to 361	1.4 to 55.2	0.01 to 0.67
… + n-butane					62	328 to 394	2.8 to 16.9	0.02 to 0.27
… + isobutane	No reducing function. Linear combining rule used instead.							
… + n-pentane	No reducing function. Linear combining rule used instead.							
… + isopentane	No reducing function. Linear combining rule used instead.							
… + n-hexane	193	278 to 511	1.4 to 68.9	0.19 to 0.79	98	278 to 478	0.03 to 68.9	0.01 to 0.69
… + n-heptane					27	424 to 499	2.5 to 78.5	0.02 to 0.81
… + n-octane	No reducing function. Linear combining rule used instead.							
… + n-nonane	No reducing function. Linear combining rule used instead.							
… + n-decane					44	323 to 583	1.93 to 25.5	0.02 to 0.50
… + oxygen	No reducing function. Lorentz-Berthelot combining rule used instead.							
… + carbon monoxide	54	298	0.1 to 17.2	0.34 to 0.67	80	68.2 to 122	1.7 to 24.1	0.35 to 0.97
… + water	No reducing function. Lorentz-Berthelot combining rule used instead.							
… + hydrogen sulfide	No reducing function. Lorentz-Berthelot combining rule used instead.							
… + helium	No reducing function. Lorentz-Berthelot combining rule used instead.							
… + argon	No reducing function. Lorentz-Berthelot combining rule used instead.							

[a] The binary system hydrogen + methane is the only one with a binary-specific departure function included in the GERG-2008 model.

experimental data measured by Fandiño et al. [34]. The aim of this pressure explicit model was to improve the understanding of the thermodynamic behavior of carbon dioxide and relevant impurities (nitrogen, oxygen, and hydrogen) during the pipeline transport stage of carbon capture and storage (CCS) processes.

In the same year, Blackham [35] developed a reduced Helmholtz EoS for the thermodynamic properties of cryogenic mixtures composed of hydrogen + helium and hydrogen + neon. The application range for mixtures of hydrogen + helium was with a temperature range from (14–33) K and pressures up to 11 MPa, and for mixtures of hydrogen + neon from (24.6–42.5) K and up to 2.5 MPa. The extrapolation ranges were tested up to 1000 K and 750 MPa for hydrogen + helium, and up to 330 K and 750 MPa for hydrogen + neon.

Cubic EoS (Peng–Robinson, PR, and Soave–Redlich–Kwong, SRK) with quantum corrections for hydrogen, deuterium, helium, neon and their binary mixtures are presented by Aasen et al. [36]. Quantum corrections are needed for quantum fluids such as hydrogen and helium at very low temperatures. The quantum corrections result in a significantly better accuracy, especially for caloric properties.

Aasen et al. [37,38] have also developed a Statistical Associating Fluid Theory for Mie potentials of variable range, corrected for quantum effects, (SAFT-VRQ-Mie) EOS for pure hydrogen, deuterium, helium and neon [37], as well as for their binary mixtures [38].

Four new equations of state for the binary mixtures of hydrogen with methane, nitrogen, carbon dioxide and carbon monoxide have recently been proposed by Beckmüller et al. [39] as part of research to improve the GERG-2008 EoS [30] for the description of hydrogen enriched natural gas mixtures. These EoS are expressed in terms of the reduced Helmholtz energy and have the same mathematical structure and ranges of validity as the GERG-2008, which allows a direct implementation within the existing framework of the GERG-2008 model.

3.2.2. EoS for multicomponent hydrogen mixtures

The GERG-2008 Equation of State (EoS) [30], an expanded version of the previous GERG-2004 [29], is a valid model for multicomponent mixtures of 21 of the most frequent components of natural gas, hydrogen being one of them. The 21 components are classified as *main components* (methane, nitrogen, carbon dioxide and ethane), *secondary alkanes*

(linear alkanes, from propane to n-decane, and branched alkanes, such as isobutane and isopentane) and *other secondary components*. Hydrogen was included in the category of *other secondary components*, together with oxygen, carbon monoxide, water, hydrogen sulfide, helium and argon. The GERG-2008 EoS currently serves as the ISO standard (ISO 20765-2) for the calculation of the thermodynamic properties of natural gases [40].

The GERG-2008 EoS is based on fundamental equations of state for each of the 21 pure substances considered in the model and the correlation equations specifically developed for the 210 possible binary mixtures of the 21 components considered. This structure allows for a description of multicomponent mixtures over a wide range of compositions. Thermal and caloric properties of the most accurate experimental data are represented by the EoS within their accuracy for temperatures from (90–450) K and pressures up to 35 MPa. The range of validity can be extended, but with higher uncertainties, for temperatures from (60–700) K and pressures up to 70 MPa.

The GERG-2008 is a fundamental equation for multicomponent mixtures explicit in the Helmholtz free energy, with density, temperature and composition as independent variables. The development of a model like this for a multicomponent mixture requires [41,42]:

- pure substance equations of state for all the considered components,
- departure functions for each binary function (adjustable from experimental binary data),
- reducing functions for the mixture density and temperature, dependent on the composition (adjustable from experimental binary data, or obtained from combining rules, without any fitting).

Equations of state for hydrogen, carbon monoxide, water and helium were developed specifically for the development of the GERG equation of state. For the rest of the pure constituents, existing equations of state were used [28,43,44]. The range of validity for the new hydrogen EoS [29], developed for this purpose, is (14–700) K at pressures up to 300 MPa. The new equation of state is explicit in the Helmholtz free energy, with 14 terms. At the time of the development of the GERG-2004, there was already a pressure explicit equation for hydrogen [27], based on the modified BWR equation of state with 32 terms. The complex structure of

this equation and its poor performance in the liquid phase and the supercritical region were the reasons for the necessity to develop a new equation of state for hydrogen.

Departure functions were developed from binary experimental data for 15 of the 210 possible binary mixtures. Seven of these departure functions are *binary specific departure functions*, and the other eight are less accurate *generalized departure functions*. For the other 205 binary systems, no departure functions were adjusted from experimental data, due to the lack of accurate and reliable binary data.

The experimental data available for the binary mixture consisting of hydrogen with methane at the time of the development of the GERG-2004 were considered satisfactory and a binary specific departure function was developed. This binary specific departure function consists of only four polynomial terms, when most of the other departure functions have 10 or even 12 terms (polynomial and exponential). The parameters of the reducing functions were also fitted to the experimental data.

For the 19 other binary mixtures with hydrogen, no departure functions were developed, only the reducing functions were obtained. For the binary mixtures of hydrogen with nitrogen, carbon dioxide, ethane, propane, n-butane, n-hexane, n-heptane and carbon monoxide, the parameters of the reducing functions were fitted to the experimental data; while, for the other ten binary systems, linear or Lorentz-Berthelot combining rules were used to obtain the reducing functions (without any fitting to experimental data). Table 1 summarizes the number of experimental data points used for the fitting of these reducing functions.

The basis for the development of the GERG-2008 EoS was the simultaneous fitting of the coefficients of the equations (departure functions and reducing functions) to experimental data for several thermodynamic properties of binary mixtures (density, speed of sound, isobaric and isochoric heat capacities, enthalpy differences, saturated liquid densities, and VLE data), following the so-called multi-property fitting. The quality and extent of these data determine the accuracy of the model. Approximately 53 000 binary data were used for the development of the GERG-2008, and another 42 000 were used to check the resulting model. For the hydrogen binary mixtures, only 3851 density data and 689 VLE data were used. No speed of sound or other thermodynamic properties were used.

Hassanpouryouzband et al. [5] used the GERG-2008 EoS to predict the thermo-physical properties of H_2 mixed with a typical natural gas from the North Sea and for binary mixtures of hydrogen with selected components of natural gas (CH_4, N_2, CO_2). The predictions are performed over wide ranges of the mole fraction of H_2 (10–90 mol %), pressures (0.01–100 MPa), and temperatures (200–500 K). The results are available through a free-access software called H2Themobank [5].

The AGA8-DC92 [45] is another EoS that enables the calculation of thermodynamic properties of multicomponent mixtures of up to 21 components of natural gas, hydrogen among them. This equation is applicable only to the gas phase and has several limitations compared to the GERG-2008 [30].

Demetriades and Graham [33] have proposed a general framework for deriving pressure-explicit EoS for impure CO_2. This framework generalizes a previous EoS for pure CO_2 [46] to binary mixtures with N_2, O_2 and H_2. This model is valid for pressures up to 16 MPa and temperatures between 273 K and the critical temperature of pure CO_2. In this region, the model achieves close agreement with experimental data. When compared to the GERG EoS, the authors state that this model has a comparable level of agreement with (CO_2 + N_2) VLE experiments and superior agreement with the (CO_2 + O_2) and (CO_2 + H_2) VLE data.

Other simpler EoS, such as the Peng-Robinson EoS or other pressure-explicit cubic EoS, are often used in industrial applications to describe multicomponent hydrogen mixtures. The accuracy obtained with these simpler EoS are not comparable to the more complex models described before within the range for which the latter have been designed.

Binary, ternary and quaternary mixtures of hydrogen, water, and the three main components of air, nitrogen, oxygen and argon, have been
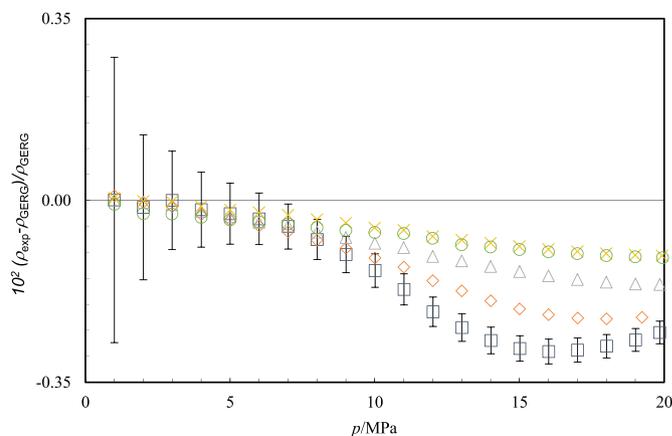
Fig. 1. Relative deviations in density of experimental (p, ρ, T) data of a 3% H_2-enriched natural gas mixture, ρexp, from density values calculated from the GERG-2008 EoS, $\rho GERG$, versus pressure p: □, T = 260 K; ◇, T = 275 K; △, T = 300 K; ×, T = 325 K; ○, T = 350 K. From Hernández-Gómez et el. [48]. Error bars on the 260-K isotherm indicate the expanded uncertainty (k = 2) of the experimental density data. The claimed uncertainty of the GERG-2008 EoS for this composition is 0.1%.

studied using molecular modeling through the Monte Carlo approach and simulation, the PC-SAFT equation of state, and sophisticated empirical equations of state by Köster et al. [47]. For that study, a new force field for hydrogen was developed. The results obtained for the thermodynamic properties, including the phase behavior, were compared to experimental data with excellent agreement in many cases.

3.3. Analysis of existing models for binary and multicomponent hydrogen mixtures

Even when it is stated that the GERG-2008 model is valid for hydrogen-enriched natural gas mixtures, with the same level of accuracy in the main ranges of temperature and pressure, the model was initially developed to characterize conventional natural gas mixtures, which usually only contain hydrogen in very small amounts, if any. Some papers [48,49] have evaluated the performance of the GERG and AGA equations of state when dealing with hydrogen-enriched natural gas samples. The results presented in Ref. [49] for hydrogen-enriched natural gas mixtures, with up to 30% of hydrogen, suggest that both equations of state are suitable for hydrogen-enriched natural-gas mixtures in the investigated temperature and pressure ranges. However, the results presented in Ref. [48] for a hydrogen enriched natural gas mixture gravimetrically prepared, with only 3% of hydrogen, show that even when the GERG-2008 EoS displays a better performance than AGA8-DC92 when applied to natural gas-type mixtures without hydrogen, it presents higher deviations for the hydrogen-enriched natural gas mixtures, even for such a low hydrogen concentration as 3%, mainly at low temperatures and high pressures. Deviations of experimental density data for that 3% hydrogen-enriched natural gas mixture from the GERG-2008 EoS can be seen in Fig. 1.

A problematic aspect of the GERG-2008 EoS has recently been reported in the research of Deiters et al. [50]. When the GERG-2008 model is applied to high asymmetric mixtures, i.e., mixtures of components with a high difference between their critical points, it leads to unexpected shapes of the phase envelope. This is the case for many of the mixtures containing hydrogen, and it is revealed as erroneously predicted open phase envelopes, which means unphysical regions of liquid-liquid equilibrium (LLE) phase separation, as depicted in Fig. S1. The problem becomes more evident at lower temperatures and correspondingly higher pressures, predicting an unreasonable maximum in the critical line with the temperature in the worst case scenario. Deiters et al. [50] studied the source of this distortion of the phase envelope

shape in the multiparametric GERG models, and concluded that the origin was in the use of empirically corrected critical exponents in the terms applied to the pure-fluid EoS to ensure the accurate prediction of the properties of the pure fluid in the vicinity of the critical point. These non-classical terms do not have to be the same for the mixture model as for the pure fluids, and considering them may have a negative side effect, as described above. Thus, they proposed building the mixture models using classical critical exponents in the pure fluid EoS and introducing the corrected exponents in the final stage of the fitting procedure of the mixture model.

In the work of Beckmüller et al. [39], the known open-phase issues of the GERG-2008 were solved for the systems $H_2 + CH_4$ at temperatures below 120 K, $H_2 + N_2$ at temperatures below 100 K, $H_2 + CO$ at temperatures below 80 K, and $H_2 + CO_2$ at temperatures below 260 K. The solution was to: (i) replace the Klimeck [28] EoS of pure hydrogen used in the GERG-2008 model with the current reference EoS of Leachman et al. [24], and (ii) reparametrize the departure function of $H_2 + CH_4$, as well as to build three new specific departures equations for $H_2 + N_2$, $H_2 + CO$ and $H_2 + CO_2$, respectively, based on more data sets of accurate VLE and density values than those used in the original model, now covering the whole pressure and temperature ranges where this problem occurred.

The works of Köster et al. [47] and Alkhatib et al. [51] tackle the performance of the widely used cubic EoS and the statistical associating fluid theory (SAFT) EoS as compared to GERG-2008 EoS. In these two studies, the assessment of the cubic and SAFT EoS compared to the GERG-2008 EoS is made without applying the improvements made to the GERG EoS by Beckmüller et al. [39], considering new binary functions for the mixtures of H_2 with CH_4, N_2, CO and CO_2.

The research of Köster et al. [47] deals with all the subsystems containing H_2, N_2, O_2, Ar, and H_2O. The version of the cubic EoS chosen was Peng-Robinson (PR) [52,53], with the alpha function of Twu et al. [54], the quadratic van der Waals one-fluid mixing rules and no volume translation. The version of the SAFT EoS used was the perturbed chain PC-SAFT [55–57], with the Lorentz-Berthelot mixing rule exclusively for the energy parameter, modeling H_2 as a spherical molecule. Pure fluid parameters were taken from the literature, and only one binary temperature-independent interaction parameter was fitted to the vapor pressure data for the PR and PC-SAFT EoS.

Focusing on hydrogen binary systems and regarding the numerous VLE data compared, PR agrees better than the other EoS with the experimental data of both the liquid and vapor saturation lines for the $H_2 + N_2$ system, and with the liquid saturation line for $H_2 + Ar$. On the contrary, PC-SAFT overestimates the critical point and the pressures of the liquid saturation line for both $H_2 + N_2$ and $H_2 + Ar$ systems, and also shows large discrepancies in the vapor saturation line for $H_2 + Ar$. GERG-2008 yields a nonphysical open phase envelope for both $H_2 + N_2$ and $H_2 + Ar$. This issue for the $H_2 + N_2$ system was subsequently corrected in the work of Beckmüller et al. [39], but remains for the mixtures of $H_2 + Ar$. All the EoS perform well for the vapor saturation line of $H_2 + H_2O$, with PC-SAFT deviating less than PR in the liquid saturation line and GERG-2008 yielding a nonreal open phase envelope again, as yet unsolved.

Density was evaluated against several equimolar mixtures, where unlike molecular interactions are more significant. For $H_2 + N_2$, PR, SAFT and GERG-2008 EoS perform well for temperatures below $T = 273$ K, but show increasing deviations at high pressures and densities, overestimating the density at $T = (323$ up to $373)$ K. Concerning the $H_2 + Ar$ system, PC-SAFT and GERG-2008 yield low discrepancies, but PR behaves the worst. In addition, PR fails to reproduce the saturated liquid density as expected from a cubic EoS. The results reveal that neither the PR nor the PC-SAFT EoS were able to qualitatively predict the very low experimental values of hydrogen solubility in water and, hence, of the Henry's law constant. Not enough VLE data for $H_2 + O_2$, density data for $H_2 + O_2$, or $H_2 + H_2O$ were available for comparison.

Furthermore, Köster et al. [47] used molecular simulation through the Monte Carlo method and non-polarizable force fields taken from literature for Ar, N_2, and O_2, with two different force fields for H_2, a new one developed for H_2 in their work and another from the literature. Overall, the Monte Carlo simulation is seen to be the more versatile and accurate of all the models analyzed for these systems.

Alkhatib et al. [51] also used the PR EoS with the same alpha function of Twu et al. [54], van der Waals mixing rules, and no volume translation, as in Köster et al. [47]. However, they shifted to the polar Soft-SAFT EoS [58,59], again with the Lorentz-Berthelot mixing rule solely for the energy parameter, modeling H_2 as a non-spherical molecule in this case. They studied the binary mixtures of H_2 with CH_4, C_2H_6, C_3H_8, N_2, and CO_2 in terms of VLE, density and some calorific properties, such as isobaric heat capacity, speed of sound and Joule-Thomson coefficient, selecting only one representative data source for each property and system.

PR and polar Soft-SAFT are the only models reproducing the entire phase envelopes for all the binary systems studied containing hydrogen, with a higher accuracy from polar Soft-SAFT, although both models overestimate the critical points. For the PR EoS, the deviations systematically increase as the temperature is reduced away from the temperature of the data used in fitting the binary parameter; while, for the polar Soft-SAFT EoS, this is less notorious. Thus, the predictive behavior of the polar Sof-SAFT is better than PR. They found that the GERG-2008 was the least accurate, mainly due to the prediction of open phase envelopes with decreasing temperatures and increasing pressure for most of these mixtures. These unexpected shapes of the phase boundary were announced in the work of Deiters et al. [50] and corrected in the work of Beckmüller et al. [39], reparametrizing the GERG-2008 with a wider range and more accurate experimental database than the original one used for the binary mixtures of $H_2 + CH_4$, $H_2 + N_2$, and $H_2 + CO_2$. Surprisingly, Alkhatib et al. [51] also report an open phase envelope in the case of $H_2 + CO_2$, not seen in the research of Köster et al. [47], even when also dealing with this system at similar temperatures around 80 K.

Regarding the system $H_2 + CH_4$, PR, polar Soft-SAFT and GERG-2008 all reproduce the density and isobaric heat capacity experimental data with similar deviations. These deviations are constant with the hydrogen content for the density but tend to increase rapidly with the hydrogen molar fraction for the heat capacity. Moreover, the GERG-2008 model clearly outperforms the others in estimating the speed of sound data, while the polar Soft-SAFT model has smaller deviations with respect to the Joule-Thomson coefficients (JT). Similar qualitative discrepancies are found for the other systems: $H_2 + C_2H_6$, $H_2 + C_3H_8$, $H_2 + N_2$, and $H_2 + CO_2$, with similar agreement for density and speed of sound of all the models, while polar Soft-SAFT again deviates less for the second-order derivative properties, such as the JT coefficient.

In addition, Alkhatib et al. [51] also computed viscosity values through the Chapman-Enskog theory for the dilute gas contribution and the residual part from either PR + friction theory, or polar Soft-SAFT + free volume theory, or GERG-2008 + extended corresponding states.

The inclusion of quantum corrections in the alpha function of the cubic EoS and in the framework of the SAFT EoS, as well as temperature dependent binary interaction parameters, is suggested to enhance the accuracy of both models, specially at low temperatures, with the disadvantage of losing simplicity and predictive capabilities, while also requiring a much larger experimental database for reparameterization.

Although, cubic EoS with classical expressions accurately reproduce the VLE data, they clearly fail to reproduce the interaction second virial coefficients and densities of the mixtures in most ultra-cryogenic states. This stems mainly from the poor description of these properties for the pure components at low temperatures. Aasen et al. deal with this issue in a subsequent work [36], adding temperature dependent quantum corrections in the covolume parameter for both PR and SRK EoS. This results in an overall improvement of the predictive capabilities of these models, highlighting the reduction of the error representing the isochoric heat capacity of liquid hydrogen at saturation from 80% to less than 4%.

Table 2
Available experimental data on vapor-liquid equilibrium (VLE) for binary H_2 mixtures.

Source	Year	Rank	Experimental technique	Mixture	x_{H_2} / y_{H_2}	T/K	p/MPa	Uncertainty ($k = 2$)
Benham et al. [118]	1957	1	Vapor-Recirculating VLE Cell - Mass Spectrometry	$CH_4 + H_2/CH_4 + C_3H_8 + H_2/CH_4 + C_3H_6 + H_2^b$	0–0.35/0–0.99	116–255	3.4–27.6	$10^6 \cdot U(x,y) =$ (3499–9990) mol mol^{-1}; $U(T) = $ (200–2000) mK; $U(p) = 68950$ Pa
Cosway et al. [119]	1959	1	Vapor-Recirculating VLE Cell - Mass Spectrometry	$CH_4 + C_2H_6 + H_2/CH_4 + N_2 + H_2/CH_4 + C_2H_6 + N_2 + H_2^b$	0–0.12/0–0.99	144–200	3.4–6.9	$10^6 \cdot U(x,y) =$ (1157–9974) mol mol^{-1}; $U(T) = $ (200–2000) mK; $U(p) = 68950$ Pa
Freeth et al. [120]	1931	1	Compression Vessel with a Volumenometer and Piezometer	$CH_4 + H_2^b$	0.004–0.10/ 0.97–0.99	90.6	1.7–20.8	$10^6 \cdot U(x,y) =$ (38–9905) mol mol^{-1}; $U(T) = 100$ mK; $U(p) = $ (1700–20800) Pa
Hong et al. [63]	1981	1	Cryogenic VLE Cell – Gas Chromatography	$CH_4 + H_2^b$	0.006–0.49/ 0.034–0.97	108–183	0.07–28.4	$10^6 \cdot U(x,y) = 3300$ mol mol^{-1}; $U(T) = 20$ mK; $U(p) \leq 57000$ Pa
Hu et al. [121]	2014	1	Static Analytic VLE Cell - Gas Chromatography	$CH_4 + H_2/CH_4 + N_2 + H_2^b$	0.002–0.04/ 0.53–0.98	100–120	0.2–4.4	$10^6 \cdot U(x,y) = 400$ mol mol^{-1}; $U(T) = 200$ mK; $U(p) = 5000$ Pa
Sagara et al. [122]	1972	1	Static Analytic VLE Cell - Gas Chromatography	$CH_4 + H_2/C_2H_6 + H_2/CH_4 + C_2H_4 + H_2/C_2H_6 + C_2H_4 + H_2^b$	0.003–0.23/ 0.03–0.99	103–248	1.0–10.8	$10^6 \cdot U(x,y) = 9950$ mol mol^{-1}; $U(T) = 200$ mK; $U(p) = 10132.5$ Pa
Tsang et al. [62]	1980	1	Vapor-Recirculating VLE Cell (Phase Envelope)	$CH_4 + H_2^b$	0.002–0.61/ 0.16–0.99	92.3–180	0.2–138	$10^6 \cdot U(x,y) = 5000$ mol mol^{-1}; $U(T) = 40$ mK; $U(p) = $ (2200–1400000) Pa
Yorizane et al. [123]	1980	1	Vapor-Recirculating VLE Cell (Phase Envelope) – Gas Chromatography	$CH_4 + H_2/N_2 + H_2/CO + H_2/CH_4 + N_2 + H_2/CH_4 + CO + H_2/N_2 + CO + H_2^b$	0.05–0.53/ 0.63–0.99	93.1–103	10.1–15.2	$10^6 \cdot U(x,y) =$ (920–19730) mol mol^{-1}; $U(T) = 200$ mK; $U(p) = 202650$ Pa
Akers et al. [124]	1960	2	Vapor-Recirculating VLE Cell – Thermal Conductivity Analysis - Gas Chromatography	$N_2 + H_2/CO + H_2/N_2 + CO + H_2^b$	0.03–0.34/ 0.08–0.93	83–122	2.2–13.8	$10^6 \cdot U(x,y) =$ (104–3728) mol mol^{-1}; $U(T) = 200$ mK; $U(p) = 68947.6$ Pa
Kremer et al. [125]	1983	1	High-pressure Low-temperature VLE Cell with View Section – Gas Chromatography	$CH_4 + N_2 + H_2/CH_4 + CO + H_2^b$	0.0–0.29/0.0–0.96	80–144	2.9–10.0	$10^6 \cdot U(x,y) =$ (5800–19000) mol mol^{-1}; $U(T) = 100$ mK; $U(p) = $ (17000–60000) Pa
Maimoni [126]	1961	1	Vapor-Recirculating VLE Cell with Mercury Variable-Volume – Optical Interferometer	$N_2 + H_2^b$	0.01–0.11/ 0.38–0.83	90–95	0.6–4.59	$U(x,y) = $ N.A.; $U(T) = $ N.A.; $U(p) = $ N.A.
Omar et al. [127]	1962	2	Flow Method - Vapor-Recirculating VLE Cell (Vapor Phase)	$N_2 + H_2^b$	0.88–0.99	63–75	0.02–0.243	$U(y) = $ N.A.; $U(T) = $ N.A.; $U(p) = 10132.5$ Pa
Streett et al. [65]	1978	1	Vapor-Recirculating VLE Cell – Thermal Conductivity Gas Analysis (Phase Envelope)	$N_2 + H_2^b$	0.002–0.54/ 0.25–0.97	63.2–110	1.0–57.2	$10^6 \cdot U(x,y) = 1000$ mol mol^{-1}; $U(T) = 40$ mK; $U(p) = $ N.A.
Verschoyle [82]	1931	1	Compression Vessel with a Volumenometer and Piezometer	$N_2 + H_2/CO + H_2/N_2 + CO + H_2^b$	0–0.55/0–0.99	63–88	0.01–22.8	$10^6 \cdot U(x,y) =$ (5490–9870) mol mol^{-1}; $U(T) = 200$ mK; $U(p) = 10132.5$ Pa
Yorizane et al. [128]	1971	1	Vapor-Recirculating VLE Cell (Phase Envelope) – Gas Chromatography	$N_2 + H_2^b$	0.05–0.47/ 0.62–0.94	77–88	1.7–19.0	$10^6 \cdot U(x,y) =$ (980–18840) mol mol^{-1}; $U(T) = 200$ mK; $U(p) = 202650$ Pa
Bezanehtak et al. [129]	2002	1	Analytical VLE Cell – Gas Chromatography (Phase Envelope)	$CO_2 + H_2$	0.009–0.16/ 0.04–0.51	278–298	4.8–19.3	$U(x,y) = $ N.A.; $U(T) = $ N.A.; $U(p) = $ N.A.

(continued on next page)

Table 2 (*continued*)

Source	Year	Rank	Experimental technique	Mixture	x_{H_2} / y_{H_2}	T/K	p/MPa	Uncertainty ($k = 2$)
Fandiño et al. [34]	2015	1	Static Analytical VLE Cell – Gas Chromatography (Phase Envelope)	CO_2 + H_2	0–0.18/0–0.93	218–303	0.6–15.4	$10^6 \cdot U(x,y) =$ (100–4300) mol mol^{-1}; $U(T) = 10$ mK; $U(p) = 6000$ Pa
Kaminishi et al. [130]	1966	2	N.A. (Phase Envelope)	CO_2 + H_2	0.01–0.18/ 0.04–0.88	233–298	5.1–20.0	$U(x) = $ N.A.; $U(T) = $ N.A.; $U(p) = $ N.A.
Ke et al. [131]^f	2017	2	Synthetic VLE Cell – Optic Fiber Sensor (Phase Envelope)	CO_2 + Ar + H_2	0.03	268–301	3.3–9.1	$10^6 \cdot U(x,y) = 180$ mol mol^{-1}; $U(T) = 100$ mK; $U(p) = 50000$ Pa
Ke et al. [132]^f	2014	2	Synthetic VLE Cell – Optic Fiber Sensor (Phase Envelope)	CO_2 + H_2	0.05	273–293	3.5–10.5	$10^6 \cdot U(x,y) = 250$ mol mol^{-1}; $U(T) = 100$ mK; $U(p) = 50000$ Pa
Ke et al. [133]^f	2005	2	Synthetic VLE Cell - Shear Mode Piezoelectric Sensor (Phase Envelope)	CO_2 + H_2	0.09	293–312	8.5–13.5	$10^6 \cdot U(x,y) = 910$ mol mol^{-1}; $U(T) = 500$ mK; $U(p) = $ N.A.
Spano et al. [134]	1968	1	Vapor-Recirculating VLE Cell (Phase Envelope) – Gas Chromatography	CO_2 + H_2	0.001–0.14/ 0.11–0.93	220–290	1.1–20.3	$10^6 \cdot U(x,y) =$ (35–46675) mol mol^{-1}; $U(T) = 200$ mK; $U(p) = 30397.5$ Pa
Tenorio et al. [135]	2015	1	Synthetic VLE Cell – Optic Fiber Sensor (Phase Envelope)	CO_2 + H_2/CO_2 + N_2 + H_2	0.03–0.05/ 0.03–0.05	253–303	2.0–10.6	$10^6 \cdot U(x,y) = 200$ mol mol^{-1}; $U(T) = 100$ mK; $U(p) = 50000$ Pa
Tsang et al. [70]	1981	1	Vapor-Recirculating VLE Cell (Phase Envelope)	CO_2 + H_2	0.001–0.56/ 0.16–0.93	220–290	0.9–171	$10^6 \cdot U(x,y) = 5000$ mol mol^{-1}; $U(T) = 40$ mK; $U(p) =$ (9300–1700000) Pa
Tsankova et al. [136]	2019	1	Microwave Re-entrant Resonance Cavity (Dew Points)	CO_2 + H_2	0.05–0.25	250–297	1.9–7.1	$10^6 \cdot U(y) = 700$ mol mol^{-1}; $U(T) = 81$ mK; $U(p) = 21800$ Pa
Yorizane et al. [137]	1970	1	Vapor-Recirculating VLE Cell (Phase Envelope) – Gas Chromatography	CO_2 + H_2	0.05–0.47/ 0.28–0.65	273.15	6.1–37.5	$10^6 \cdot U(x,y) =$ (940–13020) mol mol^{-1}; $U(T) = 200$ mK; $U(p) = 202650$ Pa
Heintz et al. [138]	1982	1	Vapor-Recirculating High-Pressure VLE Cell (Phase Envelope)	C_2H_6 + H_2^b	0.007–0.75/ 0.20–1.0	92.5–280	3.2–559	$10^6 \cdot U(x,y) \leq 20000$ mol mol^{-1}; $U(T) = 40$ mK; $U(p) =$ (31800–5595000) Pa
Hiza et al. [75]	1968	1	Vapor-Recirculating VLE Cell (Phase Envelope) – Gas Chromatography	C_2H_6 + H_2^b	0.007–0.077/ 0.93–0.99	108–190	0.5–15.6	$10^6 \cdot U(x,y) =$ (134–19999) mol mol^{-1}; $U(T) = 40$ mK; $U(p) = $ N.A.
Williams et al. [139]	1954	1	Vapor-Recirculating VLE Cell (Phase Envelope) – Infrared Spectrometry	C_2H_6 + H_2/C_2H_4 + H_2/C_3H_8 + H_2/C_3H_6 + H_2/C_2H_6 + C_2H_4 + H_2/C_2H_4 + C_3H_6 + H_2/C_3H_8 + C_3H_6 + H_2^b	N.A./N.A.	88.7–297	1.7–55.2	$10^6 \cdot U(x,y) \geq 150$ mol mol^{-1}; $U(T) =$ (100–1000) mK; $U(p) =$ (8619–275791) Pa
Burriss et al. [76]	1953	1	Static VLE Cell with Mercury Variable-Volume (Phase Envelope) – Gas gravimetry	C_3H_8 + H_2	0.01–0.57/ 0.13–0.94	278–361	2.5–52.8	$U(x,y) = $ N.A.; $U(T) = 40$ mK; $U(p) = 2757.9$ Pa
Trust et al. [140]	1971	1	Static Analytical VLE Cell (Phase Envelope) – Gas Chromatography	C_3H_8 + H_2/CO + C_3H_8 + H_2^b	0.002–0.35/ 0.03–0.99	88.1–348	1.0–20.7	$U(x,y) = $ N.A.; $U(T) = 100$ mK; $U(p) = 41368.5$ Pa
Aroyan et al. [79]	1951	1	Flow Method - Vapor-Recirculating VLE Cell (Phase Envelope) – Gas gravimetry	n-C_4H_{10} + H_2^b	0.008–0.34/ 0.87–1.0	144–297	2.1–54.1	$10^6 \cdot U(x,y) =$ (2000–5000) mol mol^{-1}; $U(T) = 500$ mK; $U(p) = 137895$ Pa
Klink et al. [141]	1975	1	Static Analytical VLE Cell with Mercury Variable-Volume – Gas Chromatography	n-C_4H_{10} + H_2	0.02–0.27/ 0.21–0.93	328–394	2.8–16.9	$10^6 \cdot U(x,y) = 80000$ mol mol^{-1}; $U(T) = 100$ mK; $U(p) = 10132.5$ Pa
Nelson et al. [142]	1943	2	High Pressure Bomb – Oxidation Analyses	n-C_4H_{10} + H_2	0.020–0.11/ 0.42–0.83	297–389	2.2–10.7	$10^6 \cdot U(x,y) = $ N.A.; $U(T) = $ N.A.;

Table 2 (*continued*)

Source	Year	Rank	Experimental technique	Mixture	x_{H_2} / y_{H_2}	T/K	p/MPa	Uncertainty ($k = 2$)
Dean et al. [80]	1946	2	Static Analytical VLE Cell with Mercury Variable-Volume – Distillation columns + Calibrated balloons	i-C_4H_{10} + H_2	0.02–0.25/ 0.25–0.96	311–394	3.4–20.7	$U(p)$ = N.A. $10^6 \cdot U(x,y)$ = N.A; $U(T)$ = N.A.; $U(p)$ = N.A.
Connolly et al. [143]	1986	2	Mercury Glass Capillary (Solubility)	n-C_5H_{12} + H_2	0.03–0.12	308–463	2.9–14.1	$U(x,y)$ = N.A.; $U(T)$ = N.A.; $U(p)$ = N.A.
Freitag et al. [144]	1986	1	VLE Cell with View Section – Gas Chromatography	CH_4 + CO_2 + H_2/n-C_5H_{12} + CO_2 + H_2/n-C_5H_{12} + H_2	0.0–0.27/0.0–0.99	227–373	0.3–27.6	$10^6 \cdot U(x,y) \leq$ (30000–110000) mol mol^{-1}; $U(T)$ = 250 mK; $U(p)$ = (2100–170000) Pa
Brunner et al. [145]	1985	1	Static VLE Cell with Stripping + VLE Cell with View Section (Solubility)	n-C_6H_{14} + H_2	0–0.09	298–373	0.02–9.8	$10^6 \cdot U(x)$ = 3800 mol mol^{-1}; $U(T)$ = 200 mK; $U(p) \leq$ 39000 Pa
Fu et al. [146]	1994	2	Cocurrent-Flow Type - VLE Packed Columns - Gas Chromatography	n-C_6H_{14} + H_2/n-C_6H_{14} + DCPD + H_2	0.02–0.05/ 0.91–0.99	311–378/ 313–363	3.4/2.1–5.5	$U(x,y)$ = N.A.; $U(T)$ = 400 mK; $U(p)$ = 6000 Pa
Gao et al. [147]	2001	2	Static VLE Cell with Mercury Variable-Volume (Bubble Points)	n-C_6H_{14} + H_2	0.01–0.14	344–410	1.2–15.1	$10^6 \cdot U(x)$ = 2000 mol mol^{-1}; $U(T)$ = 200 mK; $U(p)$ = (40000–400000) Pa
Katayama et al. [148]	1976	2	Static VLE Cell with Mercury Variable-Volume (Solubility)	n-C_6H_{14} + H_2	N.A.	213–298	Atmospheric	$U(x,y)$ = N.A.; $U(T)$ = N.A.; $U(p)$ = N.A.
Nichols et al. [81]	1957	1	Static Analytical VLE Cell with Mercury Variable-Volume – Weighing bombs + Calibrated balloons	n-C_6H_{14} + H_2	0.03–0.77/ 0.31–0.99	278–478	3.4–68.9	$10^6 \cdot U(x,y)$ = 4000 mol mol^{-1}; $U(T)$ = 40 mK; $U(p)$ = 2757.9 Pa
Tsang et al. [83]	1981	1	Vapor-Recirculating VLE Cell (Phase Envelope)	CO + H_2^b	0.008–0.56/ 0.11–0.99	70–125	0.5–52.9	$10^6 \cdot U(x,y)$ = 5000 mol mol^{-1}; $U(T)$ = 40 mK; $U(p)$ = 530000 Pa
Kling et al. [87]	1991	2	Static High-Pressure VLE Cell of Variable Volume (Solubility)	H_2O + H_2	0.0004–0.0022	323–423	3.2–15.4	$U(x)$ = N.A.; $U(T)$ = 40 mK; $U(p)$ = N.A.
Purwanto et al. [149]	1996	2	Stirred Autoclave (Solubility)	H_2O + H_2	N.A.	298–323	0.1	$U(x)$ = N.A.; $U(T)$ = 2000 mK; $U(p)$ = 2000 Pa
Setthanan et al. [86]	2006	1	Ambient Pressure Saturator + Gas Extraction System (Standard ASTM D2780-92) - (Solubility)	H_2O + H_2	(1.3–1.4)·10^{-5}	298–353	Standard Atmospheric Pressure	$10^6 \cdot U(x)$ = 0.81 mol mol^{-1}; $U(T)$ = N.A.; $U(p)$ = N.A.
Shoor et al. [89]	1969	2	VLE Cell - Gas Chromatography	H_2O + H_2	(1.3–1.4)·10^{-5}	298–353	0.1	$U(x,y)$ = N.A.; $U(T)$ = N.A.; $U(p)$ = N.A.
Symons [150]	1971	2	Gas Stripping VLE Cell – Gas Chromatography (Solubility)	H_2O + H_2	0.000015	298.15	0.1	$10^6 \cdot U(x,y)$ = 0.580 mol mol^{-1}; $U(T)$ = N.A.; $U(p)$ = N.A.
Wiebe et al. [88]	1934	1	High-Pressure VLE Cell - Volumetric Determination	H_2O + H_2	0.00033–0.014	273–373	2.5–101.3	$10^6 \cdot U(x,y)$ = (3.3–140) mol mol^{-1}; $U(T)$ = N.A.; $U(p)$ = N.A.
Yorizane et al. [90]	1969	1	Vapor-Recirculating VLE Cell (Phase Envelope) – Gas Chromatography	H_2S + H_2	0.002–0.020/ 0.32–0.99	243–273	1.0–5.1	$10^6 \cdot U(x,y)$ = (40–19800) mol mol^{-1}; $U(T)$ = 200 mK; $U(p)$ = 202650 Pa
Hiza [92]	1972	2	Vapor-Recirculating VLE Cell – Gas Chromatography	He (4) + H_2/He (3) + H_2^c	0.94–0.99	20–28	0.09–2.1	$U(x)$ = N.A.; $U(T)$ = 2000 mK; $U(p)$ = 2000 Pa
Hiza [93]	1981	2	Vapor-Recirculating VLE Cell – Gas Chromatography	He (4) + H_2/He (3) + H_2^c	0.95–0.99/ 0.10–0.76	20–28	0.6–2.1	$U(x)$ = N.A.; $U(T)$ = 2000 mK; $U(p)$ = 2000 Pa
Sneed et al. [94]	1968	1	Vapor-Recirculating VLE Cell - Mass Spectrometry	He + H_2^c	0.64–0.99/ 0.03–0.70	15.5–30	2.0–10.4	$10^6 \cdot U(x,y)$ = (250–9910) mol mol^{-1}; $U(T)$ = 20 mK; $U(p)$ = 10342.1 Pa
Sonntag et al. [96]	1964	1	Vapor-Recirculating VLE Cell - Mass Spectrometry	He + H_2^d	0.82–0.99/ 0.03–0.94	20.4–31	0.2–3.5	$U(x,y)$ = N.A.; $U(T)$ = 40 mK;

Table 2 (*continued*)

Source	Year	Rank	Experimental technique	Mixture	x_{H_2} / y_{H_2}	T/K	p/MPa	Uncertainty (k = 2)
Streett et al. [95]	1964	2	Vapor-Recirculating VLE Cell - Mass Spectrometry	He + H$_2^c$	0.79–0.99/ 0.03–0.97	15.5–32	0.2–3.4	$U(p) = 6894.8$ Pa $U(x,y) = $ N.A.; $U(T) = 40$ mK; $U(p) = 6894.8$ Pa
Yamanishi et al. [91]	1992	1	Cryogenic VLE Cell – Gas Chromatography	He + H$_2^c$	0.9982–0.9997/ 0.37–0.72	15.8–20	0.06–0.16	$10^6 \cdot U(x,y) = 180$ mol mol^{-1}; $U(T) = 200$ mK; $U(p) = 130$ Pa
Calado et al. [97]	1979	1	Vapor-Recirculating VLE Cell - Thermal Conductivity Gas Analysis (Phase Envelope)	Ar + H$_2^b$	0–0.62/0–0.98	83.1–141	0.08–51.8	$10^6 \cdot U(x,y) = 5000$ mol mol^{-1}; $U(T) = 40$ mK; $U(p) = 100000$ Pa
Volk et al. [98]	1960	1	Static VLE Autoclave – Volumetric Determination (Solubility)	Ar + H$_2^b$	0.02–0.13	87–140	1.7–10.2	$10^6 \cdot U(x) = (378–2598)$ mol·mol^{-1}; $U(T) = 100$ mK; $U(p) = 5066.25$ Pa
Heck et al. [100]	1966	1	Vapor-Recirculating VLE Cell - Gas Chromatography (Phase Envelope)	Ne + H$_2^c$	0.014–0.96/ 0.031–0.94	26–42.5	0.21–2.5	$10^6 \cdot U(x,y) = (560–38000)$ mol mol^{-1}; $U(T) = 100$ mK; $U(p) = (1000–10000)$ Pa
Streett et al. [99]	1965	1	Vapor-Recirculating VLE Cell – Thermal Conductivity Gas Analysis (Phase envelope)	Ne + H$_2^c$	0.0083–0.99/ 0.19–0.99	24.6–33.7	0.17–1.4	$10^6 \cdot U(x,y) = (17–2000)$ mol mol^{-1}; $U(T) = 20$ mK; $U(p) = (350–29000)$ Pa
Zelfde et al. [101]	1974	2	Variable Volume Calorimeter – Synthetic Mixtures (Vapor Pressure)	Ne + H$_2^b$	0.0010–0.0087	20.4–26.6	0.014–0.11	$U(x,y) = $ N.A.; $U(T) = $ N.A.; $U(p) = $ N.A.
Moore et al. [151]	1972	2	Static Analytical VLE Cell – Distillation columns + Weighing + Calibrated balloons + (Solubility)	NH$_3$ + H$_2$	0.000012–0.000096	203–303	0.1	$U(x) = $ N.A.; $U(T) = $ N.A.; $U(p) = $ N.A.
Reamer et al. [112]	1959	1	Static VLE Cell with Mercury Variable-Volume (Phase Envelope) – Gas gravimetry	NH$_3$ + H$_2$	0.0021–0.15/ 0.053–0.97	278–394	1.5–4.2	$10^6 \cdot U(x,y) = 4000$ mol mol^{-1}; $U(T) = 40$ mK; $U(p) = (900–2500)$ Pa
Wiebe et al. [110]	1934	1	Static Analytical VLE Cell – Distillation columns + Weighing + Calibrated balloons + (Solubility)	NH$_3$ + H$_2$	0.0034–0.30	298–373	5–101	$U(x,y) = $ N.A.; $U(T) = $ N.A.; $U(p) = $ N.A.
Wiebe et al. [111]	1937	1	Static Analytical VLE Cell – Distillation columns + Weighing + Calibrated balloons + (Solubility)	NH$_3$ + H$_2$	0.0025–0.038	273	5–101	$U(x,y) = $ N.A.; $U(T) = $ N.A.; $U(p) = $ N.A.

[a] N.A.: not available.

[b] Not specified concentration of para/ortho hydrogen.

[c] Normal-hydrogen.

[d] Parahydrogen.

[e] Orthohydrogen.

[f] Numerical data not available in the source.

The implementation of quantum corrections in the framework of the SAFT-type EoS has been addressed in the works of Aasen et al., focusing on ultra-cryogenic conditions; first for pure hydrogen, helium, neon, and deuterium [37], and then extended to their mixtures [38]. The strategy followed was to use Monte Carlo simulations via Mie potential with Feynman-Hibbs quantum corrections to optimize the parameters of two different force fields by fitting to experimental VLE data and interaction second virial coefficients B_{ij} (from the literature and ab initio calculations) for the mixtures of the mentioned fluids. Then, the already adjusted force field was introduced into the statistical associating fluid theory-variable range (SAFT-VR) EoS by a proper perturbation theory so as to yield the statistical associating fluid theory of quantum corrected Mie potentials (SAFT-VRQ Mie) EoS. In this work, the cubic EoS of Soave–Redlich–Kwong (SKR) is used in the comparison as a classical and simple reference model to know if the increase in accuracy of the SAFT-VRQ Mie EoS is justified by the increase in complexity by adding quantum corrections.

Regarding the mixtures containing hydrogen, for H$_2$ + Ne, both the SAFT-VRQ Mie EoS and SRK EoS simulations adequately reproduce the phase envelope data, with SRK EoS being the slightly more accurate. However, the SAFT-VRQ Mie EoS shows a great improvement in representing B_{ij}, and the liquid densities: the SRK EoS systematically overestimates liquid densities at low temperatures and underestimates them at high temperatures. The SAFT-VRQ Mie EoS also surpasses the SRK EoS at estimating experimental speeds of sound. With respect to H$_2$ + He mixtures, there is a close agreement between experimental phase envelope data and both simulations and SRK EoS, although SRK systematically overpredicts the concentration of helium in the saturated liquid line. SAFT-VRQ Mie performs extremely well away from the critical region, but sharply overpredicts the critical pressure. Despite this, the quantum corrections do represent an improvement in the estimation of saturated liquid density. Finally, the comparison with ab initio computations of B_{ij} for these mixtures is satisfactory for SAFT-VRQ Mie EoS and the simulations with one of the force fields, showing clear

Table 3
Available experimental data on density and compressibility factors for binary H_2 mixtures.

Source	Year	Rank	Experimental technique	Mixture	x_{H_2} / y_{H_2}	T/K	p/MPa	Uncertainty ($k = 2$)
Hernández-Gómez et al. [152]	2018	1	Single-Sinker Magnetic Suspension Densimeter	$CH_4 + H_2$	0.05–0.50	240–350	1.0–19.9	$U(\rho) = (440–5600)$ ppm; $10^6 \cdot U(y) < 400$ mol mol^{-1}; $U(T) = 4$ mK; $U(p) = 5000$ Pa
Jaeschke et al. [153]	1996	1	Several Methods (Pycnometer and Direct-Weighing Gas-density Meter, Pressure-relative Volume Expansion Technique or Burnett type Apparatus, Optical Interferometry, Sinker Magnetic Suspension Densimeter)	$CH_4 + H_2/CO_2 + H_2/C_2H_6 + H_2$	0.15–0.75	270–353	0.2–30.5	$U(\rho) =$ N.A.; $U(y) =$ N.A.; $U(T) =$ N.A.; $U(p) =$ N.A.
Jett et al. [154]	1994	2	Low-Temperature Cryogenic Isochoric Apparatus + High-Temperature Burnett type Apparatus	$CH_4 + H_2^b$	0.05	140–273	0.8–68.2	$U(\rho) =$ N.A.; $U(x) =$ N.A.; $U(T) =$ N.A.; $U(p) =$ N.A.
Machado et al. [64]	1988	1	Gas Expansion PVT Apparatus – Burnett type Apparatus	$CH_4 + H_2^b$	0.08–0.91	130–159	5.3–106	$U(\rho) = 4000$ ppm; $10^6 \cdot U(x) = 6000$ mol mol^{-1}; $U(T) = 60$ mK; $U(p) = (11000–210000)$ Pa
Magee et al. [155]	1985	1	Burnett type Apparatus	$CH_4 + H_2$	0.20	273–600	0.3–71.5	$U(\rho) = 1000$ ppm; $10^6 \cdot U(y) = 1000$ mol mol^{-1}; $U(T) = (55–120)$ mK; $U(p) = (700–12000)$ Pa
Magee et al. [156]	1986	2	Burnett type Apparatus	$CH_4 + H_2^b$	0.20	157–273	1.8–70	$U(\rho) = 1000$ ppm; $10^6 \cdot U(y) = 1000$ mol mol^{-1}; $U(T) = (55–120)$ mK; $U(p) = (700–12000)$ Pa
Mason et al. [78]	1961	2	Burnett type Apparatus	$CH_4 + H_2/C_2H_6 + H_2/C_3H_8 + H_2/C_4H_{10} + H_2/C_5H_{12} + H_2/C_2H_4 + H_2/C_3H_6 + H_2$	0.28–0.76	289	0.1	$U(\rho) =$ N.A.; $U(y) =$ N.A.; $U(T) =$ N.A.; $U(p) =$ N.A.
Mihara et al. [157]	1977	1	Burnett type Apparatus	$CH_4 + H_2/C_2H_6 + H_2/C_3H_8 + H_2$	0.22–0.84	298–348	0.2–9.3	$U(\rho) = 1400$ ppm; $10^6 \cdot U(y) = 20000$ mol mol^{-1}; $U(T) = 20$ mK; $U(p) = 1000$ Pa
Mueller et al. [158]	1961	2	Burnett type Apparatus	$CH_4 + H_2^b$	0.20–0.78	144–283	0.3–48.3	$U(\rho) = 1300$ ppm; $10^6 \cdot U(x) = 1000$ mol mol^{-1}; $U(T) = 20$ mK; $U(p) = (110–19305)$ Pa
Bartlett et al. [159,160]	1928/1930	1	Burnett type Apparatus	$N_2 + H_2$	0.75	203–572	0.1–101	$U(\rho) = 3000$ ppm; $U(x) =$ N.A.; $U(T) =$ N.A.; $U(p) =$ N.A.
Bartlett et al. [161,162]	1927	1	Burnett type Apparatus	$N_2 + H_2$	0.06–0.88	273	0.1–101	$U(\rho) = 2000$ ppm; $U(x) =$ N.A.; $U(T) =$ N.A.; $U(p) =$ N.A.
Bennett et al. [68]	1952	1	Burnett type Apparatus	$N_2 + H_2$	0.25–0.75	298–398	99.9–307	$U(\rho) = 3700$ ppm; $10^6 \cdot U(x) = 2000$ mol mol^{-1}; $U(T) =$ N.A. mK; $U(p) =$ N.A Pa
Hernández-Gómez et al. [163]	2017	1	Single-Sinker Magnetic Suspension Densimeter	$N_2 + H_2$	0.05–0.50	240–350	1.0–20.1	$U(\rho) = (330–4400)$ ppm; $10^6 \cdot U(y) < 100$ mol mol^{-1}; $U(T) = 4$ mK; $U(p) = 5000$ Pa
Jaeschke et al. [164]	1991	1	Burnett type Apparatus and Two Coupled Grating Interferometers (Refractive Index)	$N_2 + H_2$	0.15–0.75	270–353	0.3–30.2	$U(\rho) = 1400$ ppm; $10^6 \cdot U(y) \leq 300$ mol mol^{-1}; $U(T) = 20$ mK; $U(p) \leq 6000$ Pa

Table 3 (*continued*)

Source	Year	Rank	Experimental technique	Mixture	x_{H_2} / y_{H_2}	T/K	p/MPa	Uncertainty (k = 2)
Kestin et al. [165]	1982	2	Gravimetric Method	$N_2 + H_2$	0.28–0.74	296 & 299.7	0.8–9.9	$U(\rho)$ = N.A.; $U(y)$ = N.A.; $U(T)$ = N.A.; $U(p)$ = N.A.
Mastinu et al. [66]	1967	2	Pycnometer – Mass spectrometry	$N_2 + H_2^b$	0.006–0.020	77.4	1.2	$U(\rho)$ = 1000 ppm; $U(x)$ = N.A.; $U(T)$ = N.A.; $U(p)$ = N.A.
Michels et al. [67]	1949	1	Pycnometer (piezometer)	$N_2 + H_2$	0.75	273–423	≤34.5	$U(\rho)$ = N.A.; $U(x)$ = N.A.; $U(T)$ = N.A.; $U(p)$ = N.A.
Verschoyle [166]	1926	1	Compression Vessel with a Volumenometer and Piezometer	$N_2 + H_2$	0.25–0.75	273–293	3.7–20.8	$U(\rho)$ = 1000 ppm; $U(x)$ = N.A.; $U(T)$ = 100 mK; $U(p)$ ≤ (3703–20819) Pa
Wiebe et al. [167]	1938	1	Burnett type Apparatus	$N_2 + H_2$	0.26–0.87	273–573	2.5–101	$U(\rho)$ = N.A.; $U(x)$ = N.A.; $U(T)$ = N.A.; $U(p)$ = N.A.
Zandbergen et al. [104]	1967	2	Burnett type Apparatus	$N_2 + H_2/Ar + H_2^b$	0.14–0.74	170–292	0.2–10.0	$U(\rho)$ = N.A.; $U(x)$ = N.A.; $U(T)$ = N.A.; $U(p)$ = N.A.
Ababio et al. [168]	1993	1	Gravimetric Method using a Calibrated High-Pressure Cell and a Mass Comparator	$CO_2 + H_2$	0.35–0.50	303–343	0.6–12.7	$U(\rho)$ = N.A.; $10^6 \cdot U(x)$ = 1200 mol mol^{-1}; $U(T)$ = 10 mK; $U(p)$ = 200 Pa.
Alsiyabi [169]	2013	2	High-Pressure Vibrating U-Tube Densimeter	$CO_2 + H_2$	0.03–0.05	283–423	7.9–49.2	$U(\rho)$ = N.A.; $10^6 \cdot U(x)$ = 6000 mol mol^{-1}; $U(T)$ = N.A.; $U(p)$ = N.A.
Cheng et al. [74]	2019	1	Modified Burnett type Apparatus	$CO_2 + H_2/CH_4 + CO_2 + H_2$	0.60–0.70	673	0.6–25.1	$U(\rho)$ = 4700 ppm; $10^6 \cdot U(x)$ = 20000 mol mol^{-1}; $U(T)$ = 200 mK; $U(p)$ = (2000–6000) Pa
Cipollina et al. [72]	2007	2	Fixed Volume Calibrated Pressurized Cell (Gravimetric procedure)	$CO_2 + H_2/CO + H_2/CO_2 + CO + H_2$	0.05–0.24	308–343	8.8–49.3	$U(\rho)$ = N.A.; $10^6 \cdot U(y)$ = 5000 mol mol^{-1}; $U(T)$ = 600 mK; $U(p)$ = 100000 Pa
Mallu et al. [73]	1990	2	Burnett type Apparatus	$CO_2 + H_2$	0.23–0.86	323–423	0.1–6.0	$U(\rho)$ ≤ 1600 ppm; $U(x)$ = N.A.; $U(T)$ = N.A.; $U(p)$ = N.A.
Pinho et al. [170]	2015	2	Microfluidic Capillary Device	$CO_2 + H_2$	0.10–0.20	307	12–12.8	$U(\rho)$ = 60000 ppm; $U(x)$ = N.A.; $U(T)$ = N.A.; $U(p)$ = N.A.
Sanchez-Vicente et al. [171]	2013	2	High-Pressure Vibrating U-Tube Densimeter	$CO_2 + H_2$	0.02–0.10	288–333	1.5–22.7	$U(\rho)$ = (1060–41000) ppm; $10^6 \cdot U(x)$ = 5000 mol mol^{-1}; $U(T)$ = N.A; $U(p)$ = N.A.
Souissi et al. [71]	2017	1	Two-Sinker Magnetic Suspension Densimeter	$CO_2 + H_2$	0.05	273–323	0.5–6.0	$U(\rho)$ = 1500 ppm; $10^6 \cdot U(y)$ < 400 mol mol^{-1}; $U(T)$ = 5 mK; $U(p)$ = (35–420) Pa
Tsankova et al. [136]	2019	1	Microwave Re-entrant Resonance Cavity	$CO_2 + H_2$	0.05–0.25	251–313	0.5–8.2	$U(\rho)$ ≤ 3300 ppm; $10^6 \cdot U(y)$ = 700 mol mol^{-1}; $U(T)$ = 20 mK; $U(p)$ = 1400 Pa
Zhang et al. [172]	2002	2	Gravimetric Method using a Calibrated High-Pressure Cell and an Analytical Balance	$CO_2 + H_2$	0.003	308	5.5–12.9	$U(\rho)$ = N.A.; $U(x)$ = N.A.; $U(T)$ = 60 mK; $U(p)$ = 20000 Pa
Freitag et al. [144]	1986	2			0.0–0.27/ 0.0–0.99	227–373	0.3–27.6	$U(\rho)$ = (20000–40000) ppm;

(continued on next page)

Table 3 (*continued*)

Source	Year	Rank	Experimental technique	Mixture	x_{H_2} / y_{H_2}	T/K	p/MPa	Uncertainty ($k = 2$)
			Computed from Refractive-Index Measurements using a VLE Cell with View Section	$CH_4 + CO_2 + H_2$/n-$C_5H_{12} + CO_2 + H_2$/n-$C_5H_{12} + H_2$				$10^6 \cdot U(x) \leq$ (30000–110000) mol mol^{-1}; $U(T) = 250$ mK; $U(p) =$ (2100–170000) Pa
Nichols et al. [81]	1957	1	Pycnometer	n-$C_6H_{14} + H_2$	0.19–0.79	278–511	1.4–68.9	$U(\rho) = (2500$–$5000)$ ppm; $10^6 \cdot U(x) = 4000$ mol mol^{-1}; $U(T) = 40$ mK; $U(p) = 2757.9$ Pa
Scott [84]	1929	2	Pycnometer	$CO + H_2$	0.33–0.66	298	0.1–17.2	$U(\rho) = $ N.A.; $U(x) = $ N.A.; $U(T) = $ N.A.; $U(p) = $ N.A.
Townend et al. [85]	1931	2	Pycnometer	$CO + H_2$	0.33–0.67	273–298	0.1–60.8	$U(\rho) = $ N.A.; $U(x) = $ N.A.; $U(T) = $ N.A.; $U(p) = $ N.A.
Scholz et al. [102]	2020	1	Two-sinker Magnetic Suspension Densimeter	$Ar + H_2$	0.06–0.55	273–323	0.5–9.0	$U(\rho) = 150$ ppm; $10^6 \cdot U(x) = 1500$ mol mol^{-1}; $U(T) = 5.0$ mK; $U(p) = (36$–$630)$ Pa
Tanner et al. [103]	1930	2	Pycnometer	$Ar + H_2$	0.17	298–447	3.0–12.7	$U(\rho) = $ N.A.; $U(x) = $ N.A.; $U(T) = $ N.A.; $U(p) = $ N.A.
Güsewell et al. [106]	1970	1	Pycnometer	$Ne + H_2^c$	0.8–0.9	25–31	0.33–0.98	$U(\rho) = 10000$ ppm; $U(x) = $ N.A.; $U(T) = 40$ mK; $U(p) = 2900$ Pa
Streett [105]	1973	2	Burnett type Apparatus	$Ne + H_2^c$	0.027–0.94	25–31.1	0.42–10.3	$U(\rho) = 2000$ ppm; $10^6 \cdot U(x) = (50$–$1900)$ mol mol^{-1}; $U(T) = 20$ mK; $U(p) = (420$–$10300)$ Pa
Hongo et al. [109]	1978	2	Calculated data from ideal reduced molar volumes	$NH_3 + H_2$	0.19–0.80	298–373	0.12–6.6	$U(\rho) = $ N.A.; $U(x) = $ N.A.; $U(T) = $ N.A.; $U(p) = $ N.A.
Kazarnovskiy et al. [108]	1968	1	Pycnometer (piezometer)	$NH_3 + H_2$	0.43–0.65	423–573	8.4–155	$U(\rho) = 10000$ ppm; $U(x) = $ N.A.; $U(T) = 300$ mK; $U(p) =$ (59000–1100000) Pa

[a] N.A.: not available.
[b] Not specified concentration of para/ortho hydrogen.
[c] Normal-hydrogen.
[d] Parahydrogen.
[e] Orthohydrogen.

deviations with the SRK EoS.

4. Available experimental data for hydrogen binary mixtures

High-quality experimental data are needed to develop reliable thermodynamic models, but obtaining high-quality experimental data is expensive and time-consuming, and in general, such data are scarce [3]. This scarcity of experimental data is more acute in emerging fields such as the hydrogen economy.

The GERG-2008 EoS was developed as a reference for natural gas mixtures. In any case, the main components that accompany hydrogen in the vast majority of processes for the production, storage, transport and final use of hydrogen, are included in the list of the 21 components considered in this EoS. For this reason, we have taken the list of components of the GERG-2008 as the starting point for this literature search.

We have therefore considered only binary mixtures of hydrogen with the 20 other elements included in the GERG-2008 EoS and, additionally,

we have considered the binary mixtures of hydrogen with neon and ammonia. The thermophysical properties object of this survey are VLE equilibrium data, density, and speed of sound and other calorific properties, in the main range of applicability of the GERG-2008 EoS, as these are the more relevant data sets for the development of multiparametric EoS.

Table 2 shows the available experimental data on VLE for hydrogen binary mixtures, indicating for each reference, the authors, the experimental technique used, the composition of the binary mixture, the ranges of temperature and pressure, and the estimated uncertainty for each magnitude. Tables 3 and 4 present the same information for the available experimental data on density and speed of sound, respectively. The experimental techniques used to obtain these data are usually described in detail in the original sources, but a comprehensive review of the available experimental techniques can be found in the works of Wagner and Kleinrahm [60] and Cheng et al. [61].

The experimental data sets presented in Tables 2–4 have been

Table 4
Available experimental data on speed of sound and other calorific properties for binary H_2 mixtures.

Source	Year	Rank	Experimental technique (Calorific property)	Mixture	x_{H_2} / y_{H_2}	T/K	p/MPa	Uncertainty ($k = 2$)
Maurer [173]	2021	1	Spherical Acoustic Resonator (Speed of Sound)	$CH_4 + H_2$	0.05	250–350	0.5–10.1	$U_r(w) = (360–1060)$ ppm; $10^6 \cdot U(x) = 8$ mol mol^{-1}; $U(T) = 40$ mK; $U(p) = (600–2400)$ Pa
Lozano-Martín et al. [174]	2020	1	Spherical Acoustic Resonator (Speed of Sound)	$CH_4 + H_2$	0.05–0.50	273–375	0.4–20.2	$U_r(w) = 220$ ppm; $10^6 \cdot U(x) = 40$ mol mol^{-1}; $U(T) = 4.6$ mK; $U(p) = (240–1700)$ Pa
Randelman et al. [115]	1988	2	Flow Joule-Thomson Valve Apparatus (Joule-Thomson Coefficients)	$CH_4 + H_2$	0.13–0.57	274–295	2.2–13.8	$U(\mu_{JT}) = $ N.A.; $10^6 \cdot U(x) = 2100$ mol mol^{-1}; $U(T) = 28$ mK; $U(p) = 40000$ Pa.
Wormald et al. [114]	1977	2	Flow Calorimeter (Excess Enthalpies)	$CH_4 + H_2/N_2 + H_2^b$	0.21–0.92	201–298	1.1–11.2	$U(H^E) = 40000$ ppm; $10^6 \cdot U(x) = (2100–9200)$ mol mol^{-1}; $U(T) = 40$ mK; $U(p) = 40000$ Pa
Knapp et al. [113]	1976	1	Flow Calorimeter (Molar Heat Capacity)	$N_2 + H_2^b$	0.1–0.78	100–200	3.0–7.0	$U(C_{p,m}) = 40000$ ppm; $10^6 \cdot U(x) = (1400–10920)$ mol mol^{-1}; $U(T) = (40–80)$ mK; $U(p) = (12000–28000)$ Pa
Lozano-Martín et al. [176]	2021	1	Spherical Acoustic Resonator (Speed of Sound)	$N_2 + H_2$	0.05–0.50	260–350	0.5–19.9	$U(w) = 240$ ppm; $10^6 \cdot U(x) = 70$ mol mol^{-1}; $U(T) = 5.2$ mK; $U(p) = (240–1620)$ Pa
Van Itterbeek et al. [69]	1949	1	Ultrasonic Interferometer (Speed of sound)	$N_2 + H_2/O_2 + H_2/CO + H_2^b$	0.12–0.84	75–90	lim. $p \to 0$	$U(w) = $ N.A.; $U(x) = $ N.A.; $U(T) = $ N.A.; $U(p) = $ N.A.
Alsiyabi [169]	2013	2	Ultrasonic Cell - Time of Flight (Speed of Sound)	$CO_2 + H_2$	0.05	268–301	9.7–40.7	$U(w) = $ N.A.; $10^6 \cdot U(x) = 6000$ mol mol^{-1}; $U(T) = $ N.A.; $U(p) = $ N.A.
Maurer [173]	2021	1	Spherical Acoustic Resonator (Speed of Sound)	$CO_2 + H_2$	0.25–0.74	250–350	0.5–10.1	$U_r(w) = (380–1030)$ ppm; $10^6 \cdot U(x) = (12–53)$ mol mol^{-1}; $U(T) = 40$ mK; $U(p) = (600–2400)$ Pa
Van Itterbeek et al. [107]	1946	1	Ultrasonic Interferometer (Speed of sound)	$He + H_2/Ar + H_2^b$	0.14–0.81	20.3–90	lim. $p \to 0$	$U(w) = $ N.A.; $U(x) = $ N.A.; $U(T) = $ N.A.; $U(p) = $ N.A.
Brouwer et al. [175]	1970	2	Flow Calorimeter (Molar Heat Capacity)	$Ne + H_2^c$	0.03–0.84	24.5–30.5	0.19–0.92	$U(C_{p,m}) = $ N.A.; $U(x) = $ N.A.; $U(T) = $ N.A.; $U(p) = $ N.A.
Güsewell et al. [106]	1970	1	Parallel-plate Ultrasonic Resonator (Speed of sound)	$Ne + H_2^c$	0.8–0.9	25–31	0.33–0.98	$U_r(w) = 10000$ ppm; $U(x) = $ N.A.; $U(T) = 40$ mK; $U(p) = 2900$ Pa

[a] N.A.: not available.
[b] Not specified concentration of para/ortho hydrogen.
[c] Normal-hydrogen.
[d] Parahydrogen.
[e] Orthohydrogen.

classified in two categories based on an estimate of their quality. The ranks or priorities of the data sets are given in the third column of these tables. The rank (1 is primary, 2 is secondary) of the data set is determined based on the apparatus used for the measurements and its stated achievable uncertainty, the expertise and trajectory of the laboratory, the agreement with other data sets, and the year the data were taken. In some cases, a rank value of 1 indicates that the experimental data set was weighted during the fitting process while a rank value of 2 indicates that the experimental data sets were used as supplementary measurements in determining the real fluid behavior of the system.

The reported uncertainty in the last column of Tables 2–4 are taken from the references, when available. In general, modern references

clearly indicate the experimental expanded ($k = 2$) uncertainty of the measurement and the state point. For all other works, any indication of error, accuracy, or precision has been considered as the best estimation of what we currently understand by standard uncertainty of measurement. These are collected in Tables 2–4, after multiplying the values by two.

4.1. Analysis of the available experimental data

Tables 5–7 present the statistical analysis of the deviations of the experimental data sets presented in Tables 2–4 with respect to the GERG-2008 EoS with the improvements developed by Beckmüller et al.

Table 5
Statistical analysis of the deviation of the experimental sets of vapor-liquid equilibrium (VLE) data of binary mixtures containing hydrogen with respect to the improved GERG-2008 EoS [30,39]: Average absolute deviations (AAD), Bias, RMS and Max AD. The deviations are presented as $10^2 \cdot (\text{mol mol}^{-1})$ for bubble-point data (x) and dew-point data (y).

Source	Number of data[a]	AAD	Bias	RMS	Max AD	AAD within experimental uncertainty[b]
CH_4+H_2						
Benham et al., 1957 (x) [118]	13	1.7	−0.79	2.9	8.1	N
Benham et al., 1957 (y) [118]	13	1.5	0.82	2.0	4.7	N
Cosway et al., 1959 (x) [119]	3	0.23	−0.23	0.31	0.53	Y
Cosway et al., 1959 (y) [119]	3	3.0	3.0	3.2	4.7	N
Freeth et al., 1931 (x) [120]	15	0.88	−0.62	1.4	2.8	N
Freeth et al., 1931 (y) [120]	20	0.44	0.40	0.62	1.7	Y
Hong et al., 1981 (x) [63]	129	0.82	0.12	2.3	15	N
Hong et al., 1981 (y) [63]	133	1.2	0.74	2.5	14	N
Hu et al., 2014 (x) [121]	23	0.20	−0.20	0.26	0.55	N
Hu et al., 2014 (y) [121]	23	5.2	−4.2	6.0	12	N
Sagara et al., 1972 (x) [122]	28	0.57	−0.24	0.77	2.2	Y
Sagara et al., 1972 (y) [122]	28	1.8	1.8	2.4	5.4	N
Tsang et al., 1980 (x) [62]	169	0.7	−0.42	1.2	10	N
Tsang et al., 1980 (y) [62]	168	1.2	0.15	3.0	22	N
Yorizane et al., 1980 (x) [123]	3	0.81	−0.54	1.2	2.0	N
Yorizane et al., 1980 (y) [123]	3	0.20	0.18	0.24	0.34	Y
N_2+H_2						
Akers et al., 1957 (x) [124]	10	0.40	−0.16	0.54	1.2	N
Akers et al., 1957 (y) [124]	10	1.1	−0.93	1.3	2.4	N
Kremer et al., 1983 (x) [125]	3	0.35	−0.35	0.37	0.50	Y
Kremer et al., 1983 (y) [125]	3	0.57	−0.57	0.60	0.84	Y
Maimoni 1961 (x) [126]	11	0.060	−0.093	0.097	0.15	UNR
Maimoni 1961 (y) [126]	15	0.12	−0.069	0.22	0.65	UNR
Omar et al., 1962 (y) [127]	24	0.46	0.038	0.87	3.7	UNR
Streett et al., 1978 (x) [65]	66	1.0	−0.46	1.8	7.5	N
Streett et al., 1978 (y) [65]	64	1.4	0.013	2.3	9.6	N
Verschoyle 1931 (x) [82]	61	1.3	−1.1	3.1	14	N
Verschoyle 1931 (y) [82]	53	1.5	−0.19	3.7	20	N
Yorizane et al., 1971 (x) [128]	17	2.2	−1.9	2.8	6.3	N
Yorizane et al., 1971 (y) [128]	17	1.7	−1.2	1.8	2.6	Y
CO_2+H_2						
Bezanehtak et al., 2002 (x) [129]	41	1.0	−1.0	1.1	1.6	UNR
Bezanehtak et al., 2002 (y) [129]	33	2.5	2.6	4.0	7.8	UNR
Fandiño et al., 2015 (x) [34]	85	0.13	−0.0014	0.35	2.5	Y
Fandiño et al., 2015 (y) [34]	85	0.45	0.22	0.66	1.8	N
Kaminishi et al., 1966 (x) [130]	20	4.3	−0.0070	5.9	14	UNR
Kaminishi et al., 1966 (y) [130]	21	13	−0.38	18	41	UNR
Spano et al., 1968 (x) [134]	45	0.18	0.18	0.49	2.3	Y
Spano et al., 1968 (y) [134]	49	1.2	−1.1	2.8	14	Y
Tenorio et al., 2015 (x) [135]	37	0.15	−0.29	0.42	1.6	N
Tenorio et al., 2015 (y) [135]	36	0.15	0.16	0.41	1.3	N
Tsang et al., 1981 (x) [70]	113	1.1	−1.0	3.0	15	N
Tsang et al., 1981 (y) [70]	118	2.7	2.6	6.4	25	N
Tsankova et al., 2019 (y) [136]	27	0.70	−0.70	0.90	1.8	N
Yorizane et al., 1970 (x) [137]	11	2.8	−2.9	5.7	17	N
Yorizane et al., 1970 (y) [137]	11	2.0	1.2	3.3	8.7	N
$C_2H_6+H_2$						
Cosway et al., 1959 [119]/Williams et al., 1954 [139] (x)	5	0.63	−0.076	0.69	1.2	N
Cosway et al., 1959 [119]/Williams et al., 1954 [139] (y)	5	0.14	0.14	0.18	0.34	N
Heintz et al., 1982 (x) [138]	63	0.52	−1.0	2.9	7.7	Y
Heintz et al., 1982 (y) [138]	63	0.44	1.8	3.8	20	Y
Hiza et al., 1968 (x) [75]	31	0.43	−1.2	1.5	2.8	Y
Hiza et al., 1968 (y) [75]	70	0.012	0.0057	0.049	0.34	Y
Sagara et al., 1972 (x) [122]	16	0.47	0.17	0.58	1.2	Y
Sagara et al., 1972 (y) [122]	16	0.53	0.53	0.65	1.6	Y
$C_3H_8+H_2$						
Burris et al., 1953 (x) [76]	50	1.3	2.0	3.7	12	UNR
Burris et al., 1953 (y) [76]	54	2.5	3.2	6.5	17	UNR
Trust et al., 1971 (x) [140]	73	0.77	−0.78	1.8	4.7	UNR
Trust et al., 1971 (y) [140]	54	0.72	0.52	3.1	9.7	UNR
$C_4H_{10}+H_2$						
Aroyan et al., 1951 (x) [79]	31	2.0	−2.9	3.8	8.3	N
Aroyan et al., 1951 (y) [79]	28	0.13	0.18	0.32	1.1	Y
Klink et al., 1975 (x) [141]	60	1.0	0.80	1.2	2.5	Y
Klink et al., 1975 (y) [141]	60	2.7	2.6	3.7	12	Y
Nelson et al., 1943 (x) [142]	13	1.0	0.71	1.1	2.4	UNR
Nelson et al., 1943 (y) [142]	5	1.7	4.4	5.0	6.9	UNR
$iC_4H_{10}+H_2$						

Table 5 (*continued*)

Source	Number of data[a]	AAD	Bias	RMS	Max AD	AAD within experimental uncertainty[b]
Dean et al., 1946 (x) [80]	22	9.5	−9.5	10.8	19.0	UNR
Dean et al., 1946 (y) [80]	22	7.1	5.8	12.5	42.6	UNR
$C_5H_{12}+H_2$						
Connolly et al., 1986 (x) [143]	81	6.3	−6.3	6.9	11.5	UNR
Freitag et al., 1986 (x) [144]	29	4.8	−6.1	8.5	24	Y
Freitag et al., 1986 (y) [144]	30	0.89	1.1	1.5	4.2	Y
$C_6H_{14}+H_2$						
Brunner et al., 1985 (x) [145]	24	0.57	0.49	0.89	2.1	Y
Fu et al., 1994 (x) [146]	3	0.67	0.46	0.78	1.2	UNR
Fu et al., 1994 (y) [146]	3	0.24	0.24	0.24	0.27	UNR
Gao et al., 2001 (x) [147]	34	1.8	1.8	2.0	3.8	N
Nichols et al., 1957 (x) [81]	59	1.6	0.54	3.5	12.6	UNR
Nichols et al., 1957 (y) [81]	59	1.4	2.5	4.5	17.7	UNR
$CO + H_2$						
Akers et al., 1957 (x) [124]	11	0.28	0.10	0.31	0.53	Y
Akers et al., 1957 (y) [124]	11	0.90	−0.26	1.0	1.8	N
Tsang et al., 1981 (x) [83]	127	0.58	−0.32	1.0	4.8	Y
Tsang et al., 1981 (y) [83]	127	0.80	0.07	1.4	5.0	N
Verschoyle et al., 1931 (x) [82]	67	1.1	−0.32	1.8	7.7	N
Verschoyle et al., 1931 (y) [82]	77	1.4	−0.47	2.9	10.2	N
$H_2O + H_2$						
Kling et al., 1991 (x) [87]	10	0.12	−0.12	0.13	0.22	UNR
Setthanan et al., 2006 (x) [86]	3	0.0010	−0.0013	0.0014	0.0014	N
Shoor et al., 1969 (x) [89]	2	0.00086	−0.0013	0.0013	0.0013	UNR
Wiebe et al., 1934 (x) [88]	40	0.51	−0.51	0.67	1.4	N
$H_2S + H_2$						
Yorizane et al., 1969 (x) [90]	11	0.84	−0.84	1.0	2.0	N
Yorizane et al., 1969 (y) [90]	11	2.9	1.2	3.7	6.5	N
$He + H_2$						
Hiza et al., 1972 (x) [92]	21	0.22	0.30	0.31	0.46	UNR
Hiza et al., 1981 (x) [93]	24	0.11	−0.19	0.21	0.44	UNR
Hiza et al., 1981 (y) [93]	16	1.1	−2.7	3.0	4.4	UNR
Sneed et al., 1968 (x) [94]	60	2.4	2.0	3.7	14	N
Sneed et al., 1968 (y) [94]	60	7.1	−7.1	9.1	21	N
Sonntag et al., 1964 (x) [96]	48	0.38	0.26	1.2	6.0	UNR
Sonntag et al., 1964 (y) [96]	49	4.4	−5.4	6.3	16	UNR
Streett et al., 1964 (x) [95]	88	0.42	0.33	1.2	7.3	UNR
Streett et al., 1964 (y) [95]	86	2.4	−2.6	3.7	12	UNR
Yamanishi et al., 1992 (x) [91]	24	0.024	0.023	0.029	0.064	Y
Yamanishi et al., 1992 (y) [91]	11	2.1	4.4	5.7	12	N
$Ar + H_2$						
Calado et al., 1979 (x) [97]	132	19	−21	27	62	N
Calado et al., 1979 (y) [97]	127	8.5	9.4	14	57	N
Volk et al., 1960 (x) [98]	119	6.0	−6.1	6.6	11	N
$Ne + H_2$						
Heck et al. (x) [100]	40	1.3	−2.2	4.0	14	Y
Heck et al. (y) [100]	58	1.9	−2.2	5.0	14	Y
Streett et al. (x) [99]	50	1.6	−2.6	5.1	19	N
Streett et al. (y) [99]	77	2.8	−3.5	5.2	16	N
Zelfde et al. (x) [101]	98	0.20	−0.20	0.24	0.52	UNR
NH_3+H_2						
Moore et al., 1972 (x) [151]	4	0.00038	−0.0011	0.0013	0.0021	UNR
Reamer et al., 1959 (x) [112]	55	0.15	0.072	0.19	0.48	Y
Reamer et al., 1959 (y) [112]	104	0.78	0.54	1.2	3.8	Y
Wiebe et al., 1934 (x) [110]	72	1.1	−0.80	2.7	12	UNR
Wiebe et al., 1937 (x) [111]	11	0.35	0.29	0.44	0.78	UNR

[a] Data of pure fluid as well as data for which deviations in terms of mol-% could not be calculated are not considered.

[b] Y = yes, N = no, UNR = uncertainty not reported.

[39]. The mixture model used for estimating the properties of helium + hydrogen and neon + hydrogen is that proposed by Blackham [35] and the mixture model used for estimating the properties of ammonia + hydrogen is that proposed by Neumann et al. [32]. Unless otherwise stated, all the calculations are made considering hydrogen as normal hydrogen. The data where deviations could be not calculated because the equation of state does not converge, or where the equation of state does converge but with relative deviations greater than 100%, clearly without agreement, are not considered in the statistical analysis. The data for pure fluids are also discarded. It is indicated in Tables 5–7 if the deviations are within the reported experimental expanded ($k = 2$) uncertainty for every data set.

We have analyzed the deviations with respect to the GERG EoS in terms of Average Absolute Relative Deviations (AARD), Bias, Root Mean Square (RMS), and Maximum Absolute Relative Deviation (Max ARD), defined as follows:

$$AARD = \frac{1}{n}\sum_{i=1}^{n}\left|10^2 \cdot \frac{x_{i,exp} - x_{i,EoS}}{x_{i,EoS}}\right| \tag{1}$$

Table 6

Statistical analysis of the deviation of the experimental sets of density and compressibility factors data of binary mixtures containing hydrogen with respect to the improved GERG-2008 EoS [30,39]: Average absolute relative deviations (AARD), Bias, RMS and Max ARD.

Source	Number of data[a]	AARD/%	Bias/%	RMS/%	Max ARD/%	AARD within experimental uncertainty[b]
CH_4+H_2						
Hernández-Gómez et al., 2018 [152]	391	0.048	−0.021	0.065	0.25	Y
Jett et al., 1994 [154]	168	0.64	0.36	1.0	6.2	UNR
Machado et al., 1988 [64]	296	1.4	−0.42	1.8	11	N
Magee et al., 1985 [155]	172	0.25	−0.23	0.29	1.1	N
Magee et al., 1986 [156]	173	0.75	−0.71	1.3	3.4	N
Mason et al., 1961 [78]	2	0.014	−0.0074	0.015	0.021	UNR
Mihara et al., 1977 [90]	153	0.13	−0.13	0.20	0.79	Y
Mueller et al., 1961 [158]	344	0.86	−0.81	1.7	11	N
N_2+H_2						
Bartlett et al., 1928–1930 [159,160]	103	0.198	0.077	0.272	0.742	Y
Bartlett et al., 1927 (x2) [161,162]	72	0.158	0.096	0.202	0.471	Y
Bennett et al., 1952 [68]	77	0.296	−0.060	0.387	1.793	Y
Hernández-Gómez et al., 2017 [163]	399	0.038	−0.027	0.050	0.154	Y
Jaeschke et al., 1991 [164]	197	0.011	−0.001	0.016	0.092	Y
Kestin et al., 1982 [165]	54	1.091	1.008	1.185	2.756	UNR
Mastinu 1967 [66]	10	0.923	0.923	0.946	1.165	N
Michels et al., 1949 [67]	119	0.058	0.058	0.059	0.081	UNR
Verschoyle 1926 [166]	63	0.075	0.028	0.091	0.195	Y
Wiebe et al., 1938 [167]	175	0.118	0.096	0.155	0.457	UNR
Zandbergen et al., 1967 [104]	100	0.240	0.053	0.361	2.009	UNR
CO_2+H_2						
Ababio et al., 1993 [168]	53	0.11	−0.023	0.14	0.41	UNR
Alsiyabi 2013 [169]	67	2.7	−0.10	3.4	12	UNR
Cheng et al., 2019 [74]	16	0.41	0.023	0.57	1.5	Y
Cipollina et al., 2007 [72]	48	0.51	−0.16	0.58	1.0	UNR
Mallu et al., 1990 [73]	130	0.41	−0.45	0.55	1.7	N
Pinho et al., 2015 [170]	2	2.1	0.76	3.2	3.8	Y
Sanchez-Vicente et al., 2013 [171]	488	1.4	0.39	2.0	6.5	Y
Souissi et al., 2017 [71]	19	0.19	−0.19	0.21	0.37	Y
Tsankova et al., 2019 [136]	66	0.39	−0.21	0.46	1.2	Y
Zhang et al., 2002 [172]	20	2.2	1.3	2.7	5.1	UNR
$C_2H_6+H_2$						
Mason et al., 1961 [78]	2	0.017	−0.017	0.017	0.019	UNR
Mihara et al., 1977 [157]	154	0.23	−0.23	0.35	1.5	N
$C_3H_8+H_2$						
Mason et al., 1961 [78]	2	0.031	0.031	0.031	0.033	UNR
Mihara et al., 1977 [157]	73	0.12	−0.12	0.16	0.43	Y
$C_4H_{10}+H_2$						
Mason et al., 1961 [78]	4	0.14	0.14	0.16	0.24	UNR
$C_5H_{12}+H_2$						
Freitag et al., 1986 [144]	55	10	7.5	13	28	N
Mason et al., 1961 [78]	2	0.37	0.37	0.37	0.37	UNR
$C_6H_{14}+H_2$						
Nichols et al., 1957 [81]	421	2.0	0.034	2.8	13	N
$CO + H_2$						
Cipollina et al., 2007 [72]	48	2.40	−0.63	3.1	6.5	UNR
Scott 1929 [84]	54	0.25	−0.13	0.34	0.72	UNR
Townend et al., 1931 [85]	120	0.16	−0.054	0.24	0.79	UNR
$Ar + H_2$						
Scholz et al., 2020 [102]	144	0.32	0.32	0.41	1.1	N
Tanner et al., 1930 [103]	24	0.64	0.64	0.70	1.1	UNR
Zandbergen et al., 1967 [104]	122	1.4	1.3	2.4	9.3	UNR
$Ne + H_2$						
Güsewell et al. [106]	12	5.8	6.2	6.4	8.9	N
Streett [105]	217	5.4	3.1	6.8	27	N
NH_3+H_2						
Hongo et al. [109]	120	0.67	−0.16	0.87	2.6	UNR
Kazarnovskiy et al. [108]	52	1.1	−0.55	1.2	2.8	Y

[a] Data of pure fluid as well as data for which deviations in terms of density or compressibility factor could not be calculated are not considered.

[b] Y = yes, N = no, UNR = uncertainty not reported.

$$Bias = \frac{1}{n}\sum_{i=1}^{n}\left(10^2 \cdot \frac{x_{i,exp} - x_{i,EoS}}{x_{i,EoS}}\right) \qquad (2)$$

$$RMS = \sqrt{\frac{1}{n}\sum_{i=1}^{n}\left(10^2 \cdot \frac{x_{i,EoS} - x_{i,EoS}}{x_{i,EoS}}\right)^2} \qquad (3)$$

Table 7

Statistical analysis of the deviation of the experimental sets of speed of sound and other calorific properties data of binary mixtures containing hydrogen with respect to the improved GERG-2008 EoS [30,39]: Average absolute relative deviations (AARD), Bias, RMS and Max ARD.

Property	Source	Number of data[a]	AARD/ %	Bias/%	RMS/ %	Max ARD/%	AARD within experimental uncertainty[b]
CH₄+H₂							
Speed of sound	Maurer 2021 [173]	45	0.028	0.023	0.029	0.047	Y
Speed of sound	Lozano-Martín et al., 2020 [174]	233	0.042	−0.019	0.058	0.26	N
Joule-Thomson coefficient	Randelmand et al., 1988 [115]	56	28	28	31	78	UNR
Excess Enthalpy	Wormald et al., 1977 [114]	72	8.1	−7.9	10	22	N
N₂+H₂							
Speed of sound	Itterbeek et al., 1949 [69]	19	0.29	0.087	0.42	1.4	UNR
Molar heat capacity	Knapp et al., 1976 [113]	78	1.6	−1.2	2.5	12	Y
Speed of sound	Lozano-Martín et al., 2021 [176]	174	0.025	−0.010	0.046	0.27	Y
Excess Enthalpy	Wormald et al., 1977 [114]	63	4.6	1.4	6.2	22	Y
CO₂+H₂							
Speed of sound	Alsiyabi et al., 2013 [169]	55	6.1	6.3	6.7	19	N
Speed of sound	Maurer 2021 [173]	95	0.063	−0.043	0.10	0.45	Y
O₂+H₂							
Speed of sound	Itterbeek et al., 1949 [69]	12	0.24	−0.23	0.41	1.3	UNR
CO + H₂							
Speed of sound	Itterbeek et al., 1949 [69]	16	0.21	−0.15	0.27	0.69	UNR
He + H₂							
Speed of sound	Itterbeek et al., 1946 [107]	4	0.20	0.20	0.26	0.48	UNR
Ar + H₂							
Speed of sound	Itterbeek et al., 1946 [107]	12	0.27	−0.25	0.35	0.70	UNR
Ne + H₂							
Molar heat capacity	Brouwer et al. [175]	77	5.2	−5.8	35	42	UNR
Speed of sound	Güsewell et al. [106]	12	1.1	0.81	1.7	4.3	Y

[a] Data of pure fluid as well as data for which deviations in terms of the corresponding calorific property could not be calculated are not considered.

[b] Y = yes, N = no, UNR = uncertainty not reported.

(a)

(b)
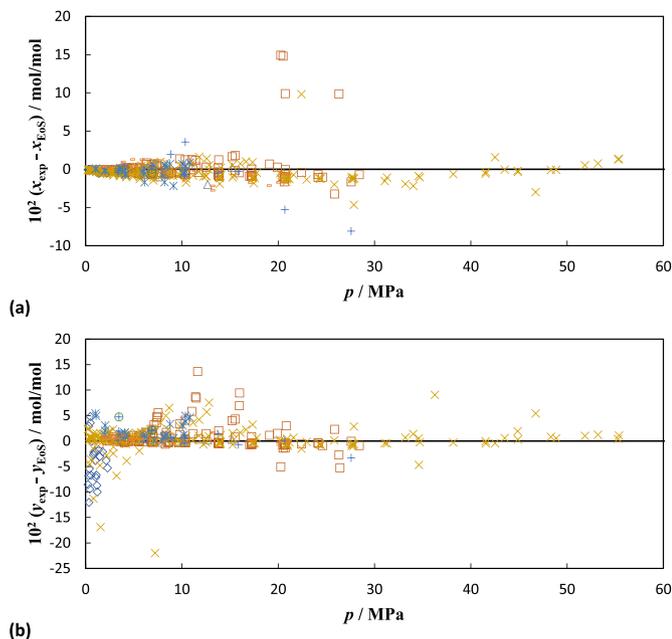
Fig. 2. Deviations of bubble-point data (a) and dew-point data (b) for the binary mixtures (CH₄ + H₂) with respect to the improved GERG-2008 EoS [30, 39]: + Benham et al. (1957), ◯ Cosway et al. (1959), ▬ Freeth et al. (1931), □ Hong et al. (1981), ◇ Hu et al. (2014), ✳ Sagara et al. (1972), ✕ Tsang et al. (1980), △ Yorizane et al. (1980).

(a)

(b)

Fig. 3. Deviations of bubble-point data (a) and dew-point data (b) for the binary mixtures (N₂ + H₂) with respect to the improved GERG-2008 EoS [30,39]: ◯ Akers et al. (1957), ◇ Kremer et al. (1983), ✳ Maimoni (1961), ✕ Omar et al. (1962), □ Street et al. (1978), + Verschoyle (1931), △ Yorizane et al. (1971).

$$Max\ RD = \max\left(\left|10^2 \cdot \frac{x_{i,exp} - x_{i,EoS}}{x_{i,EoS}}\right|\right) \tag{4}$$

The AARD and Max RD are not meaningful in the case of the VLE data. In this case, the Average Absolute Deviations (AAD) and Maximum Absolute Deviation (Max AD) in mol-% are used instead, defined as:

(a)

(b)
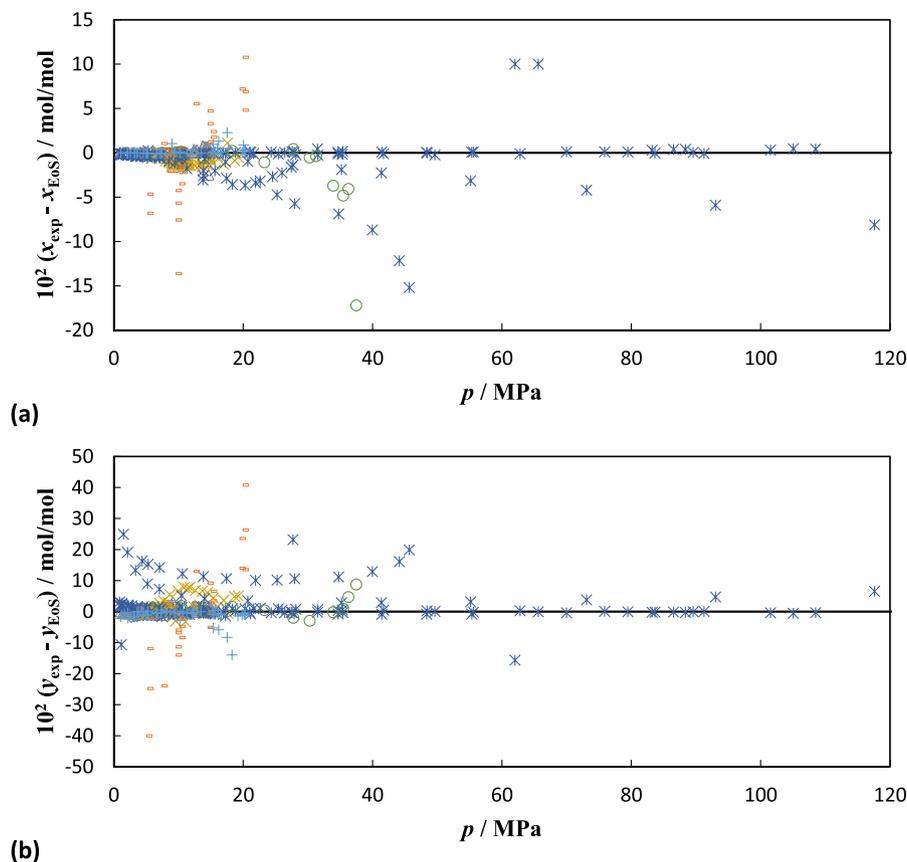
Fig. 4. Deviations of bubble-point data (a) and dew-point data (b) for the binary mixtures (CO_2 + H_2) with respect to the improved GERG-2008 EoS [30,39]: × Bezanehtak et al. (2002), △ Fandiño et al. (2015), ▬ Kaminishi et al. (1966), + Spano et al. (1968), □ Tenorio et al. (2015), ◇ Tsankova et al. (2019), ✳Tsang et al. (1981), ○ Yorizane et al. (1970).

$$AAD = \frac{1}{n} \sum_{i=1}^{n} \left| 10^2 \cdot \left(x_{i,exp} - x_{i,EoS} \right) \right| \qquad (5)$$

$$Max\ AD = \max \left(\left| 10^2 \cdot \left(x_{i,exp} - x_{i,EoS} \right) \right| \right) \qquad (6)$$

A total of 4854 experimental VLE data, corresponding to 16 binary systems (14 of the 20 possible binary systems with hydrogen considered by the GERG-2008 EoS, see Table 1), are analyzed and the results are summarized in Table 5. In the same way, the results of the analysis of the 5603 experimental density data, corresponding to 12 binary systems (10 of them from those 20 binary systems), are summarized in Table 6; while the results of the analysis of the 1043 experimental speed of sound data or other caloric properties, corresponding to 8 binary systems (7 of them from those 20 binary systems), are presented in Table 7.

Figs. 2–10 show the deviations of the bubble-point data and the dew-point data (in mol-%) for the binary mixtures of hydrogen analyzed in this work with respect to the improved GERG-2008 EoS [30,39]. In the same way, Figs. 11–17 depict the percentage deviations of homogeneous density data, and Figs. 18–21 display the percentage deviations of speed of sound, isobaric heat capacity, excess enthalpy and Joule-Thomson coefficient data.

As supplementary material, Figs. S2–S5 show the average absolute deviations of vapor-liquid equilibrium (VLE), density and compressibility, and speed of sound and other calorific properties data with respect to the improved GERG-2008 EoS [30,39]. Figs. S6–S11 depict the (p, T), (p, x), and (p, y) plots of vapor-liquid equilibrium (VLE) data. Figs. S12–16 illustrate the (p, T) and (p, x) plots of density, compressibility, speed of sound, and other calorific properties data.

Nearly half the VLE data (2260 of 4854, Figs. 2–4 and 7), and most of the density data (4199 of 5603, Figs. 11–13 and 16) and the speed of sound data, as well as other caloric properties (914 of 1043, Figs. 18–21), correspond to the binary systems of hydrogen with methane, nitrogen, carbon dioxide and carbon monoxide. The binary system hydrogen with methane is the only one for which a binary specific departure function is included in the GERG-2008 model [30], and new equations of state for the four binary systems of hydrogen with methane, nitrogen, carbon dioxide and carbon monoxide have recently been proposed by Beckmüller et al. [39]. A detailed analysis of the available experimental data for these four systems, whose deviations from the GERG-2008 EoS are presented in Figs. 2–4 and 7, can be found in that paper [39].

With respect to the VLE of CH_4 + H_2 (see Fig. 2), the AAD ranges between (0.20–5.2) mol-%, but most of the differences remain at about 1% for the saturated liquid line and twice that for the saturated vapor data. The higher AAD of the saturated vapor line are due to the data at higher temperatures, especially for compositions between the critical point and the maximum composition. However, the discrepancies are higher than the stated experimental uncertainties. For example, Tsang et al. [62] indicate an expanded (k = 2) experimental uncertainty of 0.5 mol-% and the AAD are between (0.7–1.2)%, while Hong et al. [63] report a 0.33 mol-% of uncertainty and the resulting AAD are above 0.82 mol-%. Regarding the density of this system (see Fig. 11), the AARD are between (0.014–1.4) %, with an average value of 0.5%, and within the experimental uncertainty for most of the works in non-extreme conditions: Hernández-Gómez et al. [152] report an expanded (k = 2) uncertainty of 0.5%, while the AARD are an order of magnitude lower, at
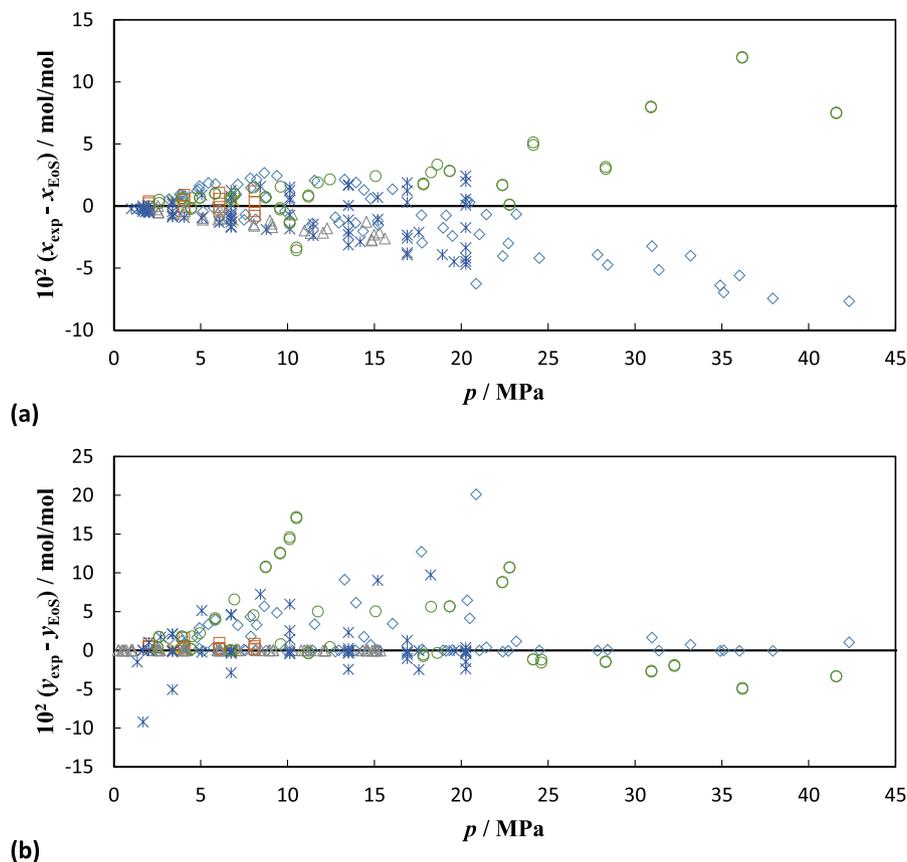
Fig. 5. Deviations of bubble-point data (a) and dew-point data (b) for the binary mixtures (C_2H_6 + H_2) and (C_3H_8 + H_2) with respect to the improved GERG-2008 EoS [30,39]: ✕Cosway et al./Williams et al. (C_2H_6 + H_2,1954), ◇ Heintz et al. (C_2H_6 + H_2, 1982), △ Hiza et al. (C_2H_6 + H_2, 1968), ☐ Sagara et al. (C_2H_6 + H_2, 1972), ◯ Burris et al. (C_3H_8 + H_2,1953), ✳Trust et al. (C_3H_8 + H_2,1971).

0.05%. At low temperatures and high pressures, up to 100 MPa, the situation is different and the data of Machado et al. [64] gives AARD of 1.4%, which are outside the claimed uncertainty of 0.2%. In addition, speed of sound data from Lozano-Martín et al. [174] and Maurer [173] is also well reproduced (see Fig. 18).

Regarding the VLE of N_2 + H_2 (see Fig. 3), the estimated dew and bubble points of the phase envelopes by the mixture model of Beckmüller et al. [39] result in a good agreement, with deviations as low as for the previous system and AAD = (0.06–2.2) mol-%, with an overall AAD of 1 mol-%. Although, these differences are outside the experimental expanded (k = 2) uncertainty reported by several authors, it seems they were determined too optimistically in general. For instance, data sets of Streett et al. [65] show differences below 1.4 mol-% in comparison to an experimental expanded (k = 2) uncertainty of 0.1 mol-%; however, some inconsistencies appear in the saturated vapor line approaching the maximum pressure of the phase boundary which are higher than the claimed uncertainty. A clear improvement over the phase envelope is reflected in the density data of Mastinu et al. [66] at low temperatures, below 100 K, accurately reproduced with an AARD = 0.9%. Other representative density data sets for this system are those of Jaeschke et al. [164] and Michels et al. [67], at temperatures between (270–420) K, which correspond well with an experimental uncertainty below 0.1% and yielding low AARDs (see Fig. 12). At even higher temperatures and pressures, the density data of Bennett et al. [68] show deviations that increase with the pressure, in line with an increasing experimental uncertainty. Apart from these properties, speed of sound data from Van Itterbeek et al. [69] also exist (see Fig. 18), but as the authors do not report an experimental uncertainty, we can only conclude the data are well represented.

For the system CO_2 + H_2 (see Fig. 4), the VLE data sets of Fandiño et al. [34] are quite comprehensive and well reproduced by the mixture model of Beckmüller et al. [39], with AAD of (0.13 and 0.45) mol-% for the saturated liquid and vapor lines, respectively. These results are within the corresponding experimental expanded (k = 2) uncertainties of (0.3 and 0.5) mol-% for the bubble and dew points, respectively. Similar good agreement is also present with the data of Tsang et al. [70], which extends the experimental pressure range up to 170 MPa. One reliable data set of density for these mixtures is the work of Souissi et al. [71] (see Fig. 13). The AARD is rather low, about 0.2%; however, the mixture model is not capable of reproducing the data within the extremely low specified uncertainty of 0.06%. Higher pressure and temperature ranges where studied by Cipollina et al. [72] and Mallu et al. [73], respectively. Unfortunately, both data sources show a large dispersion of the experimental values or the results show an offset compared to the data of Souissi et al. [71]. Finally, the density data of Cheng et al. [74] at high temperatures up to 670 K, are represented within the experimental expanded (k = 2) uncertainty by the EoS, with an AARD = 0.41%.

Fig. 5 shows the deviations of the bubble-point data and the dew-point data (in mol-%) for the binary mixtures ethane + hydrogen and propane + hydrogen. A total of 500 experimental VLE data points are included in this Fig. 5. The AAD deviations range from 0.012 for the 70 dew-point data of the system ethane + hydrogen, measured by Hiza et al. [75], to 2.5 for the 54 dew-point data of the system propane + hydrogen, measured by Burris et al. [76]. Mihara et al. [77] measured the density of these two mixtures. A total of 227 density data are analyzed. The results can be seen in Fig. 14. The AARD for the 154 data of the ethane + hydrogen system is 0.23 and 0.12 for the 73 data of the
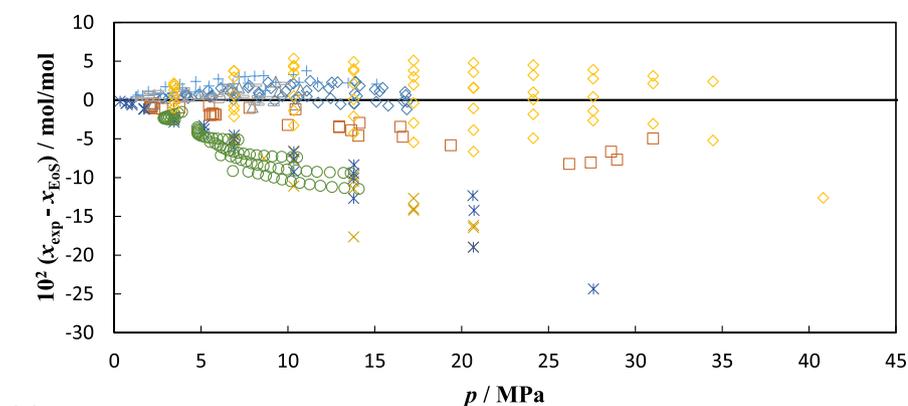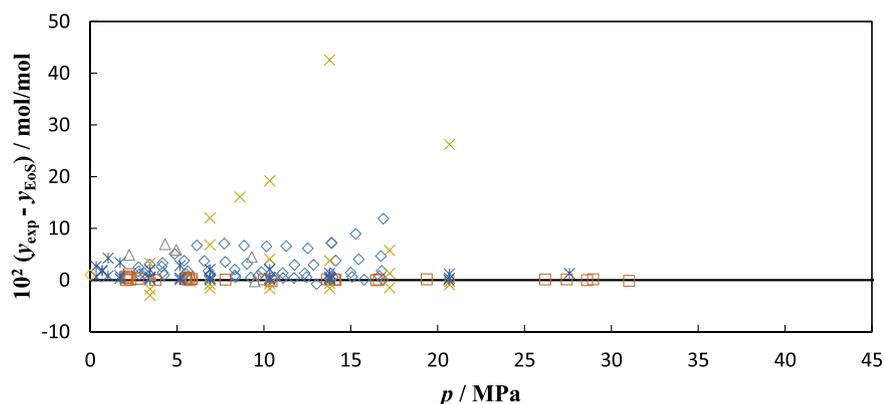
Fig. 6. Deviations of bubble-point data (a) and dew-point data (b) for the binary mixtures (n-C_4H_{10} + H_2), (i-C_4H_{10} + H_2), (n-C_5H_{12} + H_2), and (n-C_6H_{14} + H_2) with respect to the improved GERG-2008 EoS [30,39]: □ Aroyan et al. (n-C_4H_{10} + H_2, 1951), ◇ Klink et al. (n-C_4H_{10} + H_2, 1975), △ Nelson et al. (n-C_4H_{10} + H_2, 1943), × Dean et al. (i-C_4H_{10} + H_2, 1946), ○ Connolly et al. (n-C_5H_{12} + H_2, 1986), ✳Freitag et al. (n-C_5H_{12} + H_2, 1986), — Brunner et al. (n-C_6H_{14} + H_2, 1985), ▬ Fu et al. (n-C_6H_{14} + H_2, 1994), + Gao et al. (n-C_6H_{14} + H_2, 2001), ◇ Nichols et al. (n-C_6H_{14} + H_2, 1957).

propane + hydrogen system. The temperature range for these measurements is (298–348) K and the pressures are up to 9.3 MPa. Mason et al. [78] also give densities for these two systems, but only at atmospheric pressure and 289 K.

In the same way, Fig. 6 shows the deviations of the bubble-point data and dew-point data (in mol-%) for the binary mixtures n-butane + hydrogen, i-butane + hydrogen, pentane + hydrogen, and hexane + hydrogen. In this case, a total of 563 experimental VLE data points are included in Fig. 6. The AAD for these sets of data range from 0.13 for the 28 dew-point data of the system n-butane + hydrogen, measured by Aroyan et al. [79], to 9.5 for the 22 bubble-point data of the system i-butane + hydrogen, measured by Dean et al. [80]. Fig. 15 depicts the deviations of the density data of these mixtures. A total of 482 density data are analyzed, of which 421 correspond to the system hexane + hydrogen, measured by Nichols et al. [81]. These 421 experimental density data for the system hexane + hydrogen cover a temperature range from 278 K to 511 K and pressures up to 68.9 MPa. The AARD of these data is as low as 0.034, with a Max ARD of 13.

Regarding the VLE of CO + H_2 (see Fig. 7), the data base is more limited in the number of points and the temperature, pressure, and composition ranges. In addition, some authors, such as Verschoyle [82], do not report a clear overall experimental uncertainty. The most reliable data for comparison is the work of Tsang et al. [83], with the mixture model of Beckmüller et al. [39] representing the data successfully, with AAD = 0.6 mol-% for the saturated liquid line and AAD = 0.8 mol-% for the saturated vapor line. With respect to density data (see Fig. 16), the

most recent data of Cipollina et al. [72] yield AARD = 2.4%, which is too high for this system and does not match the AARD from the same authors, except for the system CO_2 + H_2 of 0.5%. Lower differences are obtained in our work when comparing to the data of Scott [84] and Townend et al. [85], with AARD of 0.25% and 0.16%, respectively. Although the authors do not report any overall experimental uncertainty, the disagreement could be explained by considering the relatively high content of impurities present in the studied mixtures. The same as mentioned above for the speed of sound data (see Fig. 18) from Van Itterbeek et al. [69] applies in this system.

The VLE of the system water + hydrogen was studied by Setthanan et al. [86], Kling et al. [87], Wiebe et al. [88], and Shoor et al. [89], while the VLE of the system hydrogen sulfide + hydrogen was studied by Yorizane et al. [90]. There is a total of 55 experimental VLE data for the system with water and 22 for the system with hydrogen sulfide, whose deviations from the GERG-2008 EoS (bubble-point data and dew-point data, in mol-%) are presented in Fig. 8. The data set from Wiebe et al. [88] is the more numerous (40) and has a broader range in temperature and pressure, from 273 K to 373 K, and up to 101 MPa. The AAD of this set of data is 0.51 with a Max AD of 1.4. Note that the GERG-2008 EoS estimates the dew points fairly well, but not the bubble points for the water + hydrogen, even taking into account the low solubility of hydrogen into liquid water. The GERG-2008 model greatly overpredicts the liquid saturation line, estimating an open phase envelope contrary to the experimental data. No experimental data on density, speed of sound or other caloric properties have been found for these two binary systems.
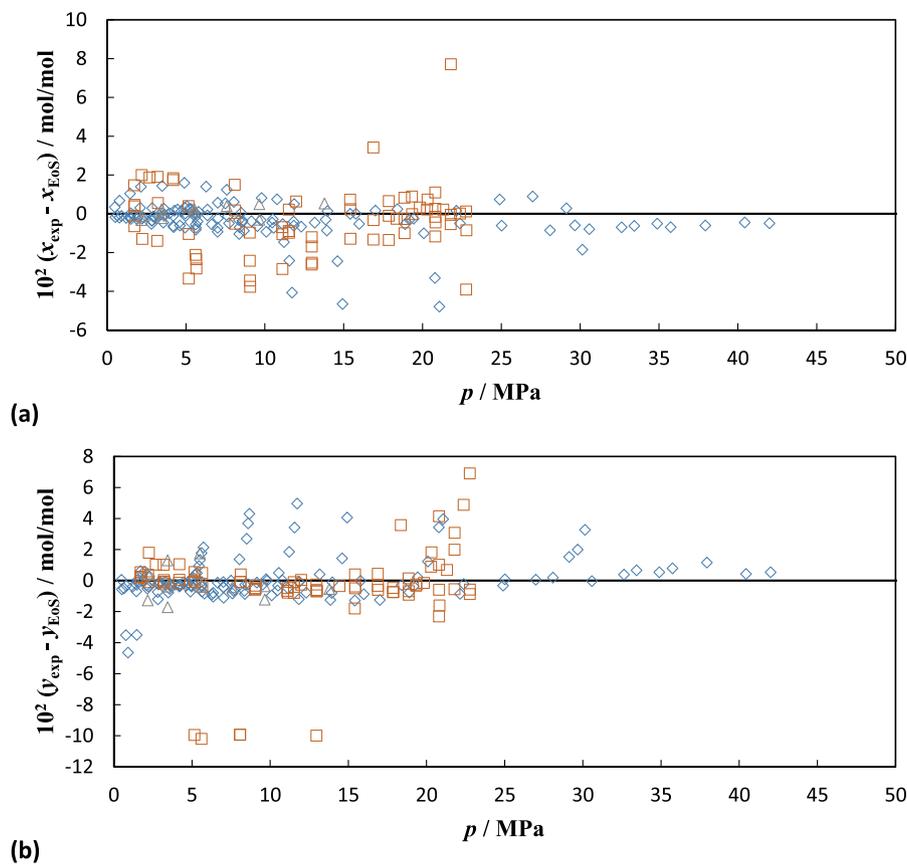
Fig. 7. Deviations of bubble-point data (a) and dew-point data (b) for the binary mixtures (CO + H$_2$) with respect to the improved GERG-2008 EoS [30,39]: △ Akers et al. (CO + H$_2$, 1957), ◇ Tsang et al. (CO + H$_2$, 1981), □ Verschoyle et al. (CO + H$_2$, 1931).
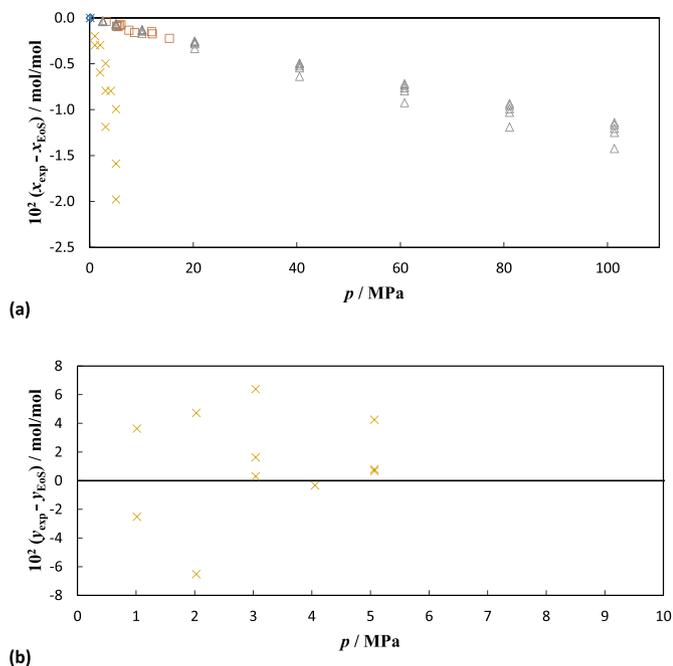
Fig. 8. Deviations of bubble-point data (a) and dew-point data (b) for the binary mixtures (H$_2$O + H$_2$) and (H$_2$S + H$_2$) with respect to the improved GERG-2008 EoS [30,39]: □ Kling et al. (H$_2$O + H$_2$, 1991), ◇ Setthanan et al. (H$_2$O + H$_2$, 2006), ✳ Shoor et al. (H$_2$O + H$_2$, 1969), △ Wiebe et al. (H$_2$O + H$_2$, 1934), ✕ Yorizane et al. (H$_2$S + H$_2$, 1969).

A total of 487 experimental VLE data points for the binary systems of helium + hydrogen have been published by Yamanishi et al. [91], Hiza [92], Hiza [93], Sneed et al. [94], Streett et al. [95], and Sonntag et al. [96]; a total of 378 points for the system argon + hydrogen can be found at Calado et al. [97] and Volk et al. [98], while a total of 323 points for the system neon + hydrogen have been reported by Streett et al. [99], Heck et al. [100], and Zelfde et al. [101]. Their deviations can be seen in Fig. 9. Most of these data are for pressures below 10 MPa, except the data from Calado et al. [97], which covers a range up to 52 MPa. Temperature ranges for the binary system helium + hydrogen are between 15 K and 30 K, and between 80 K and 140 K for the binary system argon + hydrogen. The AAD (in mol-%) for these sets of data range from 0.22 for the 21 bubble-point data of the system helium + hydrogen, measured by Hiza [92], to 19 for the 132 bubble-point data of the system argon + hydrogen, as measured by Calado et al. [97]. The weakness of the Blackham [35] mixture model is describing the VLE and density properties in the following conditions: (i) for the hydrogen + helium system, in the critical region and at temperatures below 15 K and above 32 K with pressures below 1 MPa and above 11 MPa, (ii) for the hydrogen + neon system, in the critical region and also for molar fractions of neon between (0.03–0.3). It is worth highlighting the really high discrepancy obtained for the argon + hydrogen system in the whole phase envelope according to the GERG-2008. Again, the GERG EoS yields a false open phase envelope, overestimating the pressures at the cryogenic temperatures of experimental data from Calado et al. [97] and Volk et al. [98]. This can be understood considering that the development of the GERG was focused on natural gas mixtures and its normal range of validity is for $T > 90$ K. A total of 290 density data points for the system argon + hydrogen are also available in the scientific literature at Scholz et al. [102], Tanner et al. [103], and Zandbergen et al. [104], while a total of

(a)

(b)
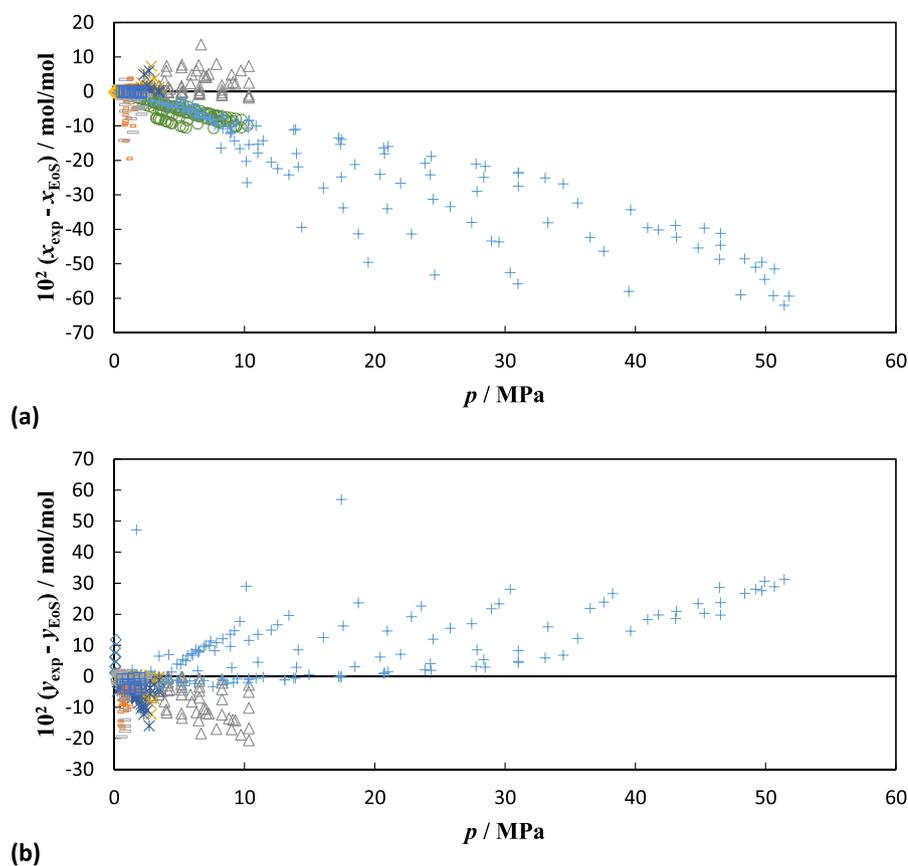
Fig. 9. Deviations of bubble-point data (a) and dew-point data (b) for the binary mixtures (He + H$_2$), (Ar + H$_2$) and (Ne + H$_2$) with respect to the improved GERG-2008 EoS [30,39]: □ Hiza et al. (He + H$_2$, 1972), □ Hiza et al. (He + H$_2$, 1981), △ Sneed et al. (He + H$_2$, 1968), ✳ Sonntag et al. (He + H$_2$, 1964), ✕ Street et al. (He + H$_2$, 1964), ◇ Yamanishi et al. (He + H$_2$, 1992), + Calado et al. (Ar + H$_2$, 1960), ○ Volk et al. (Ar + H$_2$, 1979), − Heck et al. (Ne + H$_2$, 1966), ▬ Street et al. (Ne + H$_2$, 1965), ◇ Zelfde et al. (Ne + H$_2$, 1974).

229 density points are available for the system neon + hydrogen at Streett [105] and Güsewell et al. [106]. The deviations of these density data from the GERG-2008 EoS are represented in Fig. 16. The AARD for the sets of density data for argon + hydrogen range from 0.32% for the data of Scholz et al. [102] to 1.4% for the data of Zandbergen et al. [104], while the AARD for the sets of density data of neon + hydrogen are around 5.6%. The absolute deviation for this last set of data can be as high as 9.3% for the argon + hydrogen system, but this set of data is also the one that reaches the lowest temperature (170 K). In the case of the neon + hydrogen system, the maximum absolute deviation is 27%, at temperatures between (25–31) K. The range of pressures for the three sets of data is around 10 MPa. There are also a few speed of sound data, only 8, for these two binary mixtures, published by Van Itterbeek et al. [107] in 1946, and their deviations are shown in Fig. 18.

Fig. 10 shows the deviations of the bubble-point data and the dew-point data (in mol-%) for the binary mixture ammonia + hydrogen. A total of 246 experimental VLE data points are included in this Fig. 10. The AAD deviations range from 0.0004 to 1.1 for the dew-point data and 0.78 for the bubble-point data of the system ammonia + hydrogen. A total of 172 density data are analyzed for ammonia + hydrogen mixtures by Kazarnovskiy et al. [108] and Hongo et al. [109]. These results can be seen in Fig. 17.

The huge asymmetry between ammonia and hydrogen, due to their very different critical points (T_c (NH$_3$) = 405.56 K *vs.* T_c (H$_2$) = 33.145 K), made it necessary to develop a departure function in the EoS of Neumann et al. [32]. In general, the experimental phase envelopes are well described by this model, with overall AAD from all the datasets

considered in this work of 0.5 mol-%, even for lower temperatures where the phase boundary becomes steeper. The solubility data sets of Wiebe et al. [110] and Wiebe et al. [111] agree with the model within an AAD of 1.1 mol-% and 0.35 mol-%, respectively. Unfortunately, they do not indicate any experimental uncertainty. Reamer et al. [112] measured dew points and calculated bubble points for this system in the range (280–390) K up to 4.2 MPa. They declared an experimental uncertainty of only 0.2 mol-%, which is too optimistic. A more reasonable uncertainty of 1 mol-% yields that nearly all the deviations remain within the uncertainty, with AAD of 0.15 mol-% for the dew points and 0.78 mol-% for the bubble points. Other data sets found in the literature are of lower quality. With respect to density data, Kazarnovskiy et al. [108] measured molar volumes up to 155 MPa with a 2% experimental expanded (k = 2) uncertainty. These data are represented with deviations of half the uncertainty, AARD = 1.1%. Furthermore, Hongo et al. [109] determined densities up to 6.6 MPa, but they do not claim any uncertainty. In any case, the relative discrepancies are on average of 0.67%, increasing slightly with the pressure as usual, thus suggesting a good agreement.

Fig. 19 depicts the deviation of the 78 available molar heat capacity data for the binary system nitrogen + hydrogen, measured by Knapp et al. [113]. Fig. 20 shows the deviation of the molar heat capacities measured by Wormald et al. [114] for the binary systems methane + hydrogen and nitrogen + hydrogen. Finally, Fig. 21 shows the percentage deviations of the Joule-Thompson data for the binary system methane + hydrogen, measured by Randelman et al. [115].

(a)

(b)
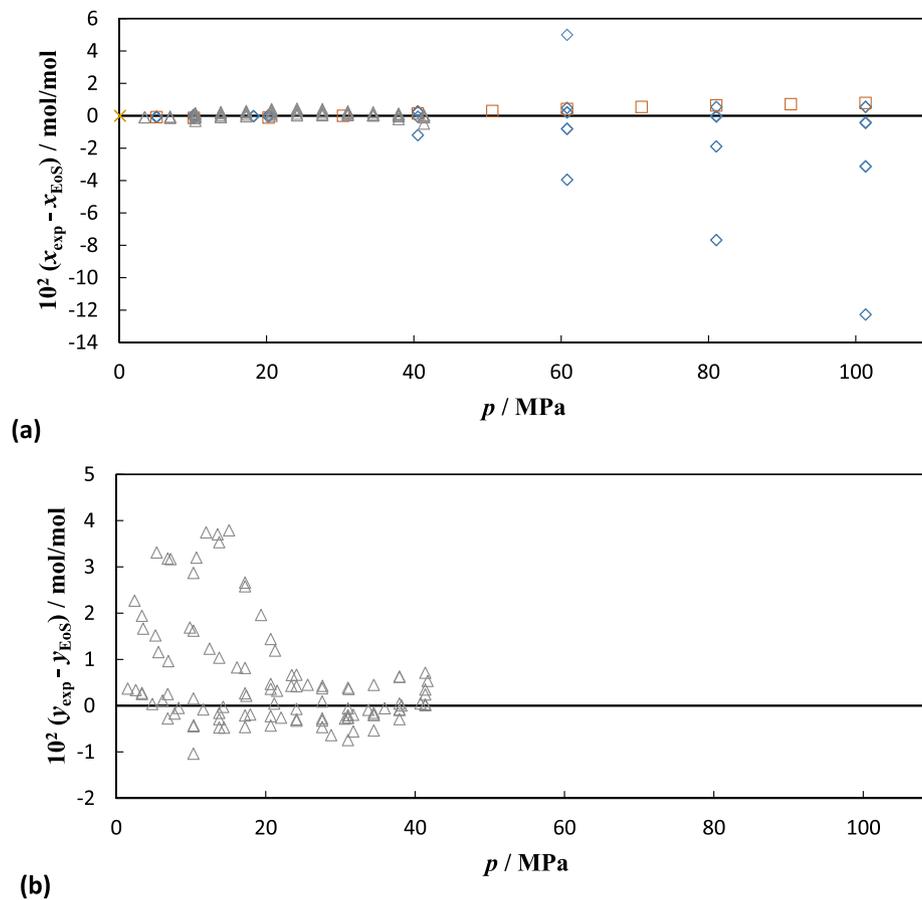
Fig. 10. Deviations of bubble-point data (a) and dew-point data (b) for the binary mixtures (NH$_3$ + H$_2$) with respect to the improved GERG-2008 EoS [30,39]: ✕ Moore et al. (1972), △ Reamer et al. (1959), ◇ Wiebe et al. (1934), □ Wiebe et al. (1937).
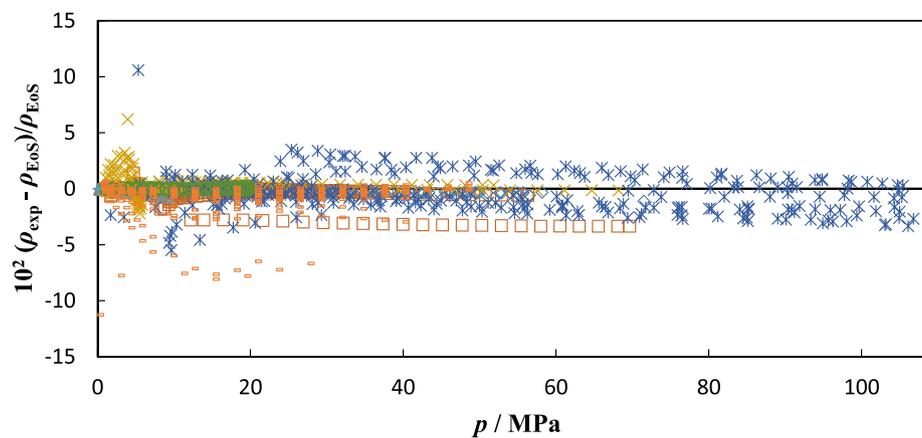
Fig. 11. Percentage deviations of homogeneous density data for the binary mixtures (CH$_4$ + H$_2$) with respect to the improved GERG-2008 EoS [30,39]: ○ Hernández-Gómez et al. (2018), ○ Jett et al. (1994), ✕ Machado et al. (1988), ✳ Magee et al. (1985), ◇ Magee et al. (1986), □ Mason et al. (1961), + Mihara et al. (1977), △ Mueller et al. (1961).

5. Conclusions

The basis for the development of multiparameter equations of state is experimental data for several thermodynamic properties. The quality and extent of these data determine the accuracy of the model. The paper describing the GERG-2008 stated that it would be worthwhile to develop different generalized departure functions for several binary mixtures, hydrogen with other components among them. For the development of

these generalized, or binary-specific, departure functions, as well as for the development of reducing functions for the mixture density and temperature, dependent on the composition, an extended set of high-quality experimental data of thermodynamic properties of binary mixtures of hydrogen with the rest of the components of natural gas is needed.

Only the methane + hydrogen binary system, of the 20 possible binary mixtures of hydrogen with the rest of the components considered
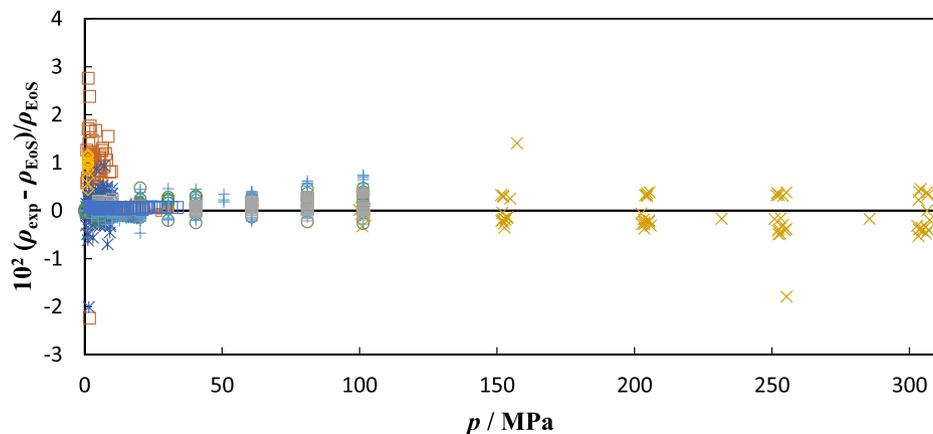
Fig. 12. Percentage deviations of homogeneous density data for the binary mixtures (N$_2$ + H$_2$) with respect to the improved GERG-2008 EoS [30,39]: ▬ Bartlett et al. (1928/1930), ╋ Bartlett et al. (1927), ○ Bennett et al. (1952), × Hernández-Gómez et al. (2017), ◇ Jaeschke et al. (1991), ▬ Kestin et al. (1982), □ Mastinu (1967), ◇ Michels et al. (1949), □ Verschoyle et al. (1926), △ Wiebe et al. (1938), − Zandbergen et al. (1967).
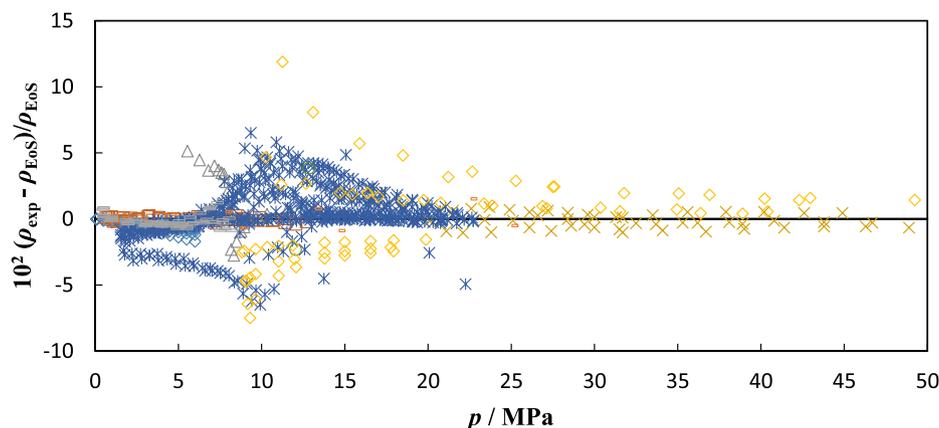
Fig. 13. Percentage deviations of homogeneous density data for the binary mixtures (CO$_2$ + H$_2$) with respect to the improved GERG-2008 EoS [30,39]: ✳ Ababio et al. (1993), □ Alsiyabi (2013), ◇ Cheng et al. (2019), ▬ Cipollina et al. (2007), × Mallu et al. (1990), ◇ Pinho et al. (2015), ○ Sanchez-Vicente et al. (2013), ✳ Souissi et al. (2017), ╋ Tsankova et al. (2019), − Zhang et al. (2002).
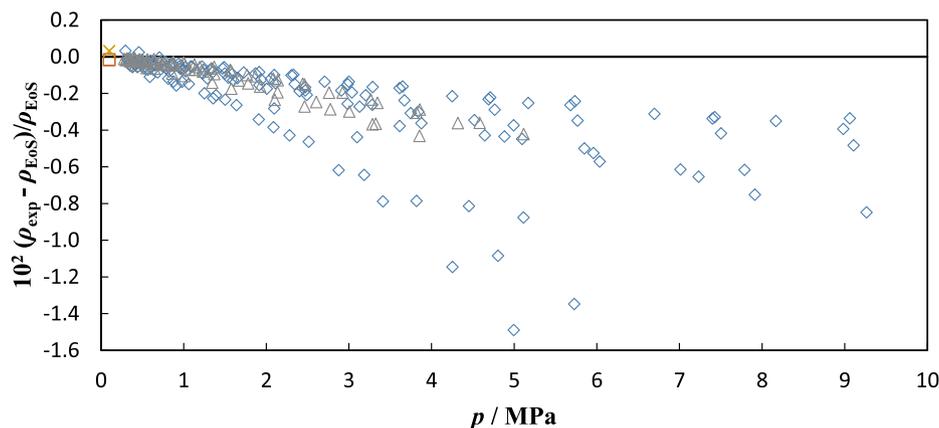
Fig. 14. Percentage deviations of homogeneous density data for the binary mixtures (C$_2$H$_6$ + H$_2$) and (C$_3$H$_8$ + H$_2$) with respect to the improved GERG-2008 EoS [30, 39]: △ Mason et al. (C$_2$H$_6$ + H$_2$, 1961), □ Mihara et al. (C$_2$H$_6$ + H$_2$, 1977), ◇ Mason et al. (C$_3$H$_8$ + H$_2$, 1961), × Mihara et al. (C$_3$H$_8$ + H$_2$, 1977).
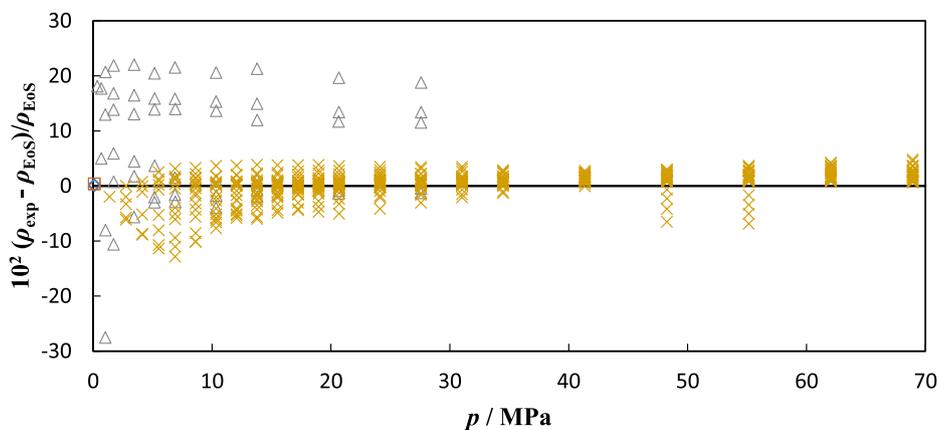
Fig. 15. Percentage deviations of homogeneous density data for the binary mixtures (C$_4$H$_{10}$ + H$_2$), (C$_5$H$_{12}$ + H$_2$) and (C$_6$H$_{14}$ + H$_2$) with respect to the improved GERG-2008 EoS [30,39]: △ Mason et al. (C$_4$H$_{10}$ + H$_2$, 1961), ◇ Freitag et al. (C$_5$H$_{12}$ + H$_2$, 1986), △ Mason et al. (C$_5$H$_{12}$ + H$_2$, 1961), □ Nichols et al. (C$_6$H$_{14}$ + H$_2$, 1957).
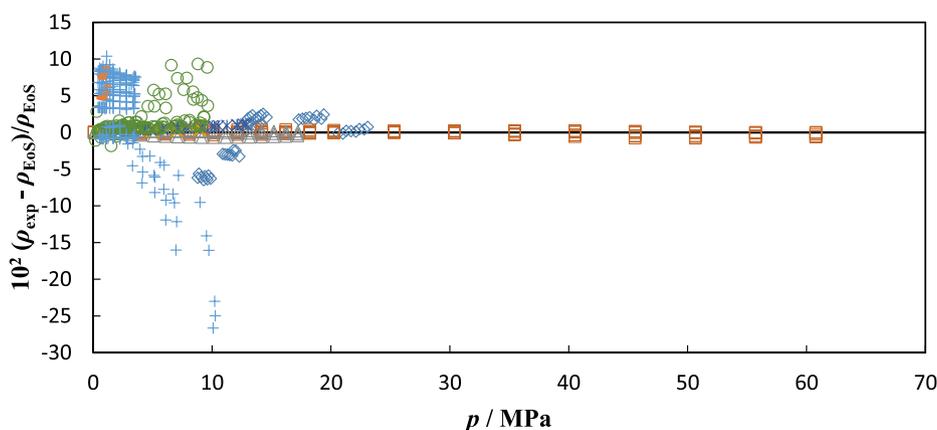
Fig. 16. Percentage deviations of homogeneous density data for the binary mixtures (CO + H$_2$), (Ar + H$_2$), and (Ne + H$_2$) with respect to the improved GERG-2008 EoS [30,39]: ✕ Cipollina et al. (CO + H$_2$, 2007), ◇ Scott et al. (CO + H$_2$, 1929), △ Townend et al. (CO + H$_2$, 1931), □ Scholz et al. (Ar + H$_2$, 2020), ✕ Tanner et al. (Ar + H$_2$, 1930), ○ Zandbergen et al. (Ar + H$_2$, 1967), ▬ Güsewell et al. (Ne + H$_2$, 1970), + + Street (Ne + H$_2$, 1973).
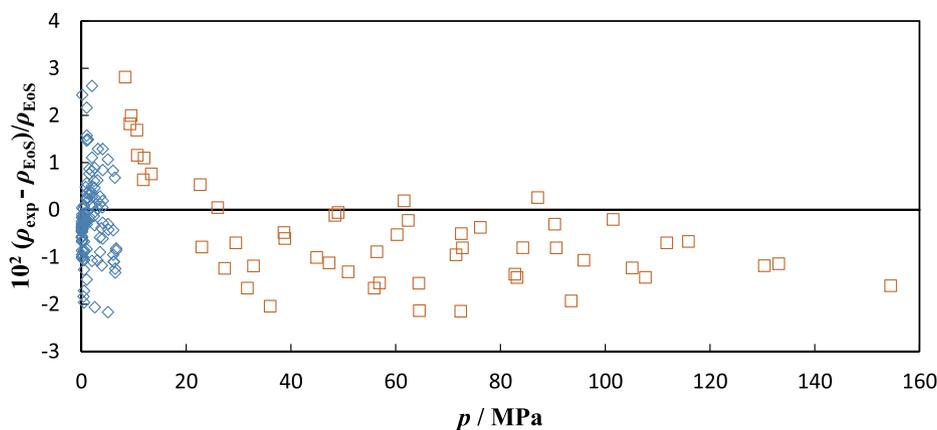
Fig. 17. Percentage deviations of homogeneous density data for the binary mixtures (NH$_3$ + H$_2$) with respect to the improved GERG-2008 EoS [30,39]: ◇ Hongo et al.(1978), □ Kanarnovskiy et al. (1968).

by the GERG-2008 model, has a binary specific departure function included in the current GERG-2008 EoS. A recent study by Beckmüller et al. [39] has developed four equations of state for the binary systems of hydrogen with methane, nitrogen, carbon dioxide, and carbon monoxide. Nevertheless, they recognize that new highly accurate data for these systems are still required for further improvements and a more comprehensive validation, especially for the binary system hydrogen + carbon monoxide. For the rest of the binary systems, the amount of
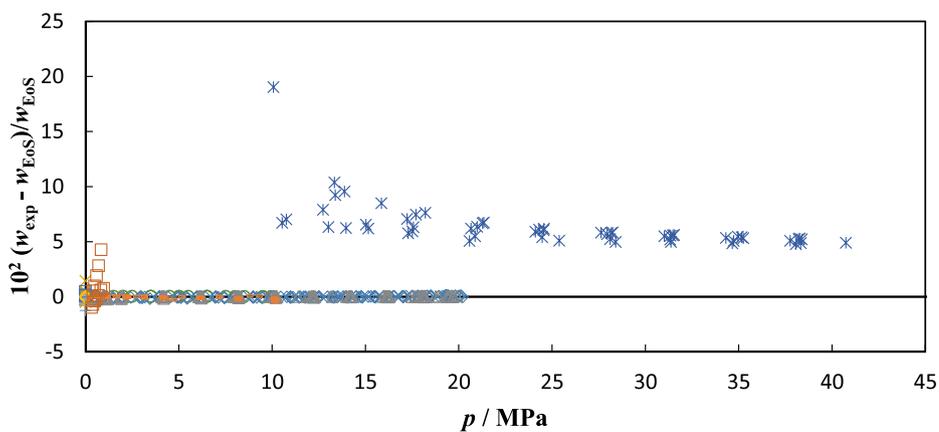
Fig. 18. Percentage deviations of speed of sound data for the binary mixtures (CH_4 + H_2), (N_2 + H_2), (CO_2 + H_2), (O_2 + H_2), (CO + H_2), (He + H_2), (Ar + H_2) and (Ne + H_2) with respect to the improved GERG-2008 EoS [30,39]: ○ Maurer (CH_4 + H_2, 2021), ◇ Lozano-Martín et al. (CH_4 + H_2, 2020), × Itterbeek et al. (N_2 + H_2, 1949), △ Lozano-Martín et al. (N_2 + H_2, 2021), ✳ Alsiyabi et al. (CO_2 + H_2, 2013), ▬ Maurer (CO_2 + H_2, 2021), + Itterbeek et al. (O_2 + H_2, 1949), − Itterbeek et al. (CO + H_2, 1949), □ Itterbeek et al. (He + H_2, 1946), ◇ Itterbeek et al. (Ar + H_2, 1946), □ Güsewell et al. (Ne + H_2, 1970).
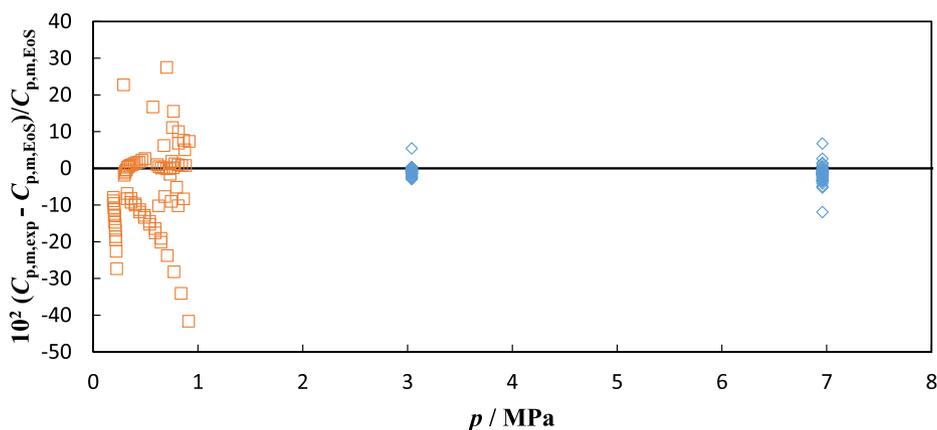
Fig. 19. Percentage deviations of molar isobaric heat capacity data for the binary mixtures (N_2 + H_2) and (Ne + H_2) with respect to the improved GERG-2008 EoS [30,39]: ◇ Knapp et al. (N_2 + H_2, 1976), □ Brouwer et al. (Ne + H_2, 1970).
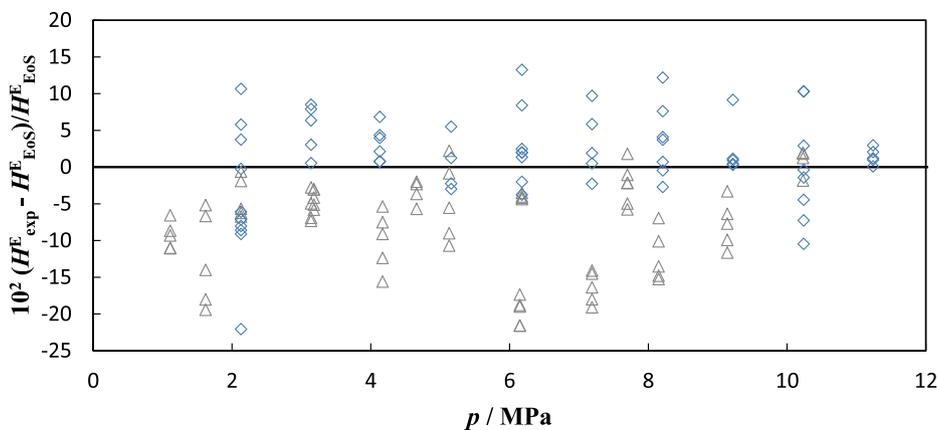
Fig. 20. Percentage deviations of excess enthalpy data for the binary mixtures (CH_4 + H_2) and (N_2 + H_2) with respect to the improved GERG-2008 EoS [30,39]: △ Wormald et al. (CH_4 + H_2, 1977), ◇ Wormald et al. (N_2 + H_2, 1977).

experimental data available is very poor. VLE data are available for the binary mixtures of hydrogen with ethane, propane, butane, iso-butane, pentane, hexane, water, hydrogen sulfide, helium, and argon. Density data are available for the binary mixtures of hydrogen with ethane,

propane, butane, pentane, hexane, and argon. Finally, very few speed of sound or other caloric properties data are available, and only for the binary mixtures of hydrogen with oxygen, helium, and argon. There is a real need for density and speed of sound data for the binary systems of
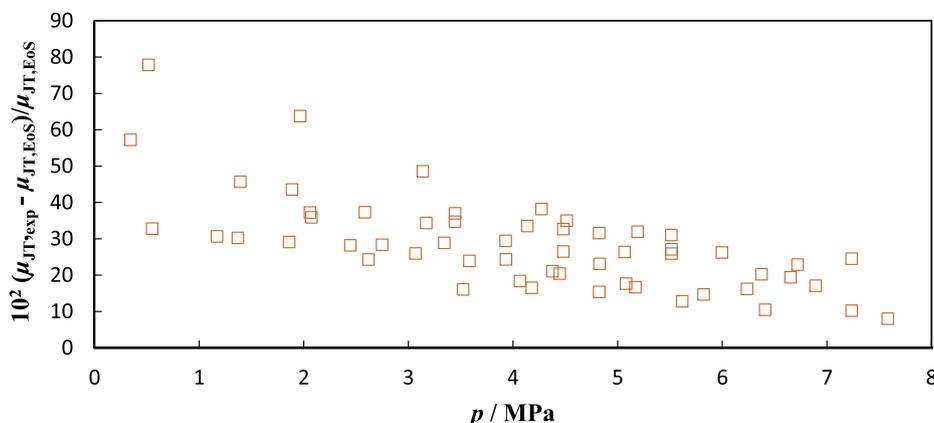
Fig. 21. Percentage deviations of Joule-Thomson data for the binary mixtures (CH_4 + H_2) with respect to the improved GERG-2008 EoS [30,39]: □ Randelmand et al. (1988).

hydrogen with water, hydrogen sulfide, helium, and argon, as well as all the linear hydrocarbons from ethane to decane, including iso-butane and iso-pentane. Not only mixtures of hydrogen with the components of natural gas are of interest for the industry. A recent survey on industrial requirements for thermodynamic and transport properties presented by Kontogeorgis et al. [4], pointed out that accurate prediction of the fluid-liquid phase equilibrium and dew point calculations for mixtures, including heavier hydrocarbons and hydrogen, is crucial.

For the development of new EoS, not only experimental data of binary mixtures with hydrogen will be necessary, but also binary mixtures between the rest of the components of natural gas. As an example, for the binary mixtures with CO_2, a review of available models and experimental data is presented by Li et al. [116,117].

Besides the experimental data of binary mixtures, which are relevant for the development of new equations of state, it is also important to check the capability of the current or newly developed EoS with multicomponent mixtures containing hydrogen. In this sense, it is important to determine the density, speed of sound or phase equilibrium properties of ternary or multicomponent mixtures containing hydrogen. Mixtures of natural gases of known composition (gravimetrically prepared, simulating typical NG mixtures) with varying amounts of hydrogen, not only up to 20 mol-% of hydrogen, but also with higher hydrogen contents, are of great interest.

It is also very important to extend the ranges of validity of temperature and pressures of the thermodynamic models, in order to cover the working ranges of some hydrogen storage systems. In this sense, it is necessary to obtain high quality experimental data of binary mixtures of hydrogen with other components at high pressures (over 70 MPa) or at very low temperatures (below 20 K). Another research field of great interest is the study of the effect of traces and small amounts of impurities in the behavior of pure hydrogen or hydrogen mixtures.

In conclusion, we can say that there is still an acute need for accurate, reliable, and thermodynamically consistent experimental data of hydrogen and hydrogen mixtures. Nevertheless, quality, and a good selection of compositions, temperature, and pressure ranges, is more important than quantity.

Declaration of competing interest

The authors declare that they have no known competing financial interests or personal relationships that could have appeared to influence the work reported in this paper.

Acknowledgements

Appendix A. Supplementary data

Supplementary data to this article can be found online at https://doi.org/10.1016/j.renene.2022.08.096.

References

[1] IEA, International Energy Agency, The Future of Hydrogen, OECD, Organisation for Economic Co-operation and Development, 2019. Paris, https://www.iea.org/reports/the-future-of-hydrogen.

[2] A. Velazquez Abad, P.E. Dodds, Green hydrogen characterisation initiatives: definitions, standards, guarantees of origin, and challenges, Energy Pol. 138 (2020) 111300, https://doi.org/10.1016/j.enpol.2020.111300.

[3] E. Hendriks, G.M. Kontogeorgis, R. Dohrn, J.C. De Hemptinne, I.G. Economou, L.F. Žilnik, et al., Industrial requirements for thermodynamics and transport properties, Ind. Eng. Chem. Res. 49 (2010) 11131–11141, https://doi.org/10.1021/ie101231b.

[4] G.M. Kontogeorgis, R. Dohrn, I.G. Economou, J.-C. de Hemptinne, A. ten Kate, S. Kuitunen, et al., Industrial requirements for thermodynamic and transport properties: 2020, Ind. Eng. Chem. Res. 60 (2021) 4987–5013, https://doi.org/10.1021/acs.iecr.0c05356.

[5] A. Hassanpouryouzband, E. Joonaki, K. Edlmann, N. Heinemann, J. Yang, Thermodynamic and transport properties of hydrogen containing streams, Sci. Data 7 (2020) 222, https://doi.org/10.1038/s41597-020-0568-6.

[6] D. Lozano-Martín, A. Moreau, D. Vega-Maza, C.R. Chamorro, Thermophysical properties of hydrogen mixtures relevant for the development of the hydrogen economy: analysis of available experimental data and thermodynamic models, SSRN Electron. J. (2021), https://doi.org/10.2139/ssrn.3939438.

[7] P. Nikolaidis, A. Poullikkas, A comparative overview of hydrogen production processes, Renew. Sustain. Energy Rev. 67 (2017) 597–611, https://doi.org/10.1016/j.rser.2016.09.044.

[8] D. Das, T.N. Veziroğlu, Hydrogen production by biological processes: a survey of literature, Int. J. Hydrogen Energy 26 (2001) 13–28, https://doi.org/10.1016/S0360-3199(00)00058-6.

[9] A. Steinfeld, Solar thermochemical production of hydrogen - a review, Sol. Energy 78 (2005) 603–615, https://doi.org/10.1016/j.solener.2003.12.012.

[10] R. Kothari, D. Buddhi, R.L. Sawhney, Comparison of environmental and economic aspects of various hydrogen production methods, Renew. Sustain. Energy Rev. 12 (2008) 553–563, https://doi.org/10.1016/j.rser.2006.07.012.

[11] J.H. Alstrum-Acevedo, M.K. Brennaman, T.J. Meyer, Chemical approaches to artificial photosynthesis. 2, Inorg. Chem. 44 (2005) 6802–6827, https://doi.org/10.1021/ic050904r.

[12] F. Razi, I. Dincer, A critical evaluation of potential routes of solar hydrogen production for sustainable development, J. Clean. Prod. 264 (2020) 121582, https://doi.org/10.1016/j.jclepro.2020.121582.

[13] Z. Abdin, A. Zafaranloo, A. Rafiee, W. Mérida, W. Lipiński, K.R. Khalilpour, Hydrogen as an energy vector, Renew. Sustain. Energy Rev. 120 (2020) 109620, https://doi.org/10.1016/j.rser.2019.109620.

[14] F. Dingenen, S.W. Verbruggen, Tapping hydrogen fuel from the ocean: a review on photocatalytic, photoelectrochemical and electrolytic splitting of seawater, Renew. Sustain. Energy Rev. 142 (2021), 110866, https://doi.org/10.1016/j.rser.2021.110866.

[15] M. Handwerker, J. Wellnitz, H. Marzbani, Comparison of hydrogen powertrains with the battery powered electric vehicle and investigation of small-scale local hydrogen production using renewable energy, Hydrogen 2 (2021) 76–100, https://doi.org/10.3390/hydrogen2010005.

[16] D.K. Ross, Hydrogen storage: the major technological barrier to the development of hydrogen fuel cell cars, Vacuum 80 (2006) 1084–1089, https://doi.org/10.1016/j.vacuum.2006.03.030.

[17] Y. Balali, S. Stegen, Review of energy storage systems for vehicles based on technology, environmental impacts, and costs, Renew. Sustain. Energy Rev. 135 (2021), 110185, https://doi.org/10.1016/j.rser.2020.110185.

[18] S. Chabab, P. Théveneau, C. Coquelet, J. Corvisier, P. Paricaud, Measurements and predictive models of high-pressure H2 solubility in brine (H2O + NaCl) for underground hydrogen storage application, Int. J. Hydrogen Energy 45 (2020) 32206–32220, https://doi.org/10.1016/j.ijhydene.2020.08.192.

[19] M. Yue, H. Lambert, E. Pahon, R. Roche, S. Jemei, D. Hissel, Hydrogen energy systems: a critical review of technologies, applications, trends and challenges, Renew. Sustain. Energy Rev. 146 (2021), 111180, https://doi.org/10.1016/j.rser.2021.111180.

[20] I.A. Hassan, H.S. Ramadan, M.A. Saleh, D. Hissel, Hydrogen storage technologies for stationary and mobile applications: review, analysis and perspectives, Renew. Sustain. Energy Rev. 149 (2021), 111311, https://doi.org/10.1016/j.rser.2021.111311.

[21] C.J. Quarton, S. Samsatli, Power-to-gas for injection into the gas grid: what can we learn from real-life projects, economic assessments and systems modelling? Renew. Sustain. Energy Rev. 98 (2018) 302–316, https://doi.org/10.1016/j.rser.2018.09.007.

[22] S. Griffiths, B.K. Sovacool, J. Kim, M. Bazilian, J.M. Uratani, Industrial decarbonization via hydrogen: a critical and systematic review of developments, socio-technical systems and policy options, Energy Res. Social Sci. 80 (2021), 102208, https://doi.org/10.1016/j.erss.2021.102208.

[23] K. Dahal, S. Brynolf, C. Xisto, J. Hansson, M. Grahn, T. Grönstedt, et al., Techno-economic review of alternative fuels and propulsion systems for the aviation sector, Renew. Sustain. Energy Rev. 151 (2021), 111564, https://doi.org/10.1016/j.rser.2021.111564.

[24] J.W. Leachman, R.T. Jacobsen, S.G. Penoncello, E.W. Lemmon, Fundamental equations of state for parahydrogen, normal hydrogen, and orthohydrogen, J. Phys. Chem. Ref. Data 38 (2009) 721–748, https://doi.org/10.1063/1.3160306.

[25] E.W. Lemmon, I.H. Bell, M.L. Huber, M.O. McLinden, E.W. Lemmon, I.H. Bell, M.L. Huber, M.O. McLinden, NIST Standard Reference Database 23: Reference Fluid Thermodynamic and Transport Properties-REFPROP, Version 10.0, Natl Inst Stand Technol Stand Ref Data Progr, 2018.

[26] R.T. Jacobsen, J.W. Leachman, S.G. Penoncello, E.W. Lemmon, Current status of thermodynamic properties of hydrogen, Int. J. Thermophys. 28 (2007) 758–772, https://doi.org/10.1007/s10765-007-0226-7.

[27] B.A. Younglove, Thermophysical properties of fluids. I. Argon, ethylene, parahydrogen, nitrogen, nitrogen trifluoride, and oxygen, J. Phys. Chem. Ref. Data 11 (Suppl. No. 1) (1982) 1–353.

[28] R. Klimeck, Entwicklung einer Fundamentalgleichung für Erdgase für das Gas- und Flüssigkeitsgebiet sowie das Phasengleichgewicht, Ph.D. Dissertation. Ruhr-Universität Bochum, Bochum, Germany, 2000.

[29] O. Kunz, R. Klimeck, W. Wagner, M. Jaeschke, GERG Technical Monograph 15 the GERG-2004 wide-range equation of state for natural gases and other mixtures. Düsseldorf, 2007.

[30] O. Kunz, W. Wagner, The GERG-2008 wide-range equation of state for natural gases and other mixtures: an expansion of GERG-2004, J. Chem. Eng. Data 57 (2012) 3032–3091, https://doi.org/10.1021/je300655b.

[31] N. Sakoda, K. Shindo, K. Shinzato, M. Kohno, Y. Takata, M. Fujii, Review of the thermodynamic properties of hydrogen based on existing equations of state, Int. J. Thermophys. 31 (2010) 276–296, https://doi.org/10.1007/s10765-009-0699-7.

[32] T. Neumann, M. Thol, I.H. Bell, E.W. Lemmon, R. Span, Fundamental thermodynamic models for mixtures containing ammonia, Fluid Phase Equil. 511 (2020), 112496, https://doi.org/10.1016/j.fluid.2020.112496.

[33] T.A. Demetriades, R.S. Graham, A new equation of state for CCS pipeline transport: calibration of mixing rules for binary mixtures of CO2 with N2, O2 and H2, J. Chem. Thermodyn. 93 (2016) 294–304, https://doi.org/10.1016/j.jct.2015.07.045.

[34] O. Fandiño, J.P.M. Trusler, D. Vega-Maza, Phase behavior of (CO2 + H2) and (CO2 + N2) at temperatures between (218.15 and 303.15) K at pressures up to 15 MPa, Int. J. Greenh. Gas Control 36 (2015) 78–92, https://doi.org/10.1016/j.ijggc.2015.02.018.

[35] T.M. Blackham, A Generalized Helmholtz Energy Functional Form For Thermodynamic Properties of Binary Mixtures Containing Hydrogen, Neon, and Helium, Washington State University, 2016.

[36] A. Aasen, M. Hammer, S. Lasala, J.N. Jaubert, Ø. Wilhelmsen, Accurate quantum-corrected cubic equations of state for helium, neon, hydrogen, deuterium and their mixtures, Fluid Phase Equil. 524 (2020), 112790, https://doi.org/10.1016/j.fluid.2020.112790.

[37] A. Aasen, M. Hammer, Å. Ervik, E.A. Müller, Ø. Wilhelmsen, Equation of state and force fields for Feynman-Hibbs-corrected Mie fluids. I. Application to pure helium, neon, hydrogen, and deuterium, J. Chem. Phys. 151 (2019) 1–19, https://doi.org/10.1063/1.5111364.

[38] A. Aasen, M. Hammer, E.A. Müller, Ø. Wilhelmsen, Equation of state and force fields for Feynman-Hibbs-corrected Mie fluids. II. Application to mixtures of helium, neon, hydrogen, and deuterium, J. Chem. Phys. 152 (2020) 074507, https://doi.org/10.1063/1.5136079.

[,39] R. Beckmüller, M. Thol, I.H. Bell, E.W. Lemmon, R. Span, New equations of state for binary hydrogen mixtures containing methane, nitrogen, carbon monoxide, and carbon dioxide, J. Phys. Chem. Ref. Data 50 (2021) 013102, https://doi.org/10.1063/5.0040533.

[40] ISO 20765-2 Natural Gas -Calculation of Thermodynamic Properties -Part 2: Single-phase Properties (Gas, Liquid, and Dense Fluid) for Extended Ranges of Application, International Organisation for Standardization, Geneva, 2015.

[41] R. Span, Multiparameter Equations of State — an Accurate Source of Thermodynamic Property Data, Springer-Verlag, Berlin, Heidelberg, 2000. https://doi.org/10.1007/978-3-662-04092-8.

[42] M. Thol, I.H. Bell, Empirical Fundamental Equations of State for Pure Fluids and Mixtures. High-Pressure Flows for Propulsion Applications, American Institute of Aeronautics and Astronautics, Inc., 2020, pp. 365–407. https://arc.aiaa.org/doi/10.2514/5.9781624105814.0365.0408.

[43] R. Span, W. Wagner, Equations of state for technical applications. II. Results for nonpolar fluids, Int. J. Thermophys. 24 (2003) 41–109, https://doi.org/10.1023/A:1022310214958.

[44] E.W. Lemmon, R. Span, Short fundamental equations of state for 20 industrial fluids, J. Chem. Eng. Data 51 (2006) 785–850, https://doi.org/10.1021/je050186n.

[45] K.E. Starling, J.L. Savidge, Compressibility factors of natural gas and other related hydrocarbon gases - AGA Transmission Measurement Committee, Report 8 (1992).

[46] T.A. Demetriades, T.C. Drage, R.S. Graham, Developing a new equation of state for carbon capture and storage pipeline transport, Proc. Inst. Mech. Eng. Part E J. Process Mech. Eng. 227 (2013) 117–124, https://doi.org/10.1177/0954408913481552.

[47] A. Köster, M. Thol, J. Vrabec, Molecular models for the hydrogen age: hydrogen, nitrogen, oxygen, argon, and water, J. Chem. Eng. Data 63 (2018) 305–320, https://doi.org/10.1021/acs.jced.7b00706.

[48] R. Hernández-Gómez, D. Tuma, D. Lozano-Martín, C.R. Chamorro, Accurate experimental (p, ρ, T) data of natural gas mixtures for the assessment of reference equations of state when dealing with hydrogen-enriched natural gas, Int. J. Hydrogen Energy 43 (2018) 21983–21998, https://doi.org/10.1016/j.ijhydene.2018.10.027.

[49] M. Richter, M.A. Ben Souissi, R. Span, P. Schley, Accurate (p, ρ, T, x) measurements of hydrogen-enriched natural-gas mixtures at T = (273.15, 283.15, and 293.15) K with pressures up to 8 MPa, J. Chem. Eng. Data 59 (2014) 2021–2029, https://doi.org/10.1021/je500181v.

[50] U.K. Deiters, I.H. Bell, Unphysical critical curves of binary mixtures predicted with GERG models, Int. J. Thermophys. 41 (2020) 1–19, https://doi.org/10.1007/s10765-020-02743-3.

[51] I.I.I. Alkhatib, A. AlHajaj, A. Almansoori, L.F. Vega, Accurate predictions of the effect of hydrogen composition on the thermodynamics and transport properties of natural gas, Ind Eng Chem Res 61 (2022) 6214–6234, https://doi.org/10.1021/acs.iecr.2c00363, acs.iecr.2c00363.

[52] D.Y. Peng, D.B. Robinson, A new two-constant equation of state, Ind. Eng. Chem. Fundam. 15 (1976) 59–64, https://doi.org/10.1021/i160057a011.

[53] J.S. Lopez-Echeverry, S. Reif-Acherman, E. Araujo-Lopez, Peng-Robinson equation of state: 40 years through cubics, Fluid Phase Equil. 447 (2017) 39–71, https://doi.org/10.1016/j.fluid.2017.05.007.

[54] C.H. Twu, J.E. Coon, J.R. Cunningham, A new generalized alpha function for a cubic equation of state Part 1. Peng-Robinson equation, Fluid Phase Equil. 105 (1995) 49–59, https://doi.org/10.1016/0378-3812(94)02601-V.

[55] J. Gross, G. Sadowski, Perturbed-chain SAFT: an equation of state based on a perturbation theory for chain molecules, Ind. Eng. Chem. Res. 40 (2001) 1244–1260, https://doi.org/10.1021/ie0003887.

[56] J. Gross, G. Sadowski, Application of the perturbed-chain SAFT equation of state to associating systems, Ind. Eng. Chem. Res. 41 (2002) 5510–5515, https://doi.org/10.1021/ie010954d.

[57] J. Gross, G. Sadowski, Reply to comment on "perturbed-chain SAFT: an equation of state based on a perturbation theory for chain molecules, Ind. Eng. Chem. Res. 58 (2019) 5744–5745, https://doi.org/10.1021/acs.iecr.9b01515.

[58] Felipe J. Blas, Lourdes F. Vega, Thermodynamic behaviour of homonuclear and heteronuclear Lennard-Jones chains with association sites from simulation and theory, Mol. Phys. 92 (1997) 135–150, https://doi.org/10.1080/002689797170707.

[59] Alkhatib III, L.M.C. Pereira, J. Torne, L.F. Vega, Polar soft-SAFT: theory and comparison with molecular simulations and experimental data of pure polar fluids, Phys. Chem. Chem. Phys. 22 (2020) 13171–13191, https://doi.org/10.1039/d0cp00846j.

[60] W. Wagner, R. Kleinrahm, Densimeters for very accurate density measurements of fluids over large ranges of temperature, pressure, and density, Metrologia 41 (2004), https://doi.org/10.1088/0026-1394/41/2/S03.

[61] S. Cheng, F. Li, F. Shang, W. Ma, H. Jin, N. Sakoda, et al., A review of experimental researches on the thermophysical properties of hydrogen-containing mixtures at high temperatures and high pressures, J. Chem. Eng. Data 66 (2021) 3361–3385, https://doi.org/10.1021/acs.jced.1c00366.

[62] C.Y. Tsang, P. Clancy, J.C.G. Calado, W.B. Streett, Phase equilibria in the H2/CH4 system at temperatures from 92.3 to 180.0 K and pressures to 140 MPa, Chem. Eng. Commun. 6 (1980) 365–383, https://doi.org/10.1080/00986448008912543.

[63] J.H. Hong, R. Kobayashi, Vapor-liquid equilibrium study of the H_2-CH_4 system at low temperatures and elevated pressures, J. Chem. Eng. Data 26 (1981) 127–131, https://doi.org/10.1021/je00024a007.

[64] J.R.S. Machado, W.B. Streett, U. Deiters, PVT measurements of hydrogen/methane mixtures at high pressures, J. Chem. Eng. Data 33 (1988) 148–152, https://doi.org/10.1021/je00052a027.

[65] W.B. Streett, J.C.G. Calado, Liquid-vapour equilibrium for hydrogen + nitrogen at temperatures from 63 to 110 K and pressures to 57 MPa, J. Chem. Thermodyn. 10 (1978) 1089–1100, https://doi.org/10.1016/0021-9614(78)90083-6.

[66] G. Mastinu, Apparatus to determine excess molar volumes. Application to the H_2-N_2 mixture, Rev. Sci. Instrum. 38 (1967) 1114–1116, https://doi.org/10.1063/1.1720980.

[67] A. Michels, T. Wassenaar, Isotherms of a nitrogen-hydrogen mixture between 0°C and 150°C up to 340 atmospheres, Appl. Sci. Res. 1 (1949) 258–262, https://doi.org/10.1007/BF02120333.

[68] C.O. Bennett, B.F. Dodge, Compressibilities of mixtures of hydrogen and nitrogen above 1000 atmospheres, Ind. Eng. Chem. 44 (1952) 180–185, https://doi.org/10.1021/ie50505a051.

[69] A. Van Itterbeek, W. Van Doninck, Measurements on the velocity of sound in mixtures of hydrogen, helium, oxygen, nitrogen and carbon monoxide at low temperatures, Proc. Phys. Soc. B 62 (1949) 62–69, https://doi.org/10.1088/0370-1301/62/1/308.

[70] C.Y. Tsang, W.B. Streett, Phase equilibria in the H_2/CO_2 system at temperatures from 220 to 290 K and pressures to 172 MPa, Chem. Eng. Sci. 36 (1981) 993–1000, https://doi.org/10.1016/0009-2509(81)80085-1.

[71] M.A. Ben Souissi, R. Kleinrahm, X. Yang, M. Richter, Vapor-phase (p, ρ, T, x) behavior and virial coefficients for the binary mixture (0.05 hydrogen + 0.95 carbon dioxide) over the temperature range from (273.15 to 323.15) K with pressures up to 6 MPa, J. Chem. Eng. Data 62 (2017) 2973–2981, https://doi.org/10.1021/acs.jced.7b00213.

[72] A. Cipollina, R. Anselmo, O. Scialdone, G. Filardo, A. Galia, Experimental P-T-ρ measurements of supercritical mixtures of carbon dioxide, carbon monoxide, and hydrogen and semiquantitative estimation of their solvent power using the solubility parameter concept, J. Chem. Eng. Data 52 (2007) 2291–2297, https://doi.org/10.1021/je700307r.

[73] B.V. Mallu, D.S. Viswanath, Compression factors and second virial coefficients of H_2, CH_4, $\{xCO_2 + (1 - x)H_2\}$, and $\{xCO_2 + (1 - x)CH_4\}$, J. Chem. Thermodyn. 22 (1990) 997–1006, https://doi.org/10.1016/0021-9614(90)90189-W.

[74] S. Cheng, F. Shang, W. Ma, H. Jin, N. Sakoda, X. Zhang, et al., Density data of two $(H_2 + CO_2)$ mixtures and a $(H_2 + CO_2 + CH_4)$ mixture by a modified burnett method at temperature 673 K and pressures up to 25 MPa, J. Chem. Eng. Data 64 (2019) 1693–1704, https://doi.org/10.1021/acs.jced.8b01206.

[75] M.J. Hiza, C.K. Heck, A.J. Kidnay, Liquid-vapor and solid-vapor equilibrium in the system hydrogen - ethane, Adv. Cryog. Eng. 13 (1968) 343–356.

[76] W.L. Burriss, N.T. Hsu, H.H. Reamer, B.H. Sage, Phase behavior of the hydrogen-propane system, Ind. Eng. Chem. 45 (1953) 210–213, https://doi.org/10.1021/ie50517a060.

[77] S. Mihara, H. Sagara, Y. Arai, S. Saito, The compressibility factors of hydrogen methane, hydrogen-ethane and hydrogen-propane gaseous mixtures, J. Chem. Eng. Jpn. 10 (1977) 395–399, https://doi.org/10.1252/jcej.10.395.

[78] D.M.A. Mason, B.E. Eakin, Compressibility factor of fuel gases at 60° F. and 1 atm, J. Chem. Eng. Data 6 (1961) 499–504, https://doi.org/10.1021/je60011a006.

[79] H.J. Aroyan, D.L. Katz, Low temperature vapor-liquid equilibria in hydrogen-n-butane system, Ind. Eng. Chem. 43 (1951) 185–189, https://doi.org/10.1021/ie50493a050.

[80] M.R. Dean, J.W. Tooke, Vapor-liquid equilibria in three hydrogen-paraffin systems, Ind. Eng. Chem. 38 (1946) 389–393, https://doi.org/10.1021/ie50436a014.

[81] W.B. Nichols, H.H. Reamer, B.H. Sage, Volumetric and phase behavior in the hydrogen–n-hexane system, AIChE J. 3 (1957) 262–267, https://doi.org/10.1002/aic.690030223.

[82] T.T.H. Verschoyle, The ternary system carbon monoxide-nitrogen-hydrogen and the component binary systems between temperatures of -185° and -215° C., and between pressures of 0 and 225 atm, Philos. Trans. R. Soc. Lond. - Ser. A Contain. Pap. a Math. or Phys. Character 230 (1931) 189–220, https://doi.org/10.1098/rsta.1932.0006.

[83] C.Y. Tsang, W.B. Streett, Phase equilibria in the H_2-CO system at temperatures from 70 to 125 K and pressures to 53 MPa, Fluid Phase Equil. 6 (1981) 261–273, https://doi.org/10.1016/0378-3812(81)85008-X.

[84] G.A. Scott, A. Prsl, The isotherms of hydrogen, carbon monoxide and their mixtures, Proc. R. Soc. Lond. - Ser. A Contain. Pap. a Math. Phys. Character 125 (1929) 330–344, https://doi.org/10.1098/rspa.1929.0171.

[85] D.T.A. Townend, L.A. Bhatt, Isotherms of hydrogen, carbon monoxide and their mixtures, Proc. R. Soc. Lond. - Ser. A Contain. Pap. a Math. Phys. Character 134 (1931) 502–512, https://doi.org/10.1098/rspa.1931.0210.

[86] U. Setthanan, D.R. Morris, D.H. Lister, Solubilities of H_2 in H_2O and D_2 in D_2O with dissolved boric acid and lithium hydroxide, Can. J. Chem. 84 (2006) 65–68, https://doi.org/10.1139/v06-010.

[87] G. Kling, G. Maurer, The solubility of hydrogen in water and in 2-aminoethanol at temperatures between 323 K and 423 K and pressures up to 16 MPa, J. Chem. Thermodyn. 23 (1991) 531–541, https://doi.org/10.1016/S0021-9614(05)80095-3.

[88] R. Wiebe, V.L. Gaddy, The solubility of hydrogen in water at 0, 50, 75 and 100° from 25 to 1000 atmospheres, J. Am. Chem. Soc. 56 (1934) 76–79, https://doi.org/10.1021/ja01316a022.

[89] S.K. Shoor, R.D. Walker, K.E. Gubbins, Salting out of nonpolar gases in aqueous potassium hydroxide solutions, J. Phys. Chem. 73 (1969) 312–317, https://doi.org/10.1021/j100722a006.

[90] M. Yorizane, S. Sadamoto, H. Masuoka, Y. Eto, Gas solubilities in methanol at high pressure, J Soc Chem Ind Japan 72 (1969) 2174–2177, https://doi.org/10.1246/nikkashi1898.72.10_2174.

[91] T. Yamanishi, K. Okuno, Y. Naruse, E. Sada, Liquid-vapor equilibrium in binary systems for He in n-hydrogen, hydrogen deuteride, and n-deuterium under ordinary pressure, J. Phys. Chem. 96 (1992) 2284–2289, https://doi.org/10.1021/j100184a048.

[92] M.J. Hiza, Technical Note 621 - Liquid-Vapor Equilibrium in the Binary Systems of He^4 and He^3 with nD_2 and nH_2, National Bureau of Standards, 1972.

[93] M.J. Hiza, Liquid-vapor equilibria in binary systems containing ^{4}He or ^{3}He with nH_2 or nD_2, Fluid Phase Equil. 6 (1981) 203–227, https://doi.org/10.1016/0378-3812(81)85005-4.

[94] C.M. Sneed, R.E. Sonntag, G.J. Van Wylen, Helium-hydrogen liquid-vapor equilibrium to 100 atm, J. Chem. Phys. 49 (1968) 2395–2404, https://doi.org/10.1063/1.1670414.

[95] W.B. Streett, R.E. Sonntag, G.J. Van Wylen, Liquid-vapor equilibrium in the system normal hydrogen-helium, J. Chem. Phys. 40 (1964) 1390–1395, https://doi.org/10.1063/1.1725322.

[96] R.E. Sonntag, G.J. Van Wylen, R.W. Crain, Liquid-vapor equilibrium in the system equilibrium hydrogen-helium, J. Chem. Phys. 41 (1964) 2399–2402, https://doi.org/10.1063/1.1726277.

[97] J.C.G. Calado, W.B. Streett, Liquid-vapor equilibrium in the system H_2-Ar at temperatures from 83 to 141 K and pressures to 52 MPa, Fluid Phase Equil. 2 (1979) 275–282, https://doi.org/10.1016/0378-3812(79)80012-6.

[98] H. Volk, G.D. Halsey, Solubility of hydrogen and deuterium in liquid argon, J. Chem. Phys. 33 (1960) 1132–1139, https://doi.org/10.1063/1.1731347.

[99] W.B. Streett, C.H. Jones, Liquid phase separation and liquid—vapor equilibrium in the system neon—hydrogen, J. Chem. Phys. 42 (1965) 3989–3994, https://doi.org/10.1063/1.1695872.

[100] C.K. Heck, P.L. Barrick, Liquid-Vapor Phase Equilffiria of the Neon-Normal Hydrogen System, Adv. Cryog. Eng., 1966, pp. 349–355.

[101] P. Van't Zelfde, Z. Dokoupil, Some vapour-pressure measurements of the condensed system Ne-H_2 near the triple point of Ne, Physica 74 (1974) 423–434, https://doi.org/10.1016/0031-8914(74)90135-9.

[102] C.W. Scholz, R. Span, Vapor-phase (p, ρ, T, x) behavior of the (hydrogen + argon) system, J. Chem. Eng. Data 65 (2020) 3728–3734, https://doi.org/10.1021/acs.jced.0c00355.

[103] C.C. Tanner, I. Masson, The pressures of gaseous mixtures. Part III, Proc. R. Soc. Lond. - Ser. A Contain. Pap. a Math. Phys. Character 126 (1930) 268–288, https://doi.org/10.1098/rspa.1930.0007.

[104] P. Zandbergen, J.J.M. Beenakker, Experimental determination of the volume change on mixing for gaseous N_2-H_2, Ar-H_2 and Ar-N_2 between 170 and 292°K up to 100 ATM, Physica 33 (1967) 343–365, https://doi.org/10.1016/0031-8914(67)90169-3.

[105] W.B. Streett, An experimental study of the equation of state of liquid mixtures of neon + normal hydrogen, J. Chem. Thermodyn. 5 (1973) 313–323, https://doi.org/10.1016/S0021-9614(73)80019-9.

[106] D. Güsewell, F. Schmeissner, J. Schmid, Density and sound velocity of saturated liquid neon-hydrogen and neon-deuterium mixtures between 25 and 31 K, Cryogenics (Guildf) 10 (1970) 150–154, https://doi.org/10.1016/0011-2275(70)90087-1.

[107] A. Van Itterbeek, W. Van Doninck, Velocity of sound in mixtures of argon, helium and hydrogen at low temperatures, Proc. Phys. Soc. 58 (1946) 615–623, https://doi.org/10.1088/0959-5309/58/5/309.

[108] Y.S. Kazarnovskii, G.B. Simonov, G.E. Arsitov, Compressibility of nitrogen-hydrogen-ammonia mixtures at high pressures and temperatures, Zh. Fiz. Khim. 14 (1968) 774–781.

[109] M. Hongo, H. Iwasaki, Viscosity of hydrogen and of hydrogen-ammonia mixtures under pressures, Rev. Phys. Chem. Jpn. 48 (1) (1978) 1–9.

[110] R. Wiebe, T.H. Tremearne, The solubility of hydrogen in liquid ammonia at 25, 50, 75 and 100° and at pressures to 1000 atmospheres, J. Am. Chem. Soc. 56 (1934) 2357–2360, https://doi.org/10.1021/ja01326a039.

[111] R. Wiebe, V.L. Gaddy, The solubility in liquid ammonia of hydrogen at 0° and of nitrogen at 0, 50, 75, 90 and 100° at pressures to 1000 atmospheres. Critical phenomena of ammonia-nitrogen mixtures at 1, J. Am. Chem. Soc. 59 (1937) 1984, https://doi.org/10.1021/ja01289a055. –7.

[112] H.H. Reamer, B.H. Sage, Phase behavior in the hydrogen-ammonia system, J. Chem. Eng. Data 4 (1959) 152–154, https://doi.org/10.1021/je60002a012.

[113] H. Knapp, K. Schmölling, A. Neumann, Measurement of the molal heat capacity of H_2-N_2 mixtures, Cryogenics (Guildf) 16 (1976) 231–237, https://doi.org/10.1016/0011-2275(76)90266-6.

[114] C.J. Wormald, K.L. Lewis, S. Mosedale, The excess enthalpies of hydrogen + methane, hydrogen + nitrogen, methane + nitrogen, methane + argon, and nitrogen + argon at 298 and 201 K at pressures up to 10.2 MPa, J. Chem. Thermodyn. 9 (1977) 27–42, https://doi.org/10.1016/0021-9614(77)90194-X.

[115] R.E. Randelman, L.A. Wenzel, Joule-thomson coefficients of hydrogen and methane mixtures, J. Chem. Eng. Data 33 (1988) 293–299, https://doi.org/10.1021/je00053a021.

[116] H. Li, J.P. Jakobsen, Ø. Wilhelmsen, J. Yan, PVTxy properties of CO_2 mixtures relevant for CO_2 capture, transport and storage: review of available experimental data and theoretical models, Appl. Energy 88 (2011) 3567–3579, https://doi.org/10.1016/j.apenergy.2011.03.052.

[117] H. Li, B. Dong, Z. Yu, J. Yan, K. Zhu, Thermo-physical properties of CO_2 mixtures and their impacts on CO_2 capture, transport and storage: progress since 2011, Appl. Energy 255 (2019), 113789, https://doi.org/10.1016/j.apenergy.2019.113789.

[118] A.L. Benham, D.L. Katz, Vapor-liquid equilibria for hydrogen–light-hydrocarbon systems at low temperatures, AIChE J. 3 (1957) 33–36, https://doi.org/10.1002/aic.690030107.

[119] H.F. Cosway, D.L. Katz, Low-temperature vapor-liquid equilibria in ternary and quaternary systems containing hydrogen, nitrogen, methane, and ethane, AIChE J. 5 (1959) 46–50, https://doi.org/10.1002/aic.690050111.

[120] F.A. Freeth, F.R. S, T.T.H. Verschoyle, Physical constants of the system methane-hydrogen, Proc. R. Soc. Lond. - Ser. A Contain. Pap. a Math. Phys. Character 130 (1931) 453–463, https://doi.org/10.1098/rspa.1931.0016.

[121] M. Hu, W. Lin, A. Gu, J. Li, Isothermal vapor-liquid equilibrium in $CH_4/H_2/N_2$ system at a cryogenic temperature range from 100.0 K to 125.0 K, Fluid Phase Equil. 366 (2014) 16–23, https://doi.org/10.1016/j.fluid.2014.01.002.

[122] H. Sagara, Y. Arai, S. Saito, Vapor-Liquid equilibria of binary and ternary systems containing hydrogen and light hydrocarbons, J. Chem. Eng. Jpn. 5 (1972) 339–348, https://doi.org/10.1252/jcej.5.339.

[123] M. Yorizane, S. Yoshimura, H. Masuoka, I. Funada, C.-T. Fu, B.C.-Y. Lu, Phase behavior of three hydrogen-containing ternary systems, Proc. Adv. Cryog. Eng. 25 (1980) 654–661.

[124] W.W. Akers, L.S. Eubanks, Vapor-liquid equilibria in the System Hydrogen-Nitrogen-Carbon Monoxide, Boston, MA: Springer US, Adv. Cryog. Eng. 389 (1960) 275–293, https://doi.org/10.1007/978-1-4684-3105-6_32.

[125] H. Kremer, H. Knapp, Vapor-liquid equilibria in ternary mixtures of H_2, N_2, CO and CH_4, Fluid Phase Equil. 11 (1983) 289–310, https://doi.org/10.1016/0378-3812(83)85030-4.

[126] A. Maimoni, Liquid-vapor equilibria in the hydrogen-nitrogen and deuterium-nitrogen systems, AIChE J. 7 (1961) 371–375, https://doi.org/10.1002/aic.690070306.

[127] M.H. Omar, Z. Dokoupil, Some supplementary measurements on the vapour-liquid equilibrium of the system hydrogen-nitrogen at temperatures higher than the triple point of nitrogen, Physica 28 (1962) 33–43, https://doi.org/10.1016/0031-8914(62)90009-7.

[128] M. Yorizane, S. Yoshimura, H. Masuoka, T. Naka, The measurement and prediction of the vapor-liquid equilibrium relation at low temperature and high pressure for H_2-N_2 system, Chem. Eng. 35 (1971) 691–696, https://doi.org/10.1252/kakoronbunshu1953.35.691, a1.

[129] K. Bezanehtak, G.B. Combes, F. Dehghani, N.R. Foster, D.L. omasko, Vapor-liquid equilibrium for binary systems of carbon dioxide + methanol, hydrogen + methanol, and hydrogen + carbon dioxide at high pressures, J. Chem. Eng. Data 47 (2002) 161–168, https://doi.org/10.1021/je010122m.

[130] G. Kaminishi, T. Toriumi, Vapor-liquid phase equilibrium in the CO_2-H_2, CO_2-N_2 and CO_2-O_2 systems, J Soc Chem Ind Japan 69 (1966) 175–178, https://doi.org/10.1246/nikkashi1898.69.2_175.

[131] J. Ke, N. Suleiman, Y. Sanchez-Vicente, T.S. Murphy, J. Rodriguez, A. Ramos, et al., The phase equilibrium and density studies of the ternary mixtures of CO_2 + Ar + N_2 and CO_2 + Ar + H_2, systems relevance to CCS technology, Int. J. Greenh. Gas Control 56 (2017) 55–66, https://doi.org/10.1016/j.ijggc.2016.11.003.

[132] J. Ke, A.J. Parrott, Y. Sanchez-Vicente, P. Fields, R. Wilson, T.C. Drage, et al., New phase equilibrium analyzer for determination of the vapor-liquid equilibrium of carbon dioxide and permanent gas mixtures for carbon capture and storage, Rev. Sci. Instrum. 85 (2014), https://doi.org/10.1063/1.4891796.

[133] J. Ke, P.J. King, M.W. George, M. Poliakoff, Method for locating the vapor-liquid critical point of multicomponent fluid mixtures using a shear mode piezoelectric sensor, Anal. Chem. 77 (2005) 85–92, https://doi.org/10.1021/ac048970i.

[134] J.O. Spano, C.K. Heck, P.L. Barrick, Liquid-vapor equilibria of the hydrogen-carbon dioxide system, J. Chem. Eng. Data 13 (1968) 168–171, https://doi.org/10.1021/je60037a007.

[135] M.J. Tenorio, A.J. Parrott, J.A. Calladine, Y. Sanchez-Vicente, A.J. Cresswell, R. S. Graham, et al., Measurement of the vapour-liquid equilibrium of binary and ternary mixtures of CO_2, N_2 and H_2, systems which are of relevance to CCS technology, Int. J. Greenh. Gas Control 41 (2015) 68–81, https://doi.org/10.1016/j.ijggc.2015.06.009.

[136] G. Tsankova, Y. Leusmann, R. Span, M. Richter, Dew points, dielectric permittivities, and densities for (hydrogen + carbon dioxide) mixtures determined with a microwave Re-entrant cavity resonator, Ind. Eng. Chem. Res. 58 (2019) 21752–21760, https://doi.org/10.1021/acs.iecr.9b04423.

[137] M. Yorizane, S. Yoshimura, H. Masuoka, Vapor liquid equilibrium at high pressure, Chem. Eng. 34 (1970) 953–957, https://doi.org/10.1252/kakoronbunshu1953.34.953, a1.

[138] A. Heintz, W.B. Streett, A. Heintz, Phase equilibria in the H_2/C_2H_6 system at temperatures from 92.5 to 280.1 K and pressures to 560 MPa, J. Chem. Eng. Data 27 (1982) 465–469, https://doi.org/10.1021/je00030a029.

[139] R.B. Williams, D.L. Katz, Vapor-liquid equilibria in binary systems. Hydrogen with ethylene, ethane, propylene, and propane, Ind. Eng. Chem. 46 (1954) 2512–2520, https://doi.org/10.1021/ie50540a033.

[140] D.B. Trust, F. Kurata, Vapor-liquid phase behavior of the hydrogen-propane and hydrogen-carbon monoxide-propane systems, AIChE J. 17 (1971) 86–91, https://doi.org/10.1002/aic.690170119.

[141] A.E. Klink, H.Y. Cheh, E.H. Amick, The vapor-liquid equilibrium of the hydrogen—n-butane system at elevated pressures, AIChE J. 21 (1975) 1142–1148, https://doi.org/10.1002/aic.690210614.

[142] E.E. Nelson, W.S. Bonnell, Solubility of hydrogen in n-butane, Ind. Eng. Chem. 35 (1943) 204–206, https://doi.org/10.1021/ie50398a016.

[143] J.F. Connolly, G.A. Kandalic, Gas solubilities, vapor—liquid equilibria, and partial molal volumes in some hydrogen-hydrocarbon systems, J. Chem. Eng. Data 31 (1986) 396–406, https://doi.org/10.1021/je00046a008.

[144] N.P. Freitag, D.B. Robinson, Equilibrium phase properties of the hydrogen-methane-carbon dioxide, hydrogen-carbon dioxide-n-pentane and hydrogen-n-pentane systems, Fluid Phase Equil. 31 (1986) 183–201, https://doi.org/10.1016/0378-3812(86)90012-9.

[145] E. Brunner, Solubility of hydrogen in 10 organic solvents at 298.15, 323.15, and 373.15 K, J. Chem. Eng. Data 30 (1985) 269–273, https://doi.org/10.1021/je00041a010.

[146] M.S. Fu, C.S. Tan, Solubility of hydrogen in a mixture of n-hexane and dicyclopentadiene from 313 to 363 K and from 2.0 to 5.5 MPa, Fluid Phase Equil. 93 (1994) 233–247, https://doi.org/10.1016/0378-3812(94)87011-X.

[147] W. Gao, R.L. Robinson, K.A.M. Gasem, Solubilities of hydrogen in hexane and of carbon monoxide in cyclohexane at temperatures from 344.3 to 410.9 K and pressures to 15 MPa, J. Chem. Eng. Data 46 (2001) 609–612, https://doi.org/10.1021/je0003546.

[148] T. Katayama, T. Nitta, Solubilities of hydrogen and nitrogen in alcohols and n-hexane, J. Chem. Eng. Data 21 (1976) 194–196, https://doi.org/10.1021/je60069a018.

[149] Purwanto, R.M. Deshpande, R.V. Chaudhari, H. Delmas, Solubility of hydrogen, carbon monoxide, and 1-octene in various solvents and solvent mixtures, J. Chem. Eng. Data 41 (1996) 1414–1417, https://doi.org/10.1021/je960024e.

[150] E.A. Symons, Hydrogen gas solubility in the dimethyl sulfoxide – water system: a further clue to solvent structure in these media, Can. J. Chem. 49 (1971) 3940–3947, https://doi.org/10.1139/v71-660.

[151] R.G. Moore, F.D. Otto, The solubility of hydrogen in aliphatic amines, Can. J. Chem. Eng. 50 (1972) 355–360, https://doi.org/10.1002/cjce.5450500308.

[152] R. Hernández-Gómez, D. Tuma, E. Pérez, C.R. Chamorro, Accurate experimental (p, ρ, and T) data for the introduction of hydrogen into the natural gas grid (II): thermodynamic characterization of the methane-hydrogen binary system from 240 to 350 K and pressures up to 20 MPa, J. Chem. Eng. Data 63 (2018) 1613–1630, https://doi.org/10.1021/acs.jced.7b01125.

[153] M. Jaeschke, H.-M.H. Dorsfen, A.E. Humphreys, GERG TM7 - Supplement to the GERG Databank of High-Accuracy Compresion Factor Measurements, 1996.

[154] M. Jett, F. Fleyfel, R. Kobayashi, The nature of (p, V_m, T) surfaces of mixtures: (Quantum + normal) and (normal + hydrogen-bonded), as summarized by their isochoric inflection loci, J. Chem. Thermodyn. 26 (1994) 561–569, https://doi.org/10.1006/jcht.1994.1064.

[155] J.W. Magee, A.G. Pollin, R.J. Martin, R. Kobayashi, Burnett-isochoric P-V-T measurements of a nominal 20 mol% hydrogen-80 mol% methane mixture at elevated temperatures and pressures, Fluid Phase Equil. 22 (1985) 155–173, https://doi.org/10.1016/0378-3812(85)85017-2.

[156] J.W. Magee, R. Kobayashi, Isochoric (p, ρ_n, T) measurements on ($0.2005H_2$ + $0.7995CH_4$) at temperatures from 140 to 273.15 K and pressures to 70 MPa, J. Chem. Thermodyn. 18 (1986) 847–858, https://doi.org/10.1016/0021-9614(86)90119-9.

[157] S. Mihara, H. Sagara, Y. Arai, S. Saito, The compressibility factors of hydrogen-methane, hydrogen-ethane and hydrogen-propane gaseous mixtures, J. Chem. Eng. Jpn. 10 (1977) 395–399, https://doi.org/10.1252/jcej.10.395.

[158] W.H. Mueller, T.W. Leland, R. Kobayashi, Volumetric properties of gas mixtures at low temperatures and high pressures by the Burnett method: the hydrogen-methane system, AIChE J. 7 (1961) 267–272, https://doi.org/10.1002/aic.690070220.

[159] E.P. Bartlett, H.D. Cupples, T.H. Tremearne, The compressibility isotherms of hydrogen, nitrogen and a 3:1 mixture of these gases at temperatures between 0 and 400° and at pressures to 1000 atmospheres, J. Am. Chem. Soc. 50 (1928) 1275–1288, https://doi.org/10.1021/ja01392a007.

[160] E.P. Bartlett, H.C. Hetherington, H.M. Kvalnes, T.H. Tremearne, The compressibility isotherms of hydrogen, nitrogen and a 3:1 mixture of these gases at temperatures of -70, -50, -25 and 20° and at pressures to 1000 atmospheres, J. Am. Chem. Soc. 52 (1930) 1363–1373, https://doi.org/10.1021/ja01367a011.

[161] E.P. Bartlett, The compressibility isotherms of hydrogen, nitrogen and mixtures of these gases at 0° and pressures to 1000 atmospheres, J. Am. Chem. Soc. 49 (1927) 687–701, https://doi.org/10.1021/ja01402a011.

[162] E.P. Bartlett, The compressibility isotherms of hydrogen, nitrogen and mixtures of these gases at 0° and pressures to 1000 atmospheres. A correction, J. Am. Chem. Soc. 49 (1927) 1955, https://doi.org/10.1021/ja01407a016. –7.

[163] R. Hernández-Gómez, D. Tuma, A. Gómez-Hernández, C.R. Chamorro, Accurate experimental (p, ρ, T) data for the introduction of hydrogen into the natural gas grid: thermodynamic characterization of the nitrogen-hydrogen binary system from 240 to 350 K and pressures up to 20 MPa, J. Chem. Eng. Data 62 (2017) 4310–4326, https://doi.org/10.1021/acs.jced.7b00694.

[164] M. Jaeschke, H.M. Hinze, H.J. Achtermann, G. Magnus, *PVT* data from burnett and refractive index measurements for the nitrogen-hydrogen system from 270 to 353 K and pressures to 30 MPa, Fluid Phase Equil. 62 (1991) 115–139, https://doi.org/10.1016/0378-3812(91)87010-7.

[165] J. Kestin, Y. Nagasaka, W.A. Wakeham, The thermal conductivity of mixtures of hydrogen with nitrogen, Berichte Der Bunsengesellschaft Für Phys. Chemie 86 (1982) 187–191, https://doi.org/10.1002/bbpc.19820860302.

[166] T.T.H. Verschoyle, Isotherms of hydrogen, of nitrogen, and of hydrogen-nitrogen mixtures, at 0° and 20° C., up to a pressure of 200 atmospheres, Proc. R. Soc. Lond. - Ser. A Contain. Pap. a Math. Phys. Character 111 (1926) 552–576, https://doi.org/10.1098/rspa.1926.0081.

[167] R. Wiebe, V.L. Gaddy, The compressibilities of hydrogen and of four mixtures of hydrogen and nitrogen at 0, 25, 50, 100, 200 and 300° and to 1000 atmospheres, J. Am. Chem. Soc. 60 (1938) 2300–2303, https://doi.org/10.1021/ja01277a007.

[168] B.D. Ababio, P.J. McElroy, (Pressure, Amount-of-Substance Density, Temperature) of $(1 - x)CO_2 + xH_2$ Using a Direct Method, J. Chem. Thermodyn. 25 (1993) 1495–1501, https://doi.org/10.1006/jcht.1993.1149.

[169] I. Al-Siyabi, Effect of Impurities on CO_2 Stream Properties, Heriot-Watt University, 2013, 1–182.

[170] B. Pinho, S. Girardon, F. Bazer-Bachi, G. Bergeot, S. Marre, C. Aymonier, Simultaneous measurement of fluids density and viscosity using HP/HT capillary devices, J. Supercrit. Fluids 105 (2015) 186–192, https://doi.org/10.1016/j.supflu.2015.04.016.

[171] Y. Sanchez-Vicente, T.C. Drage, M. Poliakoff, J. Ke, M.W. George, Densities of the carbon dioxide+hydrogen, a system of relevance to carbon capture and storage, Int. J. Greenh. Gas Control 13 (2013) 78–86, https://doi.org/10.1016/j.ijggc.2012.12.002.

[172] J. Zhang, X. Zhang, B. Han, J. He, Z. Liu, G. Yang, Study on intermolecular interactions in supercritical fluids by partial molar volume and isothermal compressibility, J. Supercrit. Fluids 22 (2002) 15–19, https://doi.org/10.1016/S0896-8446(01)00107-3.

[173] A. Maurer, Instrument Development and Speed of Sound Measurements in Hydrogen-Rich Mixtures, Dissertation zur Erlangung des Grades Doktor-Ingenieur der Fakultät für Maschinenbau der Ruhr-Universität Bochum (2021).

[174] D. Lozano-Martín, M.C. Martín, C.R. Chamorro, D. Tuma, J.J. Segovia, Speed of sound for three binary ($CH_4 + H_2$) mixtures from $p = (0.5$ up to 20) MPa at $T = (273.16$ to 375) K, Int. J. Hydrogen Energy 45 (2020) 4765–4783, https://doi.org/10.1016/j.ijhydene.2019.12.012.

[175] J.P. Brouwer, A.M. Vossepoel, C.J.N. Van Den Meijdenberg, J.J.M. Beenakker, Specific heat of the liquid mixtures of neon and hydrogen isotopes in the phase-separation region. II. The system Ne-D_2, Physica 50 (1970) 125–148, https://doi.org/10.1016/0031-8914(70)90057-1.

[176] J.J. Segovia, D. Lozano-Martín, D. Tuma, A. Moreau, M. Carmen Martín, D. Vega-Maza, Speed of sound data and acoustic virial coefficients of two binary ($N_2 + H_2$) mixtures at temperatures between (260 and 350) K and at pressures between (0.5 and 20) MPa, J. Chem. Thermodyn. 171 (2022) 106791, https://doi.org/10.1016/j.jct.2022.106791.